Modeling the influence of potassium content and heating rate on biomass pyrolysis

Anna Trubetskaya[a,*], Gerrit Surup[b], Alexander Shapiro[c], Richard B. Bates[d]

[a]*Energy Engineering Department, Luleå University of Technology, 97187, Luleå, Sweden*
[b]*Department of Engineering Sciences, University of Agder, Jon Lilletuns vei 9, 4879 Grimstad, Norway*
[c]*Department of Chemical and Biochemical Engineering, Technical University of Denmark, Søltofts Plads Bygning 229, Kgs. Lyngby 2800, Denmark*
[d]*MIT, Department of Mechanical Engineering, 02139, Cambridge, MA, USA*

Abstract

This study presents a combined kinetic and particle model that describes the effect of potassium and heating rate during the fast pyrolysis of woody and herbaceous biomass. The model calculates the mass loss rate, over a wide range of operating conditions relevant to suspension firing. The shrinking particle model considers internal and external heat transfer limitations and incorporates catalytic effects of potassium on the product yields. Modeling parameters were tuned with experimentally determined char yields at high heating rates ($>$ 200 K s^{-1}) using a wire mesh reactor, a single particle burner, and a drop tube reactor. The experimental data demonstrated that heating rate and potassium content have significant effects on the char yield. The importance of shrinkage on the devolatilization time becomes greater with increasing particle size, but showed little influence on the char yields.

*Corresponding author. anna.trubetskaya@ltu.se

Keywords: fast pyrolysis, kinetics, metaplast, potassium, heating rate

Nomenclature

AR	Aspect ratio
A_i	Pre-exponential factor (s^{-1})
A_p	Particle area (m^2)
c_p	Specific heat capacity (J (kg K)$^{-1}$)
d_p	Particle diameter (m)
d_{pore}	Particle pore diameter (m)
D_r	Reactor diameter (m)
E_i	Activation energy (J mol^{-1})
f_{sh}	Shrinkage factor
g	Gravity (m s^{-2})
h	Convective heat transfer coefficient (W ($m^{-2}K^{-1}$))
ΔH_{vap}	Heat of vaporization (J kg^{-1})
K_1, K_2	Constants for the activation energy of the char formation reaction as a function of biomass potassium content
k_i	Reaction rate constant (s^{-1})
L	Reactor's length (m)
m	Reaction order
n	Dimensionality factor
R	Gas constant (J (K mol)$^{-1}$)
r	Reaction rate (kg (kg s)$^{-1}$)
R_p	Particle radius at specified interior location (m)
r_p	**Particle radius (m)**
T	Temperature (°C)
t	Time (s)
V_p	Particle volume (m^3)

v_p	Slip velocity between gas and particle (m s^{-1})
X	Conversion
$x_{Fe,max}$	Feret maximum diameter (m)
$x_{Ma,min}$	Martin minimum diameter (m)

Dimensionless numbers

Bi	Biot number
Nu	Nusselt number
Pr	Prandlt number
Re	Reynolds number

Greek symbols

α	Particle thermal diffusivity (m^2 s^{-1})
κ	Heating rate (K s^{-1})
λ	Thermal conductivity (W (m K)$^{-1}$)
μ	Viscosity (Pa s)
Ω	Correction factor for influence of potassium content on activation energy ($E_{a,3}$)
ω	K^+ concentration (mg kg^{-1})
ψ	Biomass fraction of solid phase
ρ	Density (kg m^{-3})
σ	Stefan-Boltzmann constant (J (s m^2 K^4)$^{-1}$)
τ	Holding time (s)
ε	Emissivity
ξ	Void fraction occupied by the gas phase

Subscripts

0	initial
b	biomass
c	char
g	gas
H_2O	water
K	potassium

M	metaplast	pyr	pyrolysis
max	maximum	r	radiative
$mesh$	wire mesh	s	solid phase
min	minimum	$total$	overall
p	particle	w	wall

1. Introduction

Suspension firing of biomass is widely used for power generation. Danish pulverized fuel fired power plants are undergoing a transition to 100 % biomass firing in order to reduce greenhouse gase emissions. Straw, wood pellets and wood chips are the most abundant biofuels in Denmark [1]. The annual consumption of biomass at Danish power stations is 1.2 million tones of straw and 0.2 millions of wood chips per year [2]. **The advantage of utilizing wheat straw as a renewable energy source is that it is one of the most readily available Danish agricultural residues, while the wood pellet production depends on the supply of imported wood residues [3, 4]. The drawback, however, is that the quality of agricultural wastes is lower than that of wood due to a higher ash content leading to deposition and corrosion of the boiler units. In pulverized biomass combustion, short residence times are required for biomass devolatilization, which makes it difficult to examine the dynamics of the process. In addition, the lignocellulosic material reactivity is affected by the biomass composition, namely organic**

matter and minerals [5–7]. The differences in char properties generated under various pyrolysis conditions can lead to a range of challenges in a modeling of biomass conversion.

Fast pyrolysis at high temperatures and high heating rates is the initial step in suspension biomass firing. Fuel particles first undergo rapid drying, heating and devolatization with the formation of char and volatiles. Despite of numerous previous studies on biomass devolatilization mechanisms and particle models, there is no generally accepted model that can estimate the conversion rate and final char yield over a wide range of operating conditions. Existing kinetic models [8–14] were developed with experimental data using specific biomass samples and a narrow set of low temperature reaction conditions. The application of lower temperatures makes extrapolation to higher temperatures in combustion/gasification processes.

Most of the existing biomass pyrolysis models [10, 15–17] which describe both the devolatilization product composition and yields (light gases, tar and char) are mainly valid for low-ash fuels (hardwood, softwood); whereas **considerably** less work has been carried out with herbaceous lignocellulosic materials. In addition, these mathematical models are valid for biomass pyrolysis under slow heating rates (1-50 K min^{-1}) and long residence time (1-4 h). Many kinetic models for wood pyrolysis have been reported in the literature [18]. The simplest models are based on a single first order decomposition reaction, and are not able to estimate the influence of heating conditions on the product yields [19].

$$Fuel\ particle \longrightarrow Volatiles \cdot (1-\gamma) + \gamma \cdot Char$$

Figure 1: One-step global model [20].

Other models assume competing parallel reactions to predict the production kinetics of gas, tar and char, which is often valid only over a narrow temperature range [10, 21].

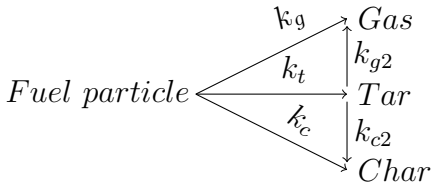

Figure 2: Competing step global model with k_g - rate constant of gas release, k_c - rate constant of char formation, k_t - rate constant of tar formation, k_{g2} - rate constant for the formation of gas from tar and k_{c2} - rate constant for the formation of char from tar [10].

Thurner and Mann [10] assumed that the activation energy for the char formation reaction is similar to the activation energy for mass loss reactions to gas and tar, and therefore, that the final residual weight (e.g. the char yield) is independent of the heating rate and heat treatment temperature. More complex models involve additional steps for tar decomposition in the gas phase [22] or an intermediate product derived from primary decomposition of biomass [15, 23, 24]. **These models can be generally applied only for a specific type of biomass. Ranzi et al. [25, 26] included the effect of holocelluloses, lignin and extractives on the product yields and composition. Previous models have not included the catalytic effect of alkali metals on biomass devolatilization, which has been shown to influence yields and product release rates sig-**

nificantly [7, 27–29]. Extrapolation kinetics fitted under low heating rate conditions to the pulverized fuel firing conditions is difficult due to the changes in devolatilization kinetics with heating rate [20]. Previous pyrolysis kinetic models have failed to extrapolate to higher temperatures because the actual particle heating rate depends on parameters which are difficult to define quantitatively [20, 30, 31].

In this study a model was developed to estimate the char yield from biomass pyrolysis at conditions relevant to suspension firing, which includes the effects of high heating rates, high heat treatment temperatures, particle size and biomass alkali content. Simulations were combined with experiments in a wire mesh reactor (WMR), a single particle burner (SPR) and a drop tube reactor (DTF) to identify the most influential fuel characteristics that explain the differences between woody and herbaceous biomass pyrolysis. The accurate knowledge of reaction rate and solid residue yields is essential for the boiler optimal operation and design.

2. Model development

The devolatilization model assumes non-isothermal and cylindrical biomass particles, and includes both chemical kinetics, and external and internal heat transfer. A single biomass particle enters a pre-heated gas flow and is heated up by convection and radiation from its surroundings (single particle reactor and drop tube reactor), or by conduction from the mesh (wire mesh reactor). The model assumes:

1. The fuel particle is a one-dimensional, cylindrical geometry.
2. Thermal gradients within the particle are only in the radial direction.
3. Particle shrinkage occurs during pyrolysis.
4. Moisture content of all fuels are low ($< 5\,\mathrm{wt.\,\%}$) and drying occurs.
5. Internal and external mass transfer are fast [32], and therefore, are not considered.
6. Only the reactor walls contribute to the radiative external heat transfer; radiation from the flame around the particle due to ignition of volatiles is neglected.
7. Heat transfer to the particle surface occurs through convection and radiation.
8. Heat transfer within a biomass particle occurs through conduction.
9. Potassium has a dominant influence on the char yield compared to other ash elements.
10. Variations in plant cell wall composition (cellulose, hemicellulose, lignin, extractives) are relatively small and have less influence on the biomass char yield than variations in the potassium content.

The last two assumptions are based on previous experimental results obtained in a wire mesh reactor and a drop tube reactor [33, 34]. The proposed model includes only primary pyrolysis reactions,

i.e. not cracking of tar [35]. The schematic view of the proposed kinetic model is shown in Figure 3.

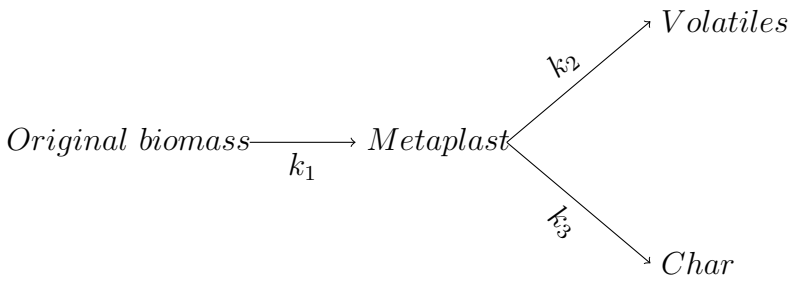

Figure 3: Three reaction model of biomass pyrolysis [12, 15, 36].

The shrinking particle is converted into an intermediate liquid compound (so called metaplast) which reacts further to form volatiles and char. Evidence of metaplast formation has been reported in the literature [23, 30, 37–40]. **The thermogravimetric results showed a change in the mass loss that was attributed to a high activation energy process during which cellulose passed from an inactive to an active form without sample mass loss [23]. High speed photography of hardwood lignin and cellulose exhibited decomposition of lignocellulosic material through an intermediate liquid with bursting bubbles [39]. Only the formation of metaplast is assumed to influence devolatilization whereas the fractional split between volatiles and char is determined by the heating rate and alkali content. The pyrolysis reactions are assumed to be irreversible and first order with an Arrhenius type of rate expression. One fixed set of kinetic parameters (activation energy and pre-exponential factor) for each of the three reactions for a generic biomass was obtained by fitting the**

model to the char yields obtained in the wire mesh and entrained flow reactors. The catalytic effect of potassium on the char yield was accounted for by decreasing the activation energy required for the reaction from metaplast to char (E_3), thereby leading to higher char yields. The particle model was solved with the initial conditions:

$$\rho_b(r_p, 0) = 1$$

$$\rho_M(r_p, 0) = 0$$

$$\rho_c(r_p, 0) = 0$$

The radial concentrations of biomass, metaplast and char are calculated from:

$$\frac{d\rho_b}{dt} = -k_1 \cdot \rho_b \tag{1}$$

$$\frac{d\rho_M}{dt} = k_1 \cdot \rho_b - (k_2 \cdot \rho_M + k_3(\omega_K) \cdot \rho_M) \tag{2}$$

$$\frac{d\rho_c}{dt} = k_3(\omega_K) \cdot \rho_M \tag{3}$$

$$k_i = A_i \cdot exp\left(-\frac{E_{a,i}}{R \cdot T}\right) \tag{4}$$

$$E_{a,3,max} = \Omega_K(\omega_K) \cdot E_{a,i} \tag{5}$$

$$\Omega_K(\omega_K) = 1 - K_1 \cdot \left(1 - exp\left(-\frac{\omega_K}{K_2}\right)^2\right) \tag{6}$$

The correction factor for the potassium content (Ω_K) becomes $\Omega_K(\omega_K = 0)$=1 and the activation energy $E_{a,3}$ is equal to the maximum activation energy $E_{a,3,max}$ when there is no potassium in the sample. Ω_K approaches the minimum value and the activation energy $E_{a,3}$ is equal to the minimum activation energy $E_{a,3,min}$ when

the biomass contains high amounts of potassium. The K_1 parameter is a constant and describes a range of activation energy; the K_2 parameter is a constant for the exponential adjustment of the potassium content (ω_K in mg kg^{-1}). Various expressions of Ω_K to describe the influence of potassium content were tested, and equation 6 was found to fit the char yield data best.

The results of the fitting showed that the kinetic parameters (A_i and $E_{a,i}$) for the metaplast formation and volatiles release are similar. The char yields were calculated in the model by keeping the kinetic parameters (k_1 and k_2) of other reactions constant, whereas the activation energy $E_{a,3}$ required for the reaction from metaplast to char was calculated according to equation 5. The modeling parameters were fitted by minimizing the sum of squares of the residuals using fmincon in Matlab (version 8.6, MathWorks Inc.).

2.1. Shrinking

The model calculates the radial shrinkage of the particle at radius r_p, which is divided into R_p grid points numbered from i=0 to i=R_p, where 0 is the center of the particle, generating a number of discrete volumes. The density distribution along the particle radius is calculated using a linear approximation between two neighboring points which form a discrete volume as shown in Figure 4.

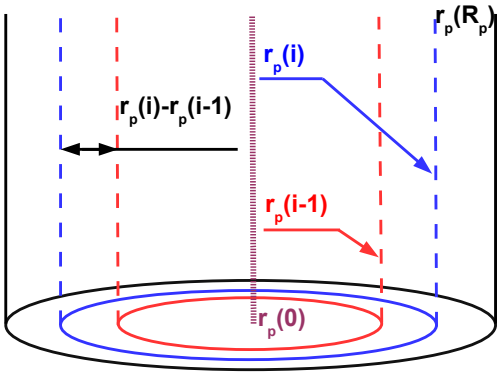

Figure 4: **Representation of a shrinking cylindrical biomass particle**.

The size of the control volume at a given time is calculated according to equation 7:

$$dV_i = 2 \cdot \pi \cdot R_p \cdot AR \cdot (r_{p(i)}^2 - r_{p(i-1)}^2) \tag{7}$$

The initial size of control volume is given by equation 8:

$$dV_{i,0} = 2 \cdot \pi \cdot R_p \cdot AR \cdot (r_{p(i,0)}^2 - r_{p(i-1,0)}^2) \tag{8}$$

In the shrinking particle model, the volume occupied by the solid structure of the particle is assumed to decrease proportionally with the conversion. The current size of the control volume is related to the initial size of the control volume through a shrinkage factor in equation 9, and further implemented in heat transfer equation 11:

$$f_{Sh} = \frac{dV_i}{dV_{i,0}} = \frac{r_{p(i)}^2 - r_{p(i-1)}^2}{r_{p(i,0)}^2 - r_{p(i-1,0)}^2} \tag{9}$$

The shrinkage factor is calculated from the density change of a fuel particle which is affected by the original biomass, metaplast and char fractions in

equation 10:

$$f_{Sh} = 1 - f_{Sh,min} \cdot \left(1 - \frac{\rho_b + \rho_M + \rho_c}{\rho_{b,0}}\right) \tag{10}$$

The shrinkage factor varies from 1 for the untreated biomass particle, to a minimum value $f_{Sh,min}$, when a particle is converted to volatiles and char. Here, the minimum shrinkage factor was varied from 0 to 0.5 according to previous experimental observations from fast pyrolysis of smaller wood particles (0.2-0.4 mm) [34], larger wood particles (3-5 mm) [41], and modeling results from Anca-Couce et al. [42].

2.2. ***Conservation of energy***

The unsteady energy equation for the particle describes internal heat transfer using Fourier's Law in cylindrical coordinates:

$$c_{p,s} \cdot \frac{dT_p}{dt} = \frac{1}{\rho_s \cdot f_{sh}} \cdot \frac{1}{r_p^n} \cdot \frac{\partial}{\partial r_p}\left(r_p^n \lambda_{eff} \frac{\partial T_p}{\partial r_p}\right) + \sum_{j=1}^{3} r_{pyr,j} \cdot (-\Delta H_{reac,j}) + r_{H_2O} \cdot (-\Delta H_{vap}) \tag{11}$$

$$r_{pyr,j} = -A_{pyr,j} \cdot exp\left(-\frac{E_{pyr,j}}{RT}\right) \cdot \left(\frac{\rho_b}{\rho_{b,0}}\right)^m \tag{12}$$

$$r_{H_2O} = -A_{H_2O} \cdot T_p^{1/2} \cdot exp\left(-\frac{E_{H_2O}}{RT}\right) \cdot \left(\frac{\rho_w}{\rho_{b,0}}\right)^m \tag{13}$$

The overall reaction enthalpy includes the heat of reaction ($\Delta H_{reac,j}$) multiplied by the pyrolysis reaction rate ($r_{pyr,j}$) for each reaction product: metaplast (j=1), char (j=2), and volatiles (j=3). The reactions from metaplast to gas or to char are competitive. **The metaplast formation was assumed to be as thermally neutral [43, 44], gas formation as endothermic, and char formation as exothermic [45, 46].** This approach resulted in the dependence of overall heat of reaction depending on the char yield [47],

which is consistent with experimental results [48, 49]. Thus the overall reaction enthalpy changes with the char yield, similar to the modeling approach of Haseli et al. [47]. The presence of potassium in fuels catalyzes pyrolysis reactions favoring the formation of char. Therefore, the endothermic heat of pyrolysis decreases with increasing char yield, and eventually shifts to an exothermic process, similar to results of Rath et al. [49] and Mack et al. [48]. Exothermic and endothermic heat of reaction (Δ $H_{reac,2}$ = -255000 J $kg^{-}1$; Δ $H_{reac,3}$ = 20000 J $kg^{-}1$) were proposed by Koufopanos et al. [45].

The rates of mass loss during drying and devolatilization were described by equations 1- 3 [50]. A first order reaction model (m=1) was chosen to describe the experimental results [51]. The heat of vaporization was assumed to be ΔH_{vap} = 2440000 J kg^{-1} [52, 53]. The initial condition is given by the ambient temperature:

$$T_p(r_p, 0) = T_{amb} \tag{14}$$

The boundary conditions specify that the particle center line is adiabatic due to symmetry shown in equation 15 and that convection and radiation entering at the particle surface is conducted into the particle as shown the equation 16 or given by the temperature of the mesh in equation 17:

$$\lambda_{eff} \frac{dT_p}{dr_p}\bigg|_{r_p=0} = 0 \tag{15}$$

$$\lambda_{eff} \frac{dT_p}{dr_p}\bigg|_{r_p=R_p} = h \cdot (T_g - T_p|_{r_p=R_p}) + \epsilon \cdot \sigma \cdot (T_w^4 - T_p^4|_{r_p=R_p}) \quad drop\ tube\ reactor \tag{16}$$

$$T_p|_{r_p=R_p} = T_{mesh}(t) \quad wire\ mesh\ reactor \tag{17}$$

When the biomass sample is heated up in the wire mesh reactor, it is assumed that the particle surface temperature is equivalent to that of the mesh. The effective thermal conductivity (λ_{eff}) inside the particle is approximated by equation 18 [16, 17]:

$$\lambda_{eff} = \xi \cdot \lambda_g + \lambda_b \cdot \psi \cdot (1-\xi) + \lambda_c \cdot (1-\psi) \cdot (1-\xi) + \lambda_r \cdot (1-\xi) \tag{18}$$

$$\lambda_r = \frac{4 \cdot \xi}{(1-\xi)} \cdot \epsilon \cdot \sigma \cdot d_{pore} \cdot T_p^3 \tag{19}$$

$$\rho_{c,0} = \frac{\rho_{b,0} \cdot Y_c}{f_{sh,min}} \tag{20}$$

$$\psi = \frac{\rho_b + \rho_M}{\rho_b + \rho_M + \rho_{c,0}} \tag{21}$$

where λ_r is the thermal conductivity induced by radiation through pores, correlated from previous investigations [16, 17], λ_g, λ_b and λ_c are the thermal conductivities of gas, unconverted biomass and char, repsectively, ξ is the void fraction occupied by the gas phase and ψ is the biomass fraction of the solid phase which varies 0 to 1. **ρ_b and $\rho_{b,0}$ are the original (reacting) biomass particle density and initial (unreacted) biomass particle density. The thermal conductivity of metaplast is assumed to be equal to the thermal conductivity of original biomass. The convection coefficient of the gas in the drop tube reactor is described in equation 22 [54]:**

$$h = \frac{Nu \cdot \lambda_g}{d_p} \tag{22}$$

The particle Reynolds, Prandtl and Nusselt numbers are defined in equa-

tions 23-25 [54]:

$$Re = \frac{d_p \cdot (v_p - v_g) \cdot \rho_g}{\mu_g} \tag{23}$$

$$Pr = \frac{c_{p,g} \cdot \mu_g}{\lambda_g} \tag{24}$$

$$Nu = 0.3 + \frac{0.62 \cdot Re^{1/2} \cdot Pr^{1/3}}{(1 + (\frac{0.4}{Pr})^{2/3})^{1/4}} \cdot \left(1 + \left(\frac{Re}{282000}\right)^{5/8}\right)^{4/5} \quad RePr > 0.2 \tag{25}$$

The terminal velocity of the biomass particle is calculated from correlations for Stokes regime, steady separated and unsteady separated flows in equations 26-28 [55]:

$$v_p = \frac{d_p^2 \cdot g \cdot (\rho_s - \rho_g)}{18 \cdot \mu_g} \qquad Re < 2 \tag{26}$$

$$v_p = 0.153 \left[\frac{(\rho_s - \rho_g) \cdot d_p^{1.6} \cdot g}{\mu_g^{0.6} \cdot \rho_g^{0.4}}\right]^{0.714} \qquad 2 < Re < 400 \tag{27}$$

$$v_p = 1.74 \cdot \sqrt{\frac{d_p \cdot (\rho_s - \rho_g) \cdot g}{\rho_g}} \qquad 400 < Re < 200000 \tag{28}$$

Stokes Law was used for small fuel particles, steady separated flow was used for intermediate fuel particles, and turbulent flow was used for large fuel particles.

2.3. Method of lines

Most of the pyrolysis models [15, 17, 56–59] involve solution schemes based on the method of lines (finite difference method) to solve the heat transfer equations. The heat transfer equation is discretized using a central difference scheme:

$$\begin{aligned} c_{p,s,i} \cdot \frac{dT_i}{dt} = &\left(\frac{\lambda_{eff,i}}{\rho_{s,i} \cdot f_{sh}} \cdot \left(\frac{T_{i-1} - 2 \cdot T_i + T_{i+1}}{\Delta r_p^2} + \frac{n}{r_{p,i}} \cdot \frac{T_{i+1} - T_{i-1}}{2 \cdot \Delta r_p}\right)\right) \\ &+ \sum_{j=1}^{3} r_{pyr,i,j} \cdot (-\Delta H_{reac,i,j}) + r_{H_2O,i} \cdot (-\Delta H_{vap,i}) \end{aligned} \tag{29}$$

In the present model, the ode15s method in MatLab was chosen as an ODE solver. The ode15s function based on the Backward Differentiation Formula (BDF) is recommended for the solution of stiff problems [60]. **Calculations were performed to verify the convergence of the adopted numerical procedure with grids having 51, 101 and 201 mesh points. Since the results showed that sufficient accuracy is attained using a grid with 101 mesh points for different biomass particle sizes, the number of mesh points was set to 101 with an error tolerance of 10^{-10} in time integration.**

2.4. Fuel characterization

Pinewood, beechwood, Danish wheat straw, leached Danish wheat straw, alfalfa straw and rice husk were used in this work to represent softwood, hardwood and agricultural residues. The low-ash containing wood (pinewood, beechwood) and grass samples (wheat straw, alfalfa straw), which are rich in potassium, were selected to investigate the effect of differences in potassium composition on the char yields. The fuels were milled on a Retsch rotor mill ZM200 and sieved to particle size fractions of 0.02-0.4 mm and 0.85-1 mm.

Table 1: Proximate and ultimate analysis of fuels (on % dry basis) and ash analysis (on mg/kg dry basis).

Fuel	Pine-wood	Beech-wood	Wheat straw	Leached wheat straw	Alfalfa straw
Proximate and ultimate analysis (% db)					
Moisture[a]	5.1	4.5	5.5	4.3	5.2
Ash (550 °C)	0.3	1.4	4.1	2	7.4
Volatiles	86.6	79.4	77.5	84.2	75.9
HHV[b]	21.6	20.2	18.8	18.7	19.7
LHV[b]	20.2	19	17.5	17.4	16.9
C	50.5	46.7	42.4	45.7	42.5
H	6.8	6.3	6.3	6.6	6.1
N	0.1	0.3	1	0.3	3.3
S	<0.01	0.02	0.1	0.02	0.03
Cl	0.01	0.02	0.1	0.01	0.5
Ash compositional analysis (mg/kg db)					
Al	10	10	150	100	600
Ca	600	2000	2500	1300	12900
Fe	20	10	200	350	-
K	200	3600	11000	1300	28000
Mg	100	600	750	350	1400
Na	30	100	150	50	1000
P	6	150	550	80	1900
Si	50	200	8500	6200	2000
Ti	2	<8	10	10	30

[a] wt. % (ar) [b] in MJ/kg

2.5. Biomass particle properties

Biomass samples were analyzed with a 2D dynamic imaging instrument by using different size measures (width and length). The diameters $x_{Ma,min}$ and $x_{Fe,max}$ were chosen to represent the biomass particle's width and length. Diameter $x_{Fe,max}$ is the largest diameter to fulfill the assumption that the

length of a particle is larger than its width. Diameter $x_{Ma,min}$ is an area bisector representing the shortest distance to the particle's opposite edges. **A biomass particle was represented as a plate, a cylinder and a sphere in planar (n=0), cylindrical (n=1), and spherical (n=2) coordinates under the assumption of similar volume to surface ratios using a different characteristic length:**

$$d_p = x_{Ma,min} \quad (cylinder) \tag{30}$$

$$d_p = \frac{1}{2} \cdot x_{Ma,min} \quad (plate) \tag{31}$$

$$d_p = \frac{3}{2} \cdot x_{Ma,min} \quad (sphere) \tag{32}$$

Biomass particles were described as infinite cylinders, corresponding to n=1 in equation 11 with a particle size equal to $R_p/2$, where R_p is represented by $x_{Ma,min}$. The thermo-physical parameters used in the devolatilization model are listed in Table 2.

Table 2: Thermophysical properties used in the devolatilization model and geometrical parameters of the drop tube reactor.

Symbol	Unit	Description	Expression	
ϵ		Emissivity	0.85	[61]
σ	$J{\cdot}(s{\cdot}m^2{\cdot}K^4)^{-1}$	Stefan-Boltzmann	$5.67{\cdot}10^{-8}$	[61]
ξ		Void fraction	1- $\frac{(\rho_b+\rho_M+\rho_{c,0})}{1500}$	[58]
$\rho_{b,0}$	$kg{\cdot}m^{-3}$	Raw biomass density	650 (wood) and 700 (straw)	[62, 63]
ρ_g	$kg{\cdot}m^{-3}$	Gas density (N_2)	$362.65{\cdot}T_g^{-1}$	[64]
d_{pore}	m	Pore diameter	$3.2{\cdot}10^{-6}$	[61]
$d_{pore,c}$	m	Char pore diameter	$2{\cdot}10^{-4}$	[65]
$c_{p,b}$	$J{\cdot}(kg{\cdot}K)^{-1}$	Raw biomass specific heat capacity	$1500+T_p$	[16]
$c_{p,c}$	$J{\cdot}(kg{\cdot}K)^{-1}$	Char specific heat capacity	$420+2.09{\cdot}T_p+6.85{\cdot}T_p^2$	[16]
$c_{p,g}$	$J{\cdot}(kg{\cdot}K)^{-1}$	Gas specific heat capacity	$770+0.629{\cdot}T_g+1.91{\cdot}10^{-4}{\cdot}T_g^2$	[17]
λ_g	$W{\cdot}(m{\cdot}K)^{-1}$	Gas thermal conductivity	0.026	[66]
λ_b	$W{\cdot}(m{\cdot}K)^{-1}$	Raw biomass thermal conductivity	0.35	[16]
λ_c	$W{\cdot}(m{\cdot}K)^{-1}$	Char thermal conductivity	0.1	[16]
μ_g	Pa·s	Gas phase dynamic viscosity	$4.847{\cdot}10^{-7}{\cdot}T_g^{0.64487}$	[58]
$\Delta H_{reac,1}$	$J{\cdot}kg^{-1}$	Heat of reaction from biomass to metaplast	0	[43, 44]
$-\Delta H_{reac,2}$	$J{\cdot}kg^{-1}$	Heat of reaction from metaplast to char	-255000	[45]
$\Delta H_{reac,3}$	$J{\cdot}kg^{-1}$	Heat of reaction from metaplast to gas	20000	[45]
ΔH_{vap}	$J\ kg^{-1}$	Heat of vaporization	2440000	[53]
A_{H_2O}	$s^{-1}K^{-0.5}$	Pre-exponential factor	$5.1{\cdot}10^{10}$	[58]
E_{H_2O}	$J\ mol^{-1}$	Activation energy	88000	[58]
L	m	Drop tube reactor's length	2.3	
D_r	m	Drop tube reactor's diameter	0.054	

2.6. Experimental

2.6.1. Small and intermediate size particles (0.2 and 1 mm)

The model was validated against data from three high-temperature reactors. The char yields of 0.2 and 1 mm pinewood particles were determined

in separate pyrolysis experiments performed at an intermediate heating rate (10-10^3 K s^{-1}) in the wire mesh reactor and at a high heating rate of (10^4 K s^{-1}) in the drop tube reactor.

The wire mesh reactor at TU Munich was previously described by Trubetskaya et al. [33]. Tests on the wire mesh reactor were conducted at 350-1400°C, with 1 s holding time on the mesh at atmospheric pressure. The DTF setup was described in detail by Trubetskaya et al. [34]. The experiments were conducted by feeding ≈ 5 g of biomass at a rate for 0.2 g min^{-1}. The residence time for 0.2 mm and 1 mm pinewood particles was estimated to be about 1 s, taking into account density changes during pyrolysis [29]. Biomass was rapidly heated and reacted as it fell through the reactor at temperatures of 1000-1400°C. Reaction products were separated into coarse particles (mainly char and fly ashes), fine particles (mainly soot and ash aerosols), and permanent gases.

The heating rate in the wire mesh reactor was set to 1000 K s^{-1}. In the drop tube reactor, the heating rate was calculated by the model using dimensions and operating parameters of the reactor shown in Table 2. Char yields of wood and herbaceous biomass in the wire mesh reactor and drop tube reactor are shown on dry ash free basis (daf) excluding ash content of original biomass and char.

2.6.2. Large size particles (3-5 mm)

The devolatilization time and char yield of 3, 4 and 5 mm pinewood particles in a temperature range of 1350-1450°C were determined by Jepsen in a single particle reactor (SPR) located at the DTU Chemical Engineering

Department [41]. The SPR was designed for oxidation and pyrolysis studies on fuel particles $> 2\,\text{mm}$ at temperatures up to 1500°C at high heating rates. **The setup consists of the reactor, a flat flame burner with 94 injection nozzles, a gas supply system and gas analyzers as shown in Figure 5.**

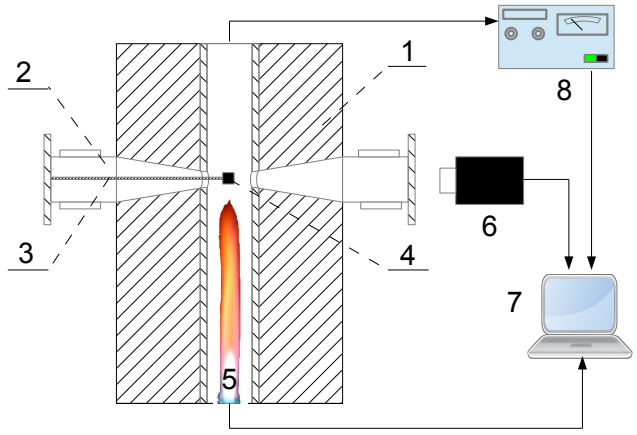

Figure 5: Schematic view of a single particle reactor at DTU: 1. Reactor corpus; 2. insertion ports with a water-cooled chamber; 3. particle holder; 4. sample particle; 5. 94 injection nozzles; 6. High-speed camera; 7. Computer; 8. Gas analyzers.

The formation of a soot cloud in the single particle reactor is associated with pyrolysis initiation. Soot formation occurs under reducing conditions. The oxygen level was kept very low ($< 0.2\,\text{vol.}\%$) during the experiments to eliminate char and soot oxidation. Devolatilization time is defined as the time from the soot cloud is seen until it extinguishes and char conversion begins due to gasification with steam and the remaining oxygen. The char yield is defined as the solid fraction of the reacted biomass, remaining on the platinum wire after an experiment.

3. Results

3.1. Kinetic parameters

The results of fitting of the rate constants, including the influence of potassium are shown in Table 3.

Table 3: The best fit values of the kinetic parameters. In the model, the constants $K_1 = 0.068$ and $K_2 = 4500$ (mg kg^{-1}) were fitted.

Metaplast		Volatiles		Char	
$E_{a,1}$	A_1	$E_{a,2}$	A_2	$E_{a,3}$	A_3
J mol^{-1}	s^{-1}	J mol^{-1}	s^{-1}	J mol^{-1}	s^{-1}
228000	$3.2{\cdot}10^{14}$	174100	$3.6{\cdot}10^{12}$	$132500{\cdot}\Omega_K$	$5.6{\cdot}10^{8}$

Figure 6 illustrates that the char yield increases with increasing potassium content in the lignocellulosic material and decreases with the higher heating rate. The activation energy of the char forming reaction decreases with increasing potassium content, and thus, the influence of potassium becomes smaller at higher heating rates. In Figure 6(b), the model estimates that char yield increases from 2.6 % to 32.5 % when the heating rates decrease from 10^4 to 2 K s^{-1}.

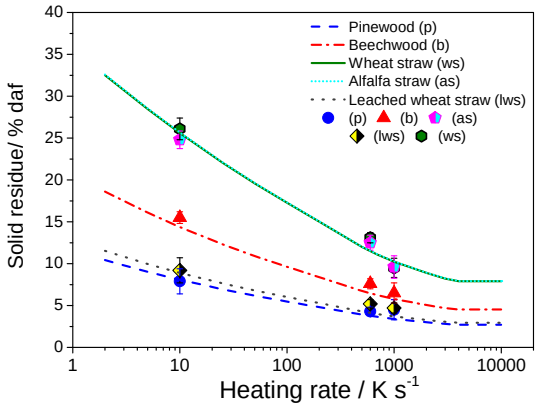

6(a): Heating rate effect on the char yield

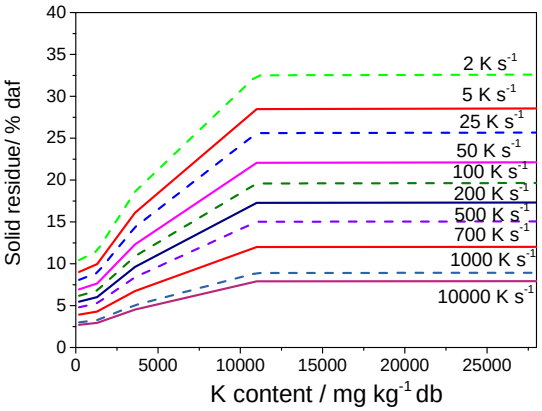

6(b): Char yields versus potassium content in the fuel

Figure 6: (a) Comparison of simulated and experimental data for the influence of heating rate on the char yield of pinewood, beechwood, wheat straw, leached wheat straw and alfalfa straw in the wire mesh reactor, and (b) Simulated char yields versus potassium content in the original fuel (heat treatment temperature: 1400°C, holding time: 1 s, particle size: 0.2 mm).

312 Estimated biomass particle mass as a function of mean particle temper-
313 ature is shown in Figure 7.

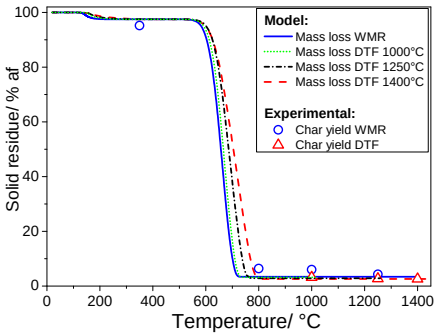

7(a): Pinewood 0.2 mm

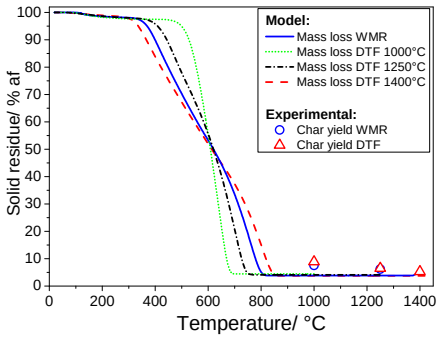

7(b): Pinewood 1 mm

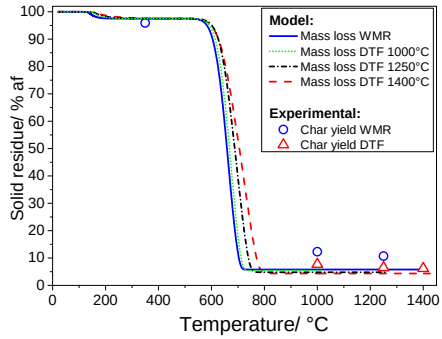

7(c): Beechwood 0.2 mm

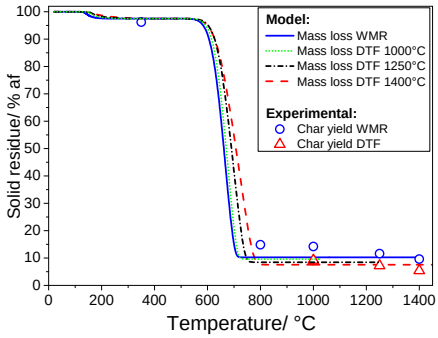

7(d): Alfalfa straw 0.2 mm

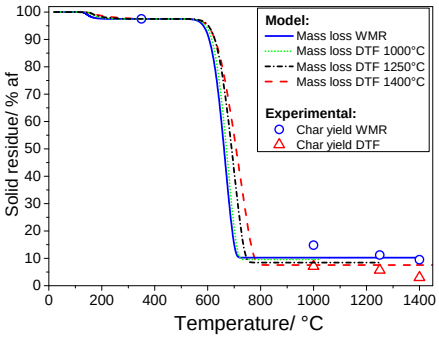

7(e): Wheat straw 0.2 mm

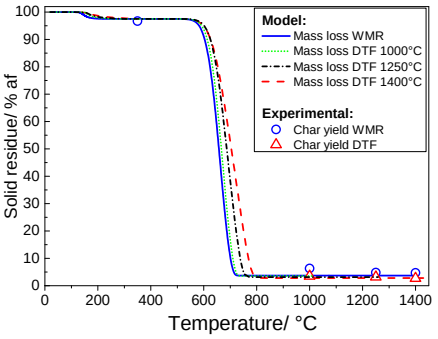

7(f): Leached wheat straw 0.2 mm

Figure 7: Simulated mass loss over the **mean particle temperature** (% af) of pinewood, beechwood, wheat straw, alfalfa straw, leached wheat straw at 1000, 1250 and 1400°C in the DTF and at 1400°C in the WMR, and comparison with the char yields determined experimentally in the wire mesh reactor at (heat treatment temperature: 350, 800, 1000, 1250 and 1400°C; heating rate: 1000 K s^{-1}; holding time: 1 s) and drop tube reactor at 1000, 1250 and 1400°C as determined by Trubetskaya et al. [33, 34].

The mass loss of smaller particles is shown only at 1400°C in the wire-mesh reactor, since pyrolysis is complete at temperatures below 800°C. The simulation results show that char yields from pyrolysis of wood and leached wheat straw in the drop tube reactor were similar over a temperature range of 1000-1400°C, whereas the char yield of wheat and alfalfa straw decreased slightly from 10.3 % to 7.6 % by weight. The present results show that the model accurately estimates the char yield for smaller (0.2 mm) biomass particles. The char yield from pyrolysis of 1 mm pinewood particles is also estimated well and is **about 3 %** lower relative to the experimentally determined char yields in the drop tube reactor. The experimental data obtained in the wire mesh reactor agree with the mass loss estimated by the model. **The lower WMR heating rate caused the reaction to take place at lower temperatures for an extended period compared to fast pyrolysis conditions in the drop tube reactor.**

Figure 8 illustrates the mass fraction of metaplast formed at the surface, middle and center of the particle as a function of time. The simulation results show that both heating rate and particle size influence metaplast formation. In general, high heating rates promote the formation of metaplast. Due to negligible temperature gradients, high heating rates cause small particles first to become fluid and form a molten sphere, then solidify into char [6, 7, 33]. For large particles, significant formation of metaplast at high heating rates is only observed at the surface.

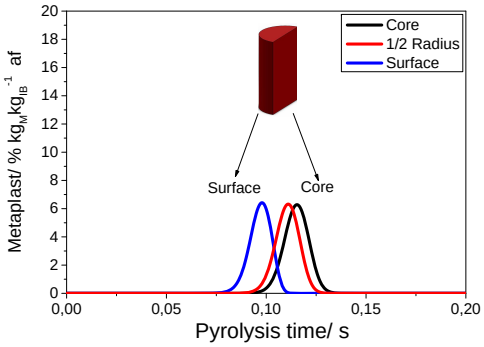

8(a): 0.2 mm, heated by 10^4 K s^{-1} gas flow

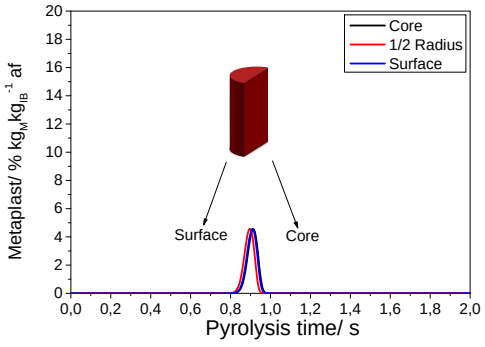

8(b): 0.2 mm, heated by 10^3 K s^{-1} gas flow

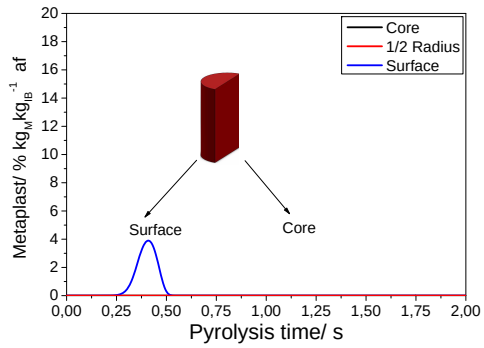

8(c): 3 mm, heated by 10^4 K s^{-1} gas flow

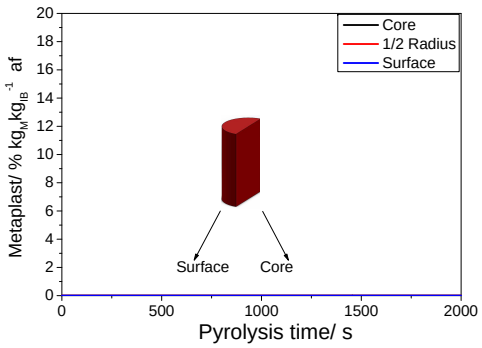

8(d): 3 mm, heated by 10 K min^{-1} gas flow

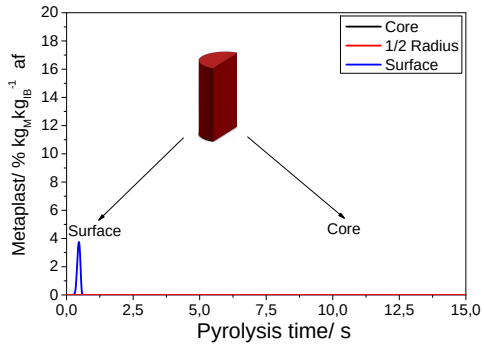

8(e): 10 mm, heated by 10^4 K s^{-1} gas flow

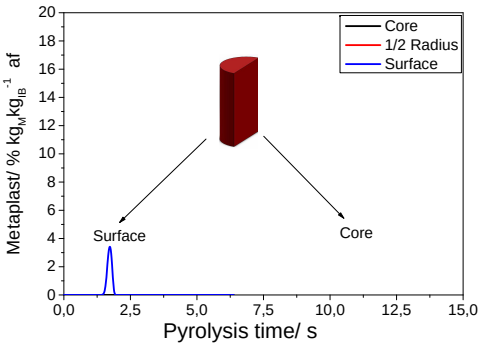

8(f): 10 mm, heated by 10^3 K s^{-1} gas flow

Figure 8: Simulated metaplast formation (% af) from pyrolysis of 0.2, 3 and 10 mm pinewood particles at slow heating rate in the thermogravimetric instrument (10 K min^{-1}), at intermediate heating rate (10^3 K s^{-1}) in the wire mesh reactor and at high heating rates in the drop tube reactor. The metaplast formation (kg_M kg_{IB}^{-1}) is showed over the pyrolysis time.

This means that the particle surface melts during pyrolysis, whereas the interior retains the original biomass structure [33]. The rate of metaplast formation was slower than formation of volatiles and char at lower temperatures. Thus, metaplast was formed faster than it was consumed at higher temperatures. At low heating rates, the particle was nearly isothermal, indicating only small differences in metaplast formation as function of position within the particle. Thus, the relatively low heating rate for the particle core increased the time for the three reactions, leading to lower metaplast yields.

*3.2. **Influence of assumed particle geometry***

Figure 9 illustrates the mass loss of 0.2, 1 and 5 mm pinewood particles. Devolatilization time decreased with the higher heating rate in the drop tube reactor compared to the wire mesh reactor. The representation of the 0.2 mm particles using different characteristics lengths does not give large deviations with respect to char yield and devolatilization time among the three particle geometries as shown in Figure 9(a).

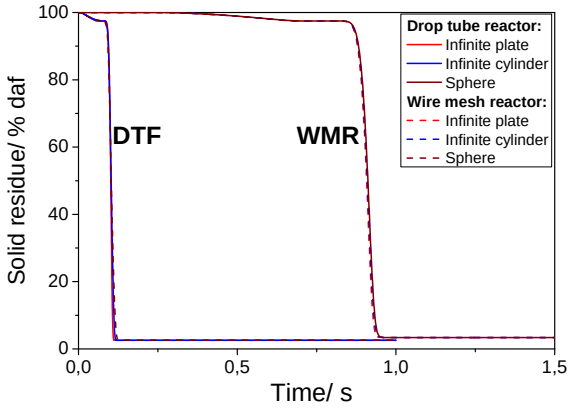

9(a): Pinewood 0.2 mm

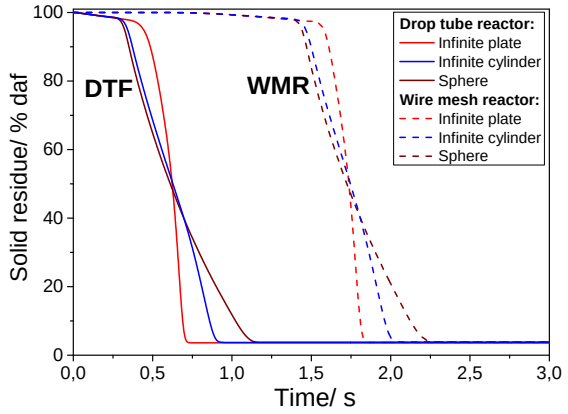

9(b): Pinewood 1 mm

Figure 9: **Mass loss histories of pinewood particles (0.2 and 1 mm) with the similar volume to surface ratio and different characteristic lengths which were calculated in plate-like (n=0), cylindrical (n=1) and spherical (n=2) geometries at the final temperature of 1400°C during pyrolysis in the wire mesh and drop tube reactors.**

352 The influence of particle shape becomes more important with the in-

creasing particle size due to the larger internal temperature gradients as shown in Figure 9(b). The relative influence of heating rate on devolatilization time of 1 mm pinewood was less compared that for smaller particles. This is because of the predominance of internal heat transfer control within the large particles.

3.3. Influence of volumetric shrinkage on devolatilization time

In the model, the shrinkage front moves from the surface towards the center. At high heating rates, the outer layers initially shrink while the inner layers remain unaffected. Later, the fuel particle shrinks due to devolatilization. During slow pyrolysis, internal thermal gradients are small, and therefore, drying followed by devolatilization takes place over throughtout the particle. Particle shrinkage takes place after the original biomass is converted into metaplast. The rate of volatiles formation determines the rate at which the particle shrinks.

Figure 10(a) shows that the particle size of 5 mm particle was reduced by 27 % during pyrolysis at high heating rates. A 26 % reduction in a particle size was measured during devolatilization of 3 mm pinewood particle in a temperature range of 1180-1440°C in the single particle reactor [41].

Figure 10(c) shows that shrinkage has a negligible influence on the devolatilization time of smaller particles, which are practically isothermal. For the large particles, the inclusion of shrinkage increases the devolatilization rate and thereby decreases the devolatilization time. Internal temperature gradients in larger particles becomes smaller as the particle shrinks which enhances the devolatilization rate. The shrinkage of 5 mm pine particle leads to the decrease of devolatilization time by 19 % during pyrolysis in the WMR

and DTF.

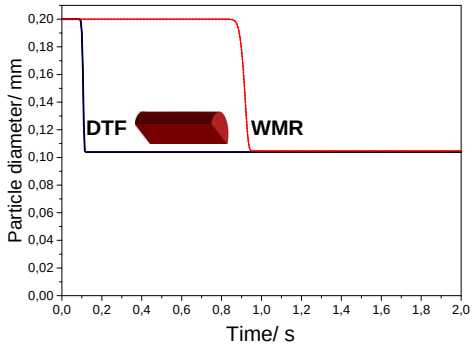

10(a): Pinewood 0.2 mm

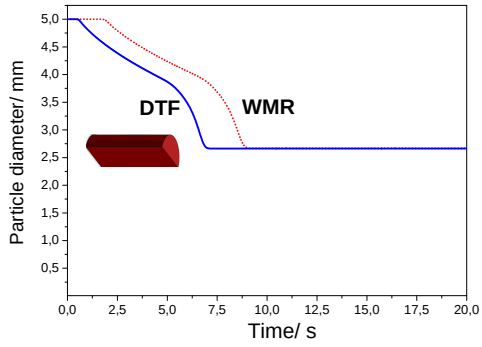

10(b): Pinewood 5 mm

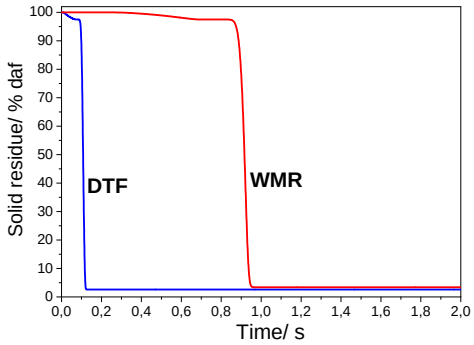

10(c): Pinewood 0.2 mm

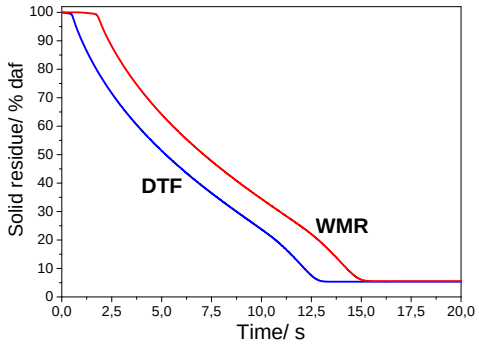

10(d): Pinewood 5 mm

Figure 10: (a)-(b) Simulated pinewood particle shrinking (0.2 and 5 mm) and (c)-(d) Simulated mass loss of shrinking pinewood particles in the wire mesh and drop tube reactors.

*3.4. **Influence of particle size on devolatilization time***

Figure 11 compares the times required for complete devolatilization of 3, 4 and 5 mm pinewood particles in the single particle reactor to those estimated by the model for particles from 0.01 to 10 mm. **In the model, the complete devolatilization time is defined as the time when 95 %**

of the volatile matter in the original pinewood particle has been released [67].

Figure 11 shows that under fast heating particles with mean diameters < 0.25 mm may be considered as thermally thin based on the modeling results with 0.1 s deviation, while the intra-particle heat conduction in larger particles plays a key role in biomass devolatilization. The diameter of 3, 4 and 5 mm pinewood cubes was recalculated for corresponding cylinders under the assumption of a similar volume to surface ratio (3, 4 and 5 mm). A comparison of experimental and estimated devolatilization times showed that the model estimates the devolatilization time of pinewood particles well. In addition, the results showed that the 1 mm pinewood particles require more than 1 s in the WMR and DTF for complete conversion. The estimated devolatilization time by the model showed a similar trend for the experiments in the drop tube reactor.

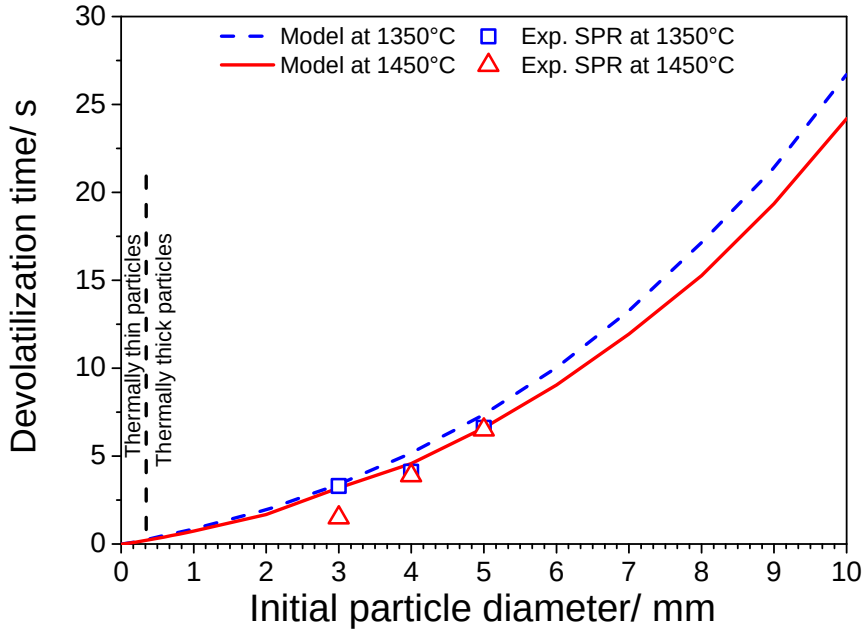

Figure 11: **Simulated devolatilization time of shrinking pinewood particles (from 0.01 mm to 10 mm) at 1000, 1250 and 1400°C, and compared with the experimental results obtained in the SPR for 3, 4 and 5 mm particles at 1350 and 1450°C. Experimental data was taken from the investigations of Jepsen [41]. The black dashed line separates the thermally thin regime ($Bi < 0.1$) from the thermally thick ($Bi > 0.1$).**

4. Discussion

The present pyrolysis model describes the char yield at high temperatures (up to 1500°C) and high heating rates $> 200\,\mathrm{K\ s^{-1}}$. In the model, an intermediate liquid (so called metaplast) is formed from the decomposition of biomass which reacts further to char and gas. It was assumed that the kinetics for metaplast formation does not depend on the biomass type and that

reaction of metaplast to char and gas is influenced by the biomass potassium content.

The impact of heating rate on the maximum metaplast formation and subsequent reaction to char and gas shown in Figure 12.

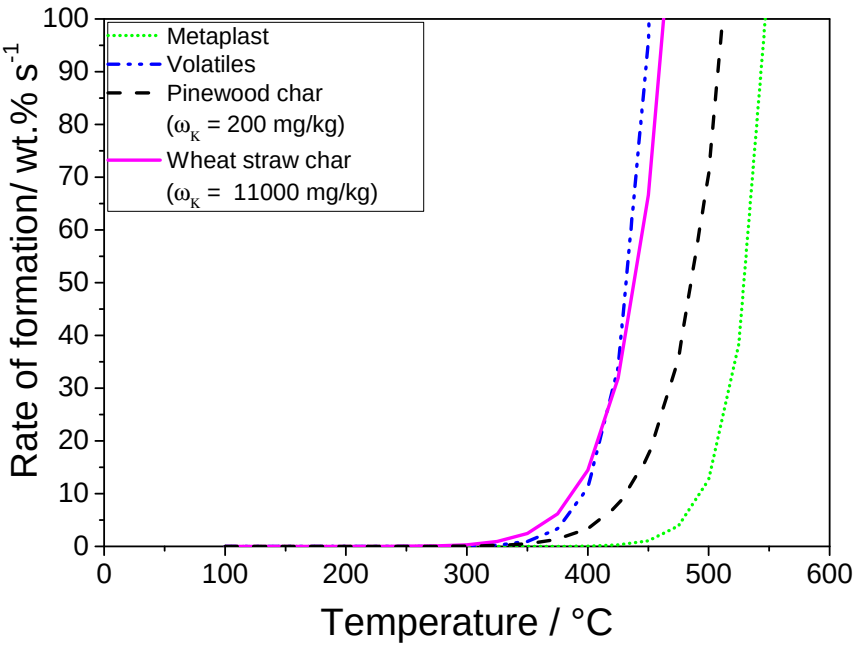

Figure 12: Simulated reaction rates (wt.% s^{-1}) of metaplast, char and volatile formation during fast pyrolysis of 0.2 mm pinewood ($\omega_K = 200\,\mathrm{mg\,kg^{-1}}$, dry basis) and wheat straw ($\omega_K = 11000\,\mathrm{mg\ kg^{-1}}$, dry basis) particles in the wire mesh reactor ($1000\,\mathrm{K\ s^{-1}}$).

Figure 12 demostrates that the rate of metaplast formation is slower than formation of volatiles and char at temperatures below 350°C. Thus, lower concentrations of metaplast are formed at lower heating rates. The particle temperature was nearly uniform over

the particle diameter, and therefore, only small differences in metaplast formation were observed. At higher temperatures, the rate of char formation was lower than the rate of metaplast formation, in agreement with experimental results from Koufopanos [15, 45]. Higher temperatures result in greater metaplast accumulation because its formation rate is faster than its rate of consumption. At high heating rates, such as in the wire mesh and drop tube reactors, lower mass fractions of metaplast were formed in the particle core compared to the particle surface. This could be due to the lower heating rates at the core compared to at the surface. At high heating rates, formation of metaplast is initially fast relative to reaction from metaplast to char and gas, so a high concentration of metaplast is obtained. With a high fraction of metaplast, the particle may become molten (locally or throughtout the whole particle), thereby leading to structural changes of the particle [33].

Particle size demonstrates a greater influence on metaplast, volatile and char formation in the drop tube reactor ($10^{-4}\,\mathrm{K\ s^{-1}}$) than in the wire mesh reactor ($10\,\mathrm{K\ s^{-1}}$). The larger internal temperature gradients led to slower pyrolysis of 3 and 10 mm pinewood particles compared to 0.2 mm particles. For large particles the formation of metaplast mainly takes place at the particle surface at high heating rates, whereas the lower heating rates result in high metaplast concentrations in the interior. At low heating rates, both small and large particles were nearly isothermal, leading to smaller local differences in metaplast formation. Differences in local mass

fractions of metaplast became larger with increasing particle size and increasing heating rates because of the predominance of internal heat transfer control within the large particles.

Char yield has been experimentally shown to increase with potassium content in the original biomass [33, 34]. This effect was accounted for in the model by modifying the activation energy for the char formation reaction as a function of the potassium content. The influence of potassium on char formation became stronger with decreasing heating rate, which corresponds to the experimental observations from the wire mesh and drop tube reactors. Calculations suggested that pyrolysis was completed at temperatures below 800°C, and thus, the char yields for woody and herbaceous biomass remain unchanged. The experimental data showed that the biomass char yields decreased with the increasing temperature due to the dehydrogeneration and cross-linking reactions [68], which are not considered in the present simulation. The simulated char yield from wheat straw pyrolysis was slightly lower than the char yield from the wire mesh and drop tube reactor experiments. The ash compositional analysis of char from the pyrolysis in the drop tube reactor showed that close to 70 % potassium in the wheat straw has been released in a temperature range of 1000-1500°C [69]. The remaining potassium in herbaceous biomass samples is still present in a larger amount than in woody chars. The large differences in herbaceous char yields between the model and experimental data might be attributed to the interactions between

potassium, other remaining alkali metals and carbonaceous char matrix which were not considered during the model development.

Moreover, the char yield of larger particles is underestimated by the model. It was hypothesized that tar inside larger particles may undergo secondary reactions, leading to higher char yields [36]. At high heat treatment temperatures of 750-1100°C, secondary reactions occurring in larger particles strongly decrease tar release and increase char formation during pyrolysis. Tar decomposition occurs by secondary reactions (i.e. cracking and polymerization), and tar release to ambient by mass transfer [35]. The evolutionary profiles of the temperatures at the pinewood particle surface and the particle center as a function of time are shown in the supplemental material. Due to the fast heat transfer in 0.2 mm particles, the differences between surface and core temperatures are small and thus, tar release remains unchanged at 1100°C. The differences between surface and core temperatures become more pronouced with the increasing particle size. Tar formation from pyrolysis of larger pinewood particles was stronger, whereas the soot yield was half lower compared to smaller particles [70]. The lower soot yields were related to the less formed PAH precursors. Tar inside larger particles underwent secondary reactions due to the lower heat flux, leading to a slower pyrolysis and thereby higher char yields and less soot, corresponding to investigations of Miller and Bellan [36]. This effect was not included in the model and could be the reason why the model slightly underpredicts the char yield for large particles.

5. Conclusion

The novelty of this work relies on the description of both low and high temperature kinetics for wood and herbaceous biomass using one set of kinetic parameters. The actual particle heating rate of biomass particles was quantitatively defined in wire mesh and drop tube reactors. The results presented in this work emphasize a stronger catalytic effect of potassium on char yield at low and intermediate heating rates compared to high heating rates. The potassium content and heating rate affected the char yield more than other operational parameters.

An innovative approach was used to implement the influence of potassium on the char yield in the model by reduction in the activation energy of char formation with increasing potassium content, and fitted to the experimental results. The simulation results showed that particle size has a more significant influence on metaplast formation and reaction to char and gas at high heating rates ($10^4\,\mathrm{K\ s^{-1}}$) compared to pyrolysis at low heating rates ($10\,\mathrm{K\ s^{-1}}$).

In addition, the model showed that the impact of shrinkage on devolatilization time increases with increasing particle size, but it has negligible influence on char yields. Results from the 1D model are in agreement with experimental data, and emphasize a key role of intra-particle heat conduction in biomass particle $> 0.25\,\mathrm{mm}$.

Acknowledgements

The authors would like to acknowledge the financial support that they received for this project from Kempestiftelserna. We also acknowledge Professor Anker Degn Jensen (DTU CHEC) for fruitful discussions. Assistant Professor Catherine Brewer is acknowledged for the article proof reading.

References

[1] Sander B, Properties of Danish Biofuels and the Requirements for Power Production, Biomass Bioenergy 12 (3) (1997) 177–83.

[2] Danish Energy Agency: Energy strategy 2050 - from coal, oil and gas to green energy, The Danish Ministry of Climate and Energy (2011) 1–66.

[3] Rosendahl LA, Yin C, Kœr SK, Friborg K, Overgaard P, Physical characterization of biomass fuels prepared for suspension firing in utility boilers for CFD modelling, Biomass Bioenergy 31 (2007) 318–25.

[4] Larsen L, Peteresen MO, Thirup L, Li HW, Iversen FK, The IBUS process - Lignocellulosic bioethanol close to a commercial reality, Chem Eng Technol 31 (2008) 765–77.

[5] Wornat MJ, Hurt RH, Yang NYC, Headley TJ, Structural and compositional transformations of biomass chars during combustion, Combust Flame 100 (1-2) (1995) 131–45.

[6] Cetin E, Moghtaderi B, Gupta R, Wall TF, Influence of pyrolysis conditions on the structure and gasification reactivity of biomass chars, Fuel 83 (2004) 2139–50.

[7] Dall'Ora M, Jensen PA, Jensen AD, Suspension combustion of wood: Influence of pyrolysis conditions on char yield, morphology, and reactivity, Energy Fuels 22 (2008) 2955–62.

[8] Tran DQ, Rai C, Pyrolytic Gasification of Bark, AIChE 75 (184) (1979) 41–9.

[9] Roberts AF, A Review of Kinetic Data for the Pyrolysis of Wood and Related Substances, Combust Flame 14 (2) (1970) 261–72.

[10] Thurner F, Mann U, Kinetic Investigation of Wood Pyrolysis, Ind Eng Chem Process Des Dev 20 (3) (1981) 482–8.

[11] Jegers HF, Klein MT, Primary and Secondary Lignin Pyrolysis Reaction Pathways, Ind Eng Chem Process Des Dev 24 (1) (1985) 173–83.

[12] Shafizadeh F, Introduction to Pyrolysis of Biomass, J Anal Appl Pyrolysis 3 (4) (1982) 283–305.

[13] Sheng C, Azevedo JLT, Modeling biomass devolatilization using the chemical percolation devolatilization model for the main components, Proc Combust Inst 29 (1) (2002) 407–14.

[14] Elfasakhany A, Klason T, Bai XS, Modelling of pulverized wood combustion using a functional group model, Combust Theory Modelling 12 (5) (2008) 883–904.

[15] Koufopanos CA, Maschio G, Lucchesi A, Kinetic Modelling of the Pyrolysis of Biomass and Biomass Components, Can J Chem Ing 67 (1) (1989) 75–84.

[16] Grønli MG, A Theoretical and Experimental Study of the Thermal Degradation of Biomass. PhD thesis, Norwegian University of Science and Technology (1996).

[17] Bellais M, Modelling of the pyrolysis of large wood particles. PhD thesis, KTH Royal Institute of Technology (2007).

[18] Di Blasi C, Modeling chemical and physical processes of wood and biomass pyrolysis, Prog Energy Combust Sci 34 (1) (2008) 47–90.

[19] Di Blasi C, Comparison of semi-global mechanisms for primary pyrolysis of lignocellulosic fuels, J Anal Appl Pyrolysis 47 (1) (1998) 43–64.

[20] Di Blasi C, Modeling and Simulation of Combustion Processes of Charring and Non-Charring Solid Fuels, Prog Energy Combust Sci 19 (1) (1993) 71–104.

[21] Chan WR, Kelbon M, Krieger BB, Modelling and experimental verification of physical and chemical processes during pyrolysis of a large biomass particle, Fuel 64 (11) (1985) 1505–13.

[22] Liden AG, Berruti F, Scott DS, A kinetic model for the production of liquids from the flash pyrolysis of biomass, Chem Eng Comm 65 (1) (1988) 207–21.

[23] Bradbury AGW, Sakai Y, Shafizadeh F, A kinetic model for pyrolysis of cellulose, J Appl Pol Sci 23 (11) (1979) 3271–80.

[24] Shafizadeh F, Bradbury AGW, Thermal Degradation of Cellulose in Air and Nitrogen at Low Temperatures, J Appl Pol Sci 23 (5) (1979) 1431–42.

[25] Ranzi E, Cuoci A, Faravelli T, Frassoldati A, Migliavacca G, Pierucci S et al., Chemical kinetics of biomass pyrolysis, Energy & Fuels 22 (6) (2008) 4292–300.

[26] Debiagi PE, Pecchi C, Gentile G, Frassoldati A, Cuici A, Ranzi E et al., Extractives extend the applicability of multistep kinetic scheme of biomass pyrolysis, Energy & Fuels 29 (10) (2015) 6544–55.

[27] Nik-Azar M, Hajaligol MR, Sohrabi M, Dabir B, Mineral matter effects in rapid pyrolysis of beechwood, Fuel Process Technol 51 (1-2) (1997) 7–17.

[28] Jensen AD, Dam-Johansen K, Wojtowicz MA, Serio MA, TG-FTIR Study of the Influence of Potassium Chloride on Wheat Pyrolysis, Energy Fuels 12 (5) (1998) 929–38.

[29] Umeki K, Kirtania K, Chen L, Bhattacharya S, Fuel Particle Conversion of Pulverized Biomass during Pyrolysis in an Entrained Flow Reactor, Ind Eng Chem Res 51 (2012) 13973–9.

[30] Lede J, Authier O, Characterization of biomass fast pyrolysis: Advantages and drawbacks of different possible criteria, Biomass Conv Bioref 1 (2011) 133–47.

595 [31] Narayan R, Antal MJ, Thermal lag, fusion and the compensation effect
596 during biomass pyrolysis, Ind Eng Chem 35 (1996) 1711–21.

597 [32] Umeki K, Biswas AK, Simplification of devolatilization models for
598 thermally-thick particles: Differences between wood logs and pellets,
599 Chem Eng J 274 (2015) 181–91.

600 [33] Trubetskaya A, PA Jensen, Jensen AD, Steibel M, Spliethoff H, Glar-
601 borg P, Influence of fast pyrolysis conditions on yield and structural
602 transformation of biomass char, Fuel Process Technol 140 (2015) 205–
603 14.

604 [34] Trubetskaya A, Jensen PA, Garcia Llamas AD, Umeki K, Jensen AD,
605 Glarborg P, Effect of fast pyrolysis conditions on biomass solid residues
606 at high temperatures, Fuel Process Tech 143 (2016) 118–29.

607 [35] Hajaligol MR, Howard JB, Longwell JP, Peters WA, An Experimental
608 and Modeling Study of Pressure Effects on Tar Release by Rapid Pyrol-
609 ysis of Cellulose Sheets in a Screen Heater, Combust Flame 95 (1993)
610 47–60.

611 [36] Miller RS, Bellan J, Tar Yield and Collection from the Pyrolysis of Large
612 Biomass Particles, Combust Sci Tech 127 (1-6) (1997) 97–118.

613 [37] Boutin O, Ferrer M, Lede J, Flash pyrolysis of cellulose pellets submitted
614 to a concentrated radiation: experiments and modeling, Chem Eng Sci
615 57 (2002) 15–25.

[38] Liu Q, Wang S, Wang K, Guo X, Luo Z, Cen K, Mechanism of Formation and Consequent Evolution of Active Cellulose during Cellulose Pyrolysis, Acta Phys Chim Sin 24 (11) (2008) 1957–63.

[39] Dauenhauer PJ, Colby JL, Balonek CM, Suszynski WJ, Schmidt LD, Reactive boiling of cellulose for integrated catalysis through an intermediate liquid, Green Chem 11 (2009) 1555–61.

[40] Teixeira AR, Mooney KG, Kruger JS, Williams CL, Suszynski WJ, Schmidt LD and etc., Aerosol generation by reactive boiling ejection of molten cellulose, Energy Environ Sci 4 (2011) 4306–21.

[41] Jepsen MS, Pyrolysis of Large Biomass Particles in a Single Particle Combustion Reactor. MSc thesis, DTU Chemical Engineering, Technical University of Denmark (2014).

[42] Anca-Couce A, Zobel N, Numerical analysis of a biomass pyrolysis particle model: Solution method optimized for the coupling to reactor models, Fuel 97 (2012) 80–8.

[43] Arseneau DF, Competitive Reactions in the Thermal Decomposition of Cellulose, Can J Chem 49 (4) (1971) 632–8.

[44] Mok WSL, Antal MJ, Effects of pressure on biomass pyrolysis. I. Cellulose pyrolysis products, Thermochimica Acta 68 (1983) 155–64.

[45] Koufopanos CA, Papayannakos N, Maschio G, Lucchesi A, Modelling of the Pyrolysis of Biomass Particles. Studies on Kinetics, Thermal and Heat Transfer Effects, Can J Chem Ing 69 (4) (1991) 907–15.

[46] Haseli Y, van Oijen JA, de Goey LPH, Modeling biomass particle pyrolysis with temperature-dependent heat of reactions, J Anal Appl Pyrolysis 90 (2) (2011) 140–54.

[47] Haseli Y, van Oijen JA, de Goey LPH, Numerical study of the conversion time of single pyrolyzing biomass particles at high heating conditions, Chem Eng J 169 (2011) 299–312.

[48] Mack CH, Donaldson DJ, Effects of Bases on the Pyrolysis of Cotton Cellulose, Textile Research J 37 (12) (1967) 1063–71.

[49] Rath J, Wolfinger MG, Steiner G, Krammer G, Barontini F, Cozzani V, Heat of wood pyrolysis, Fuel 82 (2003) 81–91.

[50] Gubba SR, Ma L, Pourkashanian M, Williams A, Influence of particle shape and internal thermal gradients of biomass particles on pulverized coal/biomass co-fired flames, Fuel Process Technol 92 (11) (2011) 2185–95.

[51] Qin K, Lin W, Jensen PA, Jensen AD, High-temperature entrained flow gasification of biomass, Fuel 93 (2012) 589–600.

[52] Ragland KW, Boerger JC, Baker AJ, A model of chunkwood combustion, Forest Prod J 38 (1988) 27–32.

[53] Borman GL, Ragland KW, Combustion engineering, McGraw Hill Book Company, 1998.

[54] Tosun I, Modeling in Transport Phenomena. A conceptual approach, Elsevier, 2007.

[55] Clement KH, Fangel P, Jensen AD, Thomsen K, Kemiske enhedsoperationer, Polyteknisk Forlag, 2004.

[56] Alves SS, Figueiredo JL, A model for pyrolysis of wet wood, Chem Eng Sci 44 (12) (1989) 2861–9.

[57] Janse AMC, Westerhout RWJ, Prins W, Modelling of flash pyrolysis of a single wood particle, Chem Eng Proc 39 (3) (2000) 239–52.

[58] Bryden KM, Hagge MJ, Modeling the combined impact of moisture and char shrinkage on the pyrolysis of a biomass particle, Fuel 82 (13) (2003) 1633–44.

[59] Fan LS, Miyanami K, Chen TY, Walawender WP, A mathematical model for pyrolysis of a solid particle: Effects of the Lewis number, Can J Chem Eng 55 (1) (1977) 47–53.

[60] Celaya EA, Aguirrezabala JJA, Chatzipantelidis P, Implementation of an Adaptive BDF2 Formula and Comparison with the MATLAB ode15s, Proc Comp Sci 29 (2014) 1014–26.

[61] Lu H, Robert W, Peirce G, Ripa B, Baxter LL, Comprehensive Study of Biomass Particle Combustion, Energy Fuels 22 (4) (2008) 2826–39.

[62] Jensen PA, Sander B, Dam-Johansen K, Pretreatment of Straw for Power Production, Biomass Bioenergy 20 (6) (2001) 431–46.

[63] Miller RS, Bellan J, Numerical Simulation of Vortex Pyrolysis Reactors for Condensable Tar Production from Biomass, Energy Fuels 12 (1) (1998) 25–40.

[64] Perry R, Perry's chemical engineers' handbook, McGraw Hill Book Company, 2007.

[65] Di Blasi C, Russo G, Modeling of Transport Phenomena and Kinetics of Biomass Pyrolysis, Adv Thermochem Biomass Conv (1994) 906–21.

[66] Di Blasi C, Modelling the Fast Pyrolysis of Cellulosic Particles in Fluid-Bed Reactors, Chem Eng Sci 55 (24) (2000) 5999–6013.

[67] Johansen JM, Jensen PA, Glarborg P, Mancini M, Weber R, Mitchell RE, Extension of apparent devolatilization kinetics from thermally think to thermally thick particles in zero dimensions for wood biomass, Energy 95 (2016) 279–90.

[68] Solomon PR, Hamblen DG, Carangelo RM, Serio MA, Deshpande GV, General Model of Coal Devolatilization, Energy Fuels 2 (1988) 405–22.

[69] Trubetskaya A, Jensen PA, Glarborg P, Steibel M, Spliethoff H, Hofmann Larsen F, Comparison of high temperature chars of wheat straw and rice husk with respect to chemistry, morphology and reactivity, Biomass Bioenergy 86 (2016) 76–87.

[70] Trubetskaya A, Fast pyrolysis of biomass at high temperatures. PhD thesis, Technical University of Denmark (2016).

Modeling the influence of potassium content and heating rate on biomass pyrolysis

Anna Trubetskaya[a,*], Gerrit Surup[b], Alexander Shapiro[c], Richard B. Bates[d]

[a]*Energy Engineering Department, Luleå University of Technology, 97187, Luleå, Sweden*
[b]*Department of Engineering Sciences, University of Agder, Jon Lilletuns vei 9, 4879 Grimstad, Norway*
[c]*Department of Chemical and Biochemical Engineering, Technical University of Denmark, Søltofts Plads Bygning 229, Kgs. Lyngby 2800, Denmark*
[d]*MIT, Department of Mechanical Engineering, 02139, Cambridge, MA, USA*

Abstract

This study presents a combined kinetic and particle model that describes the effect of potassium and heating rate during the fast pyrolysis of woody and herbaceous biomass. The model calculates the mass loss rate, over a wide range of operating conditions relevant to suspension firing. The shrinking particle model considers internal and external heat transfer limitations and incorporates catalytic effects of potassium on the product yields. Modeling parameters were tuned with experimentally determined char yields at high heating rates ($> 200\,\mathrm{K\,s^{-1}}$) using a wire mesh reactor, a single particle burner, and a drop tube reactor. The experimental data demonstrated that heating rate and potassium content have significant effects on the char yield. The importance of shrinkage on the devolatilization time becomes greater with increasing particle size, but showed little influence on the char yields.

Keywords: fast pyrolysis, kinetics, metaplast, potassium, heating rate

*Corresponding author. anna.trubetskaya@ltu.se

Nomenclature

AR	Aspect ratio		tion reaction as a function of biomass potassium content
A_i	Pre-exponential factor (s^{-1})	k_i	Reaction rate constant (s^{-1})
A_p	Particle area (m^2)	L	Reactor's length (m)
c_p	Specific heat capacity (J (kg K)$^{-1}$)	m	Reaction order
d_p	Particle diameter (m)	n	Dimensionality factor
d_{pore}	Particle pore diameter (m)	R	Gas constant (J (K mol)$^{-1}$)
D_r	Reactor diameter (m)	r	Reaction rate (kg (kg s)$^{-1}$)
E_i	Activation energy (J mol^{-1})	R_p	Particle radius at specified interior location (m)
f_{sh}	Shrinkage factor	r_p	Particle radius (m)
g	Gravity (m s^{-2})	T	Temperature (°C)
h	Convective heat transfer coefficient (W ($m^{-2}K^{-1}$))	t	Time (s)
ΔH_{vap}	Heat of vaporization (J kg^{-1})	V_p	Particle volume (m^3)
K_1, K_2	Constants for the activation energy of the char forma-	v_p	Slip velocity between gas and particle (m s^{-1})

X Conversion

$x_{Fe,max}$ Feret maximum diameter (m)

$x_{Ma,min}$ Martin minimum diameter (m)

Dimensionless numbers

Bi Biot number

Nu Nusselt number

Pr Prandlt number

Re Reynolds number

Greek symbols

α Particle thermal diffusivity ($m^2\ s^{-1}$)

κ Heating rate ($K\ s^{-1}$)

λ Thermal conductivity ($W\ (m\ K)^{-1}$)

μ Viscosity (Pa s)

Ω Correction factor for influence of potassium content on activation energy ($E_{a,3}$)

ω K^+ concentration ($mg\ kg^{-1}$)

ψ Biomass fraction of solid phase

ρ Density ($kg\ m^{-3}$)

σ Stefan-Boltzmann constant ($J\ (s\ m^2\ K^4)^{-1}$)

τ Holding time (s)

ε Emissivity

ξ Void fraction occupied by the gas phase

Subscripts

0 initial

b biomass

c char

g gas

H_2O water

K potassium

M metaplast

max maximum

$mesh$ wire mesh

min	minimum	*s*	solid phase
p	particle	*total*	overall
pyr	pyrolysis		
r	radiative	*w*	wall

1. Introduction

Suspension firing of biomass is widely used for power generation. Danish pulverized fuel fired power plants are undergoing a transition to 100 % biomass firing in order to reduce greenhouse gase emissions. Straw, wood pellets and wood chips are the most abundant biofuels in Denmark [1]. The annual consumption of biomass at Danish power stations is 1.2 million tones of straw and 0.2 millions of wood chips per year [2]. The advantage of utilizing wheat straw as a renewable energy source is that it is one of the most readily available Danish agricultural residues, while the wood pellet production depends on the supply of imported wood residues [3, 4]. The drawback, however, is that the quality of agricultural wastes is lower than that of wood due to a higher ash content leading to deposition and corrosion of the boiler units. In pulverized biomass combustion, short residence times are required for biomass devolatilization, which makes it difficult to examine the dynamics of the process. In addition, the lignocellulosic material reactivity is affected by the biomass composition, namely organic matter and minerals [5–7]. The differences in char properties generated under various pyrolysis conditions can lead to a range of challenges in a modeling of biomass conversion.

Fast pyrolysis at high temperatures and high heating rates is the initial

step in suspension biomass firing. Fuel particles first undergo rapid drying, heating and devolatization with the formation of char and volatiles. Despite of numerous previous studies on biomass devolatilization mechanisms and particle models, there is no generally accepted model that can estimate the conversion rate and final char yield over a wide range of operating conditions. Existing kinetic models [8–14] were developed with experimental data using specific biomass samples and a narrow set of low temperature reaction conditions. The application of lower temperatures makes extrapolation to higher temperatures in combustion/gasification processes.

Most of the existing biomass pyrolysis models [10, 15–17] which describe both the devolatilization product composition and yields (light gases, tar and char) are mainly valid for low-ash fuels (hardwood, softwood); whereas considerably less work has been carried out with herbaceous lignocellulosic materials. In addition, these mathematical models are valid for biomass pyrolysis under slow heating rates (1-50 K min^{-1}) and long residence time (1-4 h). Many kinetic models for wood pyrolysis have been reported in the literature [18]. The simplest models are based on a single first order decomposition reaction, and are not able to estimate the influence of heating conditions on the product yields [19].

$$Fuel\ particle \longrightarrow Volatiles \cdot (1-\gamma) + \gamma \cdot Char$$

Figure 1: One-step global model [20].

Other models assume competing parallel reactions to predict the production kinetics of gas, tar and char, which is often valid only over a narrow temperature range [10, 21].

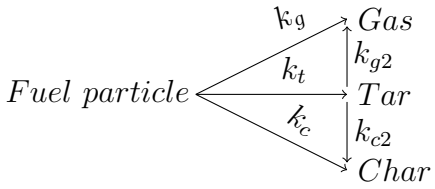

Figure 2: Competing step global model with k_g - rate constant of gas release, k_c - rate constant of char formation, k_t - rate constant of tar formation, k_{g2} - rate constant for the formation of gas from tar and k_{c2} - rate constant for the formation of char from tar [10].

Thurner and Mann [10] assumed that the activation energy for the char formation reaction is similar to the activation energy for mass loss reactions to gas and tar, and therefore, that the final residual weight (e.g. the char yield) is independent of the heating rate and heat treatment temperature. More complex models involve additional steps for tar decomposition in the gas phase [22] or an intermediate product derived from primary decomposition of biomass [15, 23, 24]. These models can be generally applied only for a specific type of biomass. Ranzi et al. [25, 26] included the effect of holocelluloses, lignin and extractives on the product yields and composition. Previous models have not included the catalytic effect of alkali metals on biomass devolatilization, which has been shown to influence yields and product release rates significantly [7, 27–29]. Extrapolation kinetics fitted under low heating rate conditions to the pulverized fuel firing conditions is difficult due to the changes in devolatilization kinetics with heating rate [20]. Previous pyrolysis kinetic models have failed to extrapolate to higher temperatures because the actual particle heating rate depends on parameters which are difficult to define quantitatively [20, 30, 31].

In this study a model was developed to estimate the char yield from

biomass pyrolysis at conditions relevant to suspension firing, which includes the effects of high heating rates, high heat treatment temperatures, particle size and biomass alkali content. Simulations were combined with experiments in a wire mesh reactor (WMR), a single particle burner (SPR) and a drop tube reactor (DTF) to identify the most influential fuel characteristics that explain the differences between woody and herbaceous biomass pyrolysis. The accurate knowledge of reaction rate and solid residue yields is essential for the boiler optimal operation and design.

2. Model development

The devolatilization model assumes non-isothermal and cylindrical biomass particles, and includes both chemical kinetics, and external and internal heat transfer. A single biomass particle enters a pre-heated gas flow and is heated up by convection and radiation from its surroundings (single particle reactor and drop tube reactor), or by conduction from the mesh (wire mesh reactor). The model assumes:

1. The fuel particle is a one-dimensional, cylindrical geometry.
2. Thermal gradients within the particle are only in the radial direction.
3. Particle shrinkage occurs during pyrolysis.
4. Moisture content of all fuels are low ($< 5\,\mathrm{wt.\,\%}$) and drying occurs.
5. Internal and external mass transfer are fast [32], and therefore, are not considered.
6. Only the reactor walls contribute to the radiative external heat transfer; radiation from the flame around the particle due to ignition of volatiles is neglected.

7. Heat transfer to the particle surface occurs through convection and radiation.
8. Heat transfer within a biomass particle occurs through conduction.
9. Potassium has a dominant influence on the char yield compared to other ash elements.
10. Variations in plant cell wall composition (cellulose, hemicellulose, lignin, extractives) are relatively small and have less influence on the biomass char yield than variations in the potassium content.

The last two assumptions are based on previous experimental results obtained in a wire mesh reactor and a drop tube reactor [33, 34]. The proposed model includes only primary pyrolysis reactions, i.e. not cracking of tar [35]. The schematic view of the proposed kinetic model is shown in Figure 3.

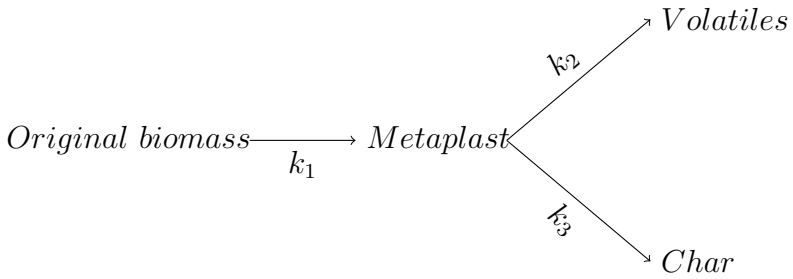

Figure 3: Three reaction model of biomass pyrolysis [12, 15, 36].

The shrinking particle is converted into an intermediate liquid compound (so called metaplast) which reacts further to form volatiles and char. Evidence of metaplast formation has been reported in the literature [23, 30, 37–40]. The thermogravimetric results showed a change in the mass loss that was attributed to a high activation energy process during which cellulose

passed from an inactive to an active form without sample mass loss [23]. High speed photography of hardwood lignin and cellulose exhibited decomposition of lignocellulosic material through an intermediate liquid with bursting bubbles [39]. Only the formation of metaplast is assumed to influence devolatilization whereas the fractional split between volatiles and char is determined by the heating rate and alkali content. The pyrolysis reactions are assumed to be irreversible and first order with an Arrhenius type of rate expression. One fixed set of kinetic parameters (activation energy and pre-exponential factor) for each of the three reactions for a generic biomass was obtained by fitting the model to the char yields obtained in the wire mesh and entrained flow reactors. The catalytic effect of potassium on the char yield was accounted for by decreasing the activation energy required for the reaction from metaplast to char (E_3), thereby leading to higher char yields. The particle model was solved with the initial conditions:

$$\rho_b(r_p, 0) = 1$$

$$\rho_M(r_p, 0) = 0$$

$$\rho_c(r_p, 0) = 0$$

The radial concentrations of biomass, metaplast and char are calculated from:

$$\frac{d\rho_b}{dt} = -k_1 \cdot \rho_b \tag{1}$$

$$\frac{d\rho_M}{dt} = k_1 \cdot \rho_b - (k_2 \cdot \rho_M + k_3(\omega_K) \cdot \rho_M) \tag{2}$$

$$\frac{d\rho_c}{dt} = k_3(\omega_K) \cdot \rho_M \tag{3}$$

$$k_i = A_i \cdot exp\left(-\frac{E_{a,i}}{R \cdot T}\right) \tag{4}$$

$$E_{a,3,max} = \Omega_K(\omega_K) \cdot E_{a,i} \tag{5}$$

$$\Omega_K(\omega_K) = 1 - K_1 \cdot \left(1 - exp\left(-\frac{\omega_K}{K_2}\right)^2\right) \tag{6}$$

The correction factor for the potassium content (Ω_K) becomes $\Omega_K(\omega_K = 0)$=1 and the activation energy $E_{a,3}$ is equal to the maximum activation energy $E_{a,3,max}$ when there is no potassium in the sample. Ω_K approaches the minimum value and the activation energy $E_{a,3}$ is equal to the minimum activation energy $E_{a,3,min}$ when the biomass contains high amounts of potassium. The K_1 parameter is a constant and describes a range of activation energy; the K_2 parameter is a constant for the exponential adjustment of the potassium content (ω_K in mg kg^{-1}). Various expressions of Ω_K to describe the influence of potassium content were tested, and equation 6 was found to fit the char yield data best.

The results of the fitting showed that the kinetic parameters (A_i and $E_{a,i}$) for the metaplast formation and volatiles release are similar. The char yields were calculated in the model by keeping the kinetic parameters (k_1 and k_2) of other reactions constant, whereas the activation energy $E_{a,3}$ required for the reaction from metaplast to char was calculated according to equation 5. The modeling parameters were fitted by minimizing the sum of squares of

the residuals using fmincon in Matlab (version 8.6, MathWorks Inc.).

2.1. Shrinking

The model calculates the radial shrinkage of the particle at radius r_p, which is divided into R_p grid points numbered from i=0 to i=R_p, where 0 is the center of the particle, generating a number of discrete volumes. The density distribution along the particle radius is calculated using a linear approximation between two neighboring points which form a discrete volume as shown in Figure 4.

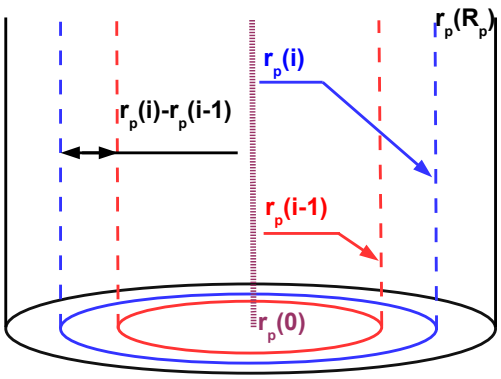

Figure 4: Representation of a shrinking cylindrical biomass particle.

The size of the control volume at a given time is calculated according to equation 7:

$$dV_i = 2 \cdot \pi \cdot R_p \cdot AR \cdot (r_{p(i)}^2 - r_{p(i-1)}^2) \tag{7}$$

The initial size of control volume is given by equation 8:

$$dV_{i,0} = 2 \cdot \pi \cdot R_p \cdot AR \cdot (r_{p(i,0)}^2 - r_{p(i-1,0)}^2) \tag{8}$$

In the shrinking particle model, the volume occupied by the solid structure of the particle is assumed to decrease proportionally with the conversion. The current size of the control volume is related to the initial size of the control volume through a shrinkage factor in equation 9, and further implemented in heat transfer equation 11:

$$f_{Sh} = \frac{dV_i}{dV_{i,0}} = \frac{r_{p(i)}^2 - r_{p(i-1)}^2}{r_{p(i,0)}^2 - r_{p(i-1,0)}^2} \tag{9}$$

The shrinkage factor is calculated from the density change of a fuel particle which is affected by the original biomass, metaplast and char fractions in equation 10:

$$f_{Sh} = 1 - f_{Sh,min} \cdot \left(1 - \frac{\rho_b + \rho_M + \rho_c}{\rho_{b,0}}\right) \tag{10}$$

The shrinkage factor varies from 1 for the untreated biomass particle, to a minimum value $f_{Sh,min}$, when a particle is converted to volatiles and char. Here, the minimum shrinkage factor was varied from 0 to 0.5 according to previous experimental observations from fast pyrolysis of smaller wood particles (0.2-0.4 mm) [34], larger wood particles (3-5 mm) [41], and modeling results from Anca-Couce et al. [42].

2.2. Conservation of energy

The unsteady energy equation for the particle describes internal heat transfer using Fourier's Law in cylindrical coordinates:

$$c_{p,s} \cdot \frac{dT_p}{dt} = \frac{1}{\rho_s \cdot f_{sh}} \cdot \frac{1}{r_p^n} \cdot \frac{\partial}{\partial r_p} \left(r_p^n \lambda_{eff} \frac{\partial T_p}{\partial r_p} \right) + \sum_{j=1}^{3} r_{pyr,j} \cdot (-\Delta H_{reac,j}) + r_{H_2O} \cdot (-\Delta H_{vap}) \quad (11)$$

$$r_{pyr,j} = -A_{pyr,j} \cdot exp\left(-\frac{E_{pyr,j}}{RT} \right) \cdot \left(\frac{\rho_b}{\rho_{b,0}} \right)^m \quad (12)$$

$$r_{H_2O} = -A_{H_2O} \cdot T_p^{1/2} \cdot exp\left(-\frac{E_{H_2O}}{RT} \right) \cdot \left(\frac{\rho_w}{\rho_{b,0}} \right)^m \quad (13)$$

The overall reaction enthalpy includes the heat of reaction ($\Delta H_{reac,j}$) multiplied by the pyrolysis reaction rate ($r_{pyr,j}$) for each reaction product: metaplast (j=1), char (j=2), and volatiles (j=3). The reactions from metaplast to gas or to char are competitive. The metaplast formation was assumed to be as thermally neutral [43, 44], gas formation as endothermic, and char formation as exothermic [45, 46]. This approach resulted in the dependence of overall heat of reaction depending on the char yield [47], which is consistent with experimental results [48, 49]. Thus the overall reaction enthalpy changes with the char yield, similar to the modeling approach of Haseli et al. [47]. The presence of potassium in fuels catalyzes pyrolysis reactions favoring the formation of char. Therefore, the endothermic heat of pyrolysis decreases with increasing char yield, and eventually shifts to an exothermic process, similar to results of Rath et al. [49] and Mack et al. [48]. Exothermic and endothermic heat of reaction ($\Delta H_{reac,2}$ = -255000 J kg^{-}1; $\Delta H_{reac,3}$ = 20000 J kg^{-}1) were proposed by Koufopanos et al. [45].

The rates of mass loss during drying and devolatilization were described

by equations 1- 3 [50]. A first order reaction model (m=1) was chosen to describe the experimental results [51]. The heat of vaporization was assumed to be $\Delta H_{vap} = 2440000\,\mathrm{J\ kg^{-1}}$ [52, 53]. The initial condition is given by the ambient temperature:

$$T_p(r_p, 0) = T_{amb} \tag{14}$$

The boundary conditions specify that the particle center line is adiabatic due to symmetry shown in equation 15 and that convection and radiation entering at the particle surface is conducted into the particle as shown the equation 16 or given by the temperature of the mesh in equation 17:

$$\lambda_{eff} \frac{dT_p}{dr_p}\bigg|_{r_p=0} = 0 \tag{15}$$

$$\lambda_{eff} \frac{dT_p}{dr_p}\bigg|_{r_p=R_p} = h \cdot (T_g - T_p|_{r_p=R_p}) + \epsilon \cdot \sigma \cdot (T_w^4 - T_p^4|_{r_p=R_p}) \quad \textit{drop tube reactor} \tag{16}$$

$$T_p|_{r_p=R_p} = T_{mesh}(t) \qquad \textit{wire mesh reactor} \tag{17}$$

When the biomass sample is heated up in the wire mesh reactor, it is assumed that the particle surface temperature is equivalent to that of the mesh. The effective thermal conductivity (λ_{eff}) inside the particle is approximated by equation 18 [16, 17]:

$$\lambda_{eff} = \xi \cdot \lambda_g + \lambda_b \cdot \psi \cdot (1 - \xi) + \lambda_c \cdot (1 - \psi) \cdot (1 - \xi) + \lambda_r \cdot (1 - \xi) \tag{18}$$

$$\lambda_r = \frac{4 \cdot \xi}{(1 - \xi)} \cdot \epsilon \cdot \sigma \cdot d_{pore} \cdot T_p^3 \tag{19}$$

$$\rho_{c,0} = \frac{\rho_{b,0} \cdot Y_c}{f_{sh,min}} \tag{20}$$

$$\psi = \frac{\rho_b + \rho_M}{\rho_b + \rho_M + \rho_{c,0}} \tag{21}$$

where λ_r is the thermal conductivity induced by radiation through pores, correlated from previous investigations [16, 17], λ_g, λ_b and λ_c are the thermal conductivities of gas, unconverted biomass and char, repsectively, ξ is the void fraction occupied by the gas phase and ψ is the biomass fraction of the solid phase which varies 0 to 1. ρ_b and $\rho_{b,0}$ are the original (reacting) biomass particle density and initial (unreacted) biomass particle density. The thermal conductivity of metaplast is assumed to be equal to the thermal conductivity of original biomass. The convection coefficient of the gas in the drop tube reactor is described in equation 22 [54]:

$$h = \frac{Nu \cdot \lambda_g}{d_p} \tag{22}$$

The particle Reynolds, Prandtl and Nusselt numbers are defined in equations 23-25 [54]:

$$Re = \frac{d_p \cdot (v_p - v_g) \cdot \rho_g}{\mu_g} \tag{23}$$

$$Pr = \frac{c_{p,g} \cdot \mu_g}{\lambda_g} \tag{24}$$

$$Nu = 0.3 + \frac{0.62 \cdot Re^{1/2} \cdot Pr^{1/3}}{(1 + (\frac{0.4}{Pr})^{2/3})^{1/4}} \cdot \left(1 + \left(\frac{Re}{282000}\right)^{5/8}\right)^{4/5} \quad RePr > 0.2 \tag{25}$$

The terminal velocity of the biomass particle is calculated from correlations for Stokes regime, steady separated and unsteady separated flows in equations 26-28 [55]:

$$v_p = \frac{d_p^2 \cdot g \cdot (\rho_s - \rho_g)}{18 \cdot \mu_g} \qquad Re < 2 \tag{26}$$

$$v_p = 0.153 \left[\frac{(\rho_s - \rho_g) \cdot d_p^{1.6} \cdot g}{\mu_g^{0.6} \cdot \rho_g^{0.4}}\right]^{0.714} \qquad 2 < Re < 400 \tag{27}$$

$$v_p = 1.74 \cdot \sqrt{\frac{d_p \cdot (\rho_s - \rho_g) \cdot g}{\rho_g}} \qquad 400 < Re < 200000 \tag{28}$$

Stokes Law was used for small fuel particles, steady separated flow was used for intermediate fuel particles, and turbulent flow was used for large fuel particles.

2.3. Method of lines

Most of the pyrolysis models [15, 17, 56–59] involve solution schemes based on the method of lines (finite difference method) to solve the heat transfer equations. The heat transfer equation is discretized using a central difference scheme:

$$c_{p,s,i} \cdot \frac{dT_i}{dt} = \left(\frac{\lambda_{eff,i}}{\rho_{s,i} \cdot f_{sh}} \cdot \left(\frac{T_{i-1} - 2 \cdot T_i + T_{i+1}}{\Delta r_p^2} + \frac{n}{r_{p,i}} \cdot \frac{T_{i+1} - T_{i-1}}{2 \cdot \Delta r_p} \right) \right) + \sum_{j=1}^{3} r_{pyr,i,j} \cdot (-\Delta H_{reac,i,j}) + r_{H_2O,i} \cdot (-\Delta H_{vap,i}) \tag{29}$$

In the present model, the ode15s method in MatLab was chosen as an ODE solver. The ode15s function based on the Backward Differentiation Formula (BDF) is recommended for the solution of stiff problems [60]. Calculations were performed to verify the convergence of the adopted numerical procedure with grids having 51, 101 and 201 mesh points. Since the results showed that sufficient accuracy is attained using a grid with 101 mesh points for different biomass particle sizes, the number of mesh points was set to 101 with an error tolerance of 10^{-10} in time integration.

2.4. Fuel characterization

Pinewood, beechwood, Danish wheat straw, leached Danish wheat straw, alfalfa straw and rice husk were used in this work to represent softwood, hardwood and agricultural residues. The low-ash containing wood (pinewood,

beechwood) and grass samples (wheat straw, alfalfa straw), which are rich in potassium, were selected to investigate the effect of differences in potassium composition on the char yields. The fuels were milled on a Retsch rotor mill ZM200 and sieved to particle size fractions of 0.02-0.4 mm and 0.85-1 mm.

Table 1: Proximate and ultimate analysis of fuels (on % dry basis) and ash analysis (on mg/kg dry basis).

Fuel	Pine-wood	Beech-wood	Wheat straw	Leached wheat straw	Alfalfa straw
Proximate and ultimate analysis (% db)					
Moisture[a]	5.1	4.5	5.5	4.3	5.2
Ash (550 °C)	0.3	1.4	4.1	2	7.4
Volatiles	86.6	79.4	77.5	84.2	75.9
HHV[b]	21.6	20.2	18.8	18.7	19.7
LHV[b]	20.2	19	17.5	17.4	16.9
C	50.5	46.7	42.4	45.7	42.5
H	6.8	6.3	6.3	6.6	6.1
N	0.1	0.3	1	0.3	3.3
S	<0.01	0.02	0.1	0.02	0.03
Cl	0.01	0.02	0.1	0.01	0.5
Ash compositional analysis (mg/kg db)					
Al	10	10	150	100	600
Ca	600	2000	2500	1300	12900
Fe	20	10	200	350	-
K	200	3600	11000	1300	28000
Mg	100	600	750	350	1400
Na	30	100	150	50	1000
P	6	150	550	80	1900
Si	50	200	8500	6200	2000
Ti	2	<8	10	10	30

[a] wt. % (ar) [b] in MJ/kg

2.5. Biomass particle properties

Biomass samples were analyzed with a 2D dynamic imaging instrument by using different size measures (width and length). The diameters $x_{Ma,min}$ and $x_{Fe,max}$ were chosen to represent the biomass particle's width and length. Diameter $x_{Fe,max}$ is the largest diameter to fulfill the assumption that the length of a particle is larger than its width. Diameter $x_{Ma,min}$ is an area bisector representing the shortest distance to the particle's opposite edges. A biomass particle was represented as a plate, a cylinder and a sphere in planar (n=0), cylindrical (n=1), and spherical (n=2) coordinates under the assumption of similar volume to surface ratios using a different characteristic length:

$$d_p = x_{Ma,min} \quad (cylinder) \tag{30}$$

$$d_p = \frac{1}{2} \cdot x_{Ma,min} \quad (plate) \tag{31}$$

$$d_p = \frac{3}{2} \cdot x_{Ma,min} \quad (sphere) \tag{32}$$

Biomass particles were described as infinite cylinders, corresponding to n=1 in equation 11 with a particle size equal to $R_p/2$, where R_p is represented by $x_{Ma,min}$. The thermo-physical parameters used in the devolatilization model are listed in Table 2.

Table 2: Thermophysical properties used in the devolatilization model and geometrical parameters of the drop tube reactor.

Symbol	Unit	Description	Expression	
ϵ		Emissivity	0.85	[61]
σ	$J{\cdot}(s{\cdot}m^2{\cdot}K^4)^{-1}$	Stefan-Boltzmann	$5.67{\cdot}10^{-8}$	[61]
ξ		Void fraction	1- $\frac{(\rho_b+\rho_M+\rho_{c,0})}{1500}$	[58]
$\rho_{b,0}$	$kg{\cdot}m^{-3}$	Raw biomass density	650 (wood) and 700 (straw)	[62, 63]
ρ_g	$kg{\cdot}m^{-3}$	Gas density (N_2)	$362.65{\cdot}T_g^{-1}$	[64]
d_{pore}	m	Pore diameter	$3.2{\cdot}10^{-6}$	[61]
$d_{pore,c}$	m	Char pore diameter	$2{\cdot}10^{-4}$	[65]
$c_{p,b}$	$J{\cdot}(kg{\cdot}K)^{-1}$	Raw biomass specific heat capacity	$1500+T_p$	[16]
$c_{p,c}$	$J{\cdot}(kg{\cdot}K)^{-1}$	Char specific heat capacity	$420+2.09{\cdot}T_p+6.85{\cdot}T_p^2$	[16]
$c_{p,g}$	$J{\cdot}(kg{\cdot}K)^{-1}$	Gas specific heat capacity	$770+0.629{\cdot}T_g+1.91{\cdot}10^{-4}{\cdot}T_g^2$	[17]
λ_g	$W{\cdot}(m{\cdot}K)^{-1}$	Gas thermal conductivity	0.026	[66]
λ_b	$W{\cdot}(m{\cdot}K)^{-1}$	Raw biomass thermal conductivity	0.35	[16]
λ_c	$W{\cdot}(m{\cdot}K)^{-1}$	Char thermal conductivity	0.1	[16]
μ_g	Pa·s	Gas phase dynamic viscosity	$4.847{\cdot}10^{-7}{\cdot}T_g^{0.64487}$	[58]
$\Delta H_{reac,1}$	$J{\cdot}kg^{-1}$	Heat of reaction from biomass to metaplast	0	[43, 44]
$-\Delta H_{reac,2}$	$J{\cdot}kg^{-1}$	Heat of reaction from metaplast to char	-255000	[45]
$\Delta H_{reac,3}$	$J{\cdot}kg^{-1}$	Heat of reaction from metaplast to gas	20000	[45]
ΔH_{vap}	$J\ kg^{-1}$	Heat of vaporization	2440000	[53]
A_{H_2O}	$s^{-1}K^{-0.5}$	Pre-exponential factor	$5.1{\cdot}10^{10}$	[58]
E_{H_2O}	$J\ mol^{-1}$	Activation energy	88000	[58]
L	m	Drop tube reactor's length	2.3	
D_r	m	Drop tube reactor's diameter	0.054	

2.6. Experimental

2.6.1. Small and intermediate size particles (0.2 and 1 mm)

The model was validated against data from three high-temperature reactors. The char yields of 0.2 and 1 mm pinewood particles were determined

in separate pyrolysis experiments performed at an intermediate heating rate (10-10^3 K s^{-1}) in the wire mesh reactor and at a high heating rate of (10^4 K s^{-1}) in the drop tube reactor.

The wire mesh reactor at TU Munich was previously described by Trubetskaya et al. [33]. Tests on the wire mesh reactor were conducted at 350-1400°C, with 1 s holding time on the mesh at atmospheric pressure. The DTF setup was described in detail by Trubetskaya et al. [34]. The experiments were conducted by feeding ≈ 5 g of biomass at a rate for 0.2 g min^{-1}. The residence time for 0.2 mm and 1 mm pinewood particles was estimated to be about 1 s, taking into account density changes during pyrolysis [29]. Biomass was rapidly heated and reacted as it fell through the reactor at temperatures of 1000-1400°C. Reaction products were separated into coarse particles (mainly char and fly ashes), fine particles (mainly soot and ash aerosols), and permanent gases.

The heating rate in the wire mesh reactor was set to 1000 K s^{-1}. In the drop tube reactor, the heating rate was calculated by the model using dimensions and operating parameters of the reactor shown in Table 2. Char yields of wood and herbaceous biomass in the wire mesh reactor and drop tube reactor are shown on dry ash free basis (daf) excluding ash content of original biomass and char.

2.6.2. Large size particles (3-5 mm)

The devolatilization time and char yield of 3, 4 and 5 mm pinewood particles in a temperature range of 1350-1450°C were determined by Jepsen in a single particle reactor (SPR) located at the DTU Chemical Engineering

Department [41]. The SPR was designed for oxidation and pyrolysis studies on fuel particles > 2 mm at temperatures up to 1500°C at high heating rates. The setup consists of the reactor, a flat flame burner with 94 injection nozzles, a gas supply system and gas analyzers as shown in Figure 5.

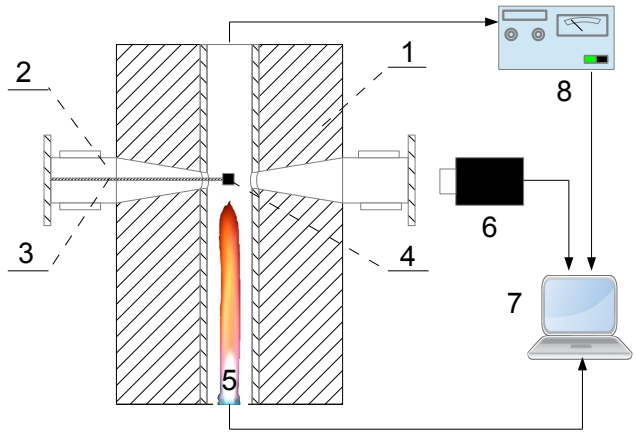

Figure 5: Schematic view of a single particle reactor at DTU: 1. Reactor corpus; 2. insertion ports with a water-cooled chamber; 3. particle holder; 4. sample particle; 5. 94 injection nozzles; 6. High-speed camera; 7. Computer; 8. Gas analyzers.

The formation of a soot cloud in the single particle reactor is associated with pyrolysis initiation. Soot formation occurs under reducing conditions. The oxygen level was kept very low (< 0.2 vol.%) during the experiments to eliminate char and soot oxidation. Devolatilization time is defined as the time from the soot cloud is seen until it extinguishes and char conversion begins due to gasification with steam and the remaining oxygen. The char yield is defined as the solid fraction of the reacted biomass, remaining on the platinum wire after an experiment.

3. Results

3.1. Kinetic parameters

The results of fitting of the rate constants, including the influence of potassium are shown in Table 3.

Table 3: The best fit values of the kinetic parameters. In the model, the constants $K_1 = 0.068$ and $K_2 = 4500$ (mg kg^{-1}) were fitted.

Metaplast		Volatiles		Char	
$E_{a,1}$	A_1	$E_{a,2}$	A_2	$E_{a,3}$	A_3
J mol^{-1}	s^{-1}	J mol^{-1}	s^{-1}	J mol^{-1}	s^{-1}
228000	$3.2{\cdot}10^{14}$	174100	$3.6{\cdot}10^{12}$	$132500{\cdot}\Omega_K$	$5.6{\cdot}10^{8}$

Figure 6 illustrates that the char yield increases with increasing potassium content in the lignocellulosic material and decreases with the higher heating rate. The activation energy of the char forming reaction decreases with increasing potassium content, and thus, the influence of potassium becomes smaller at higher heating rates. In Figure 6(b), the model estimates that char yield increases from 2.6 % to 32.5 % when the heating rates decrease from 10^4 to 2 K s^{-1}.

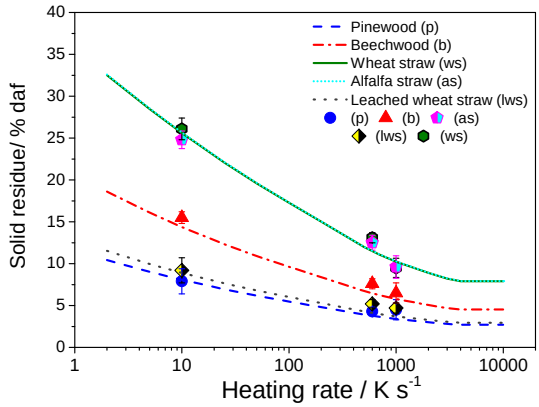

6(a): Heating rate effect on the char yield

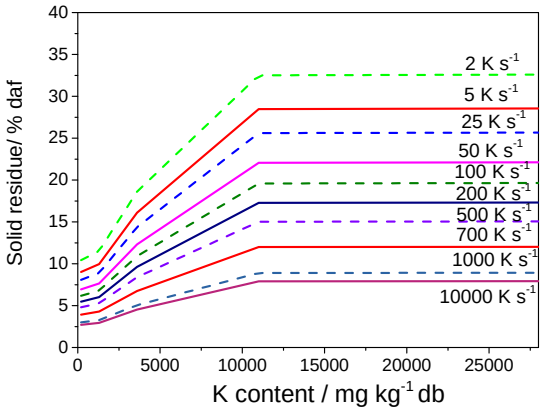

6(b): Char yields versus potassium content in the fuel

Figure 6: (a) Comparison of simulated and experimental data for the influence of heating rate on the char yield of pinewood, beechwood, wheat straw, leached wheat straw and alfalfa straw in the wire mesh reactor, and (b) Simulated char yields versus potassium content in the original fuel (heat treatment temperature: 1400°C, holding time: 1 s, particle size: 0.2 mm).

Estimated biomass particle mass as a function of mean particle temperature is shown in Figure 7.

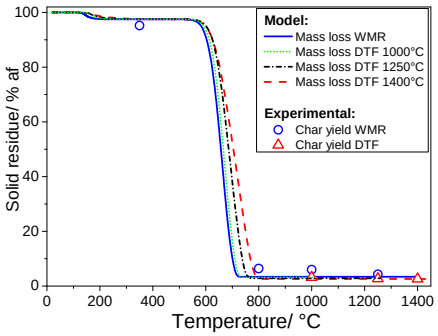

7(a): Pinewood 0.2 mm

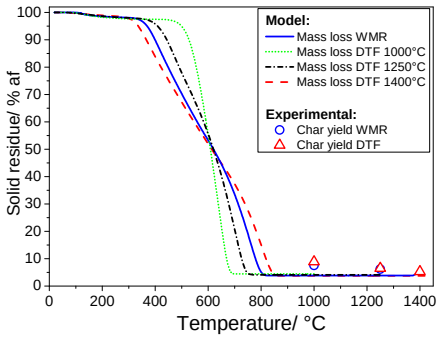

7(b): Pinewood 1 mm

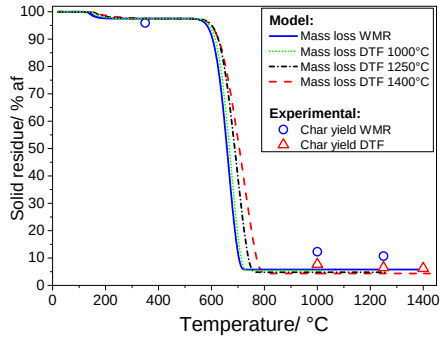

7(c): Beechwood 0.2 mm

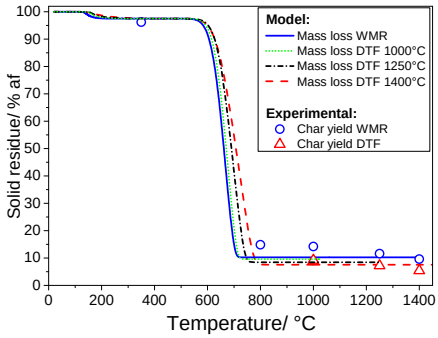

7(d): Alfalfa straw 0.2 mm

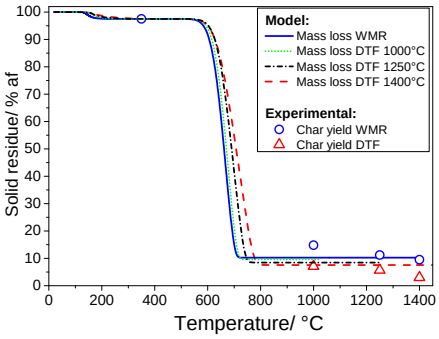

7(e): Wheat straw 0.2 mm

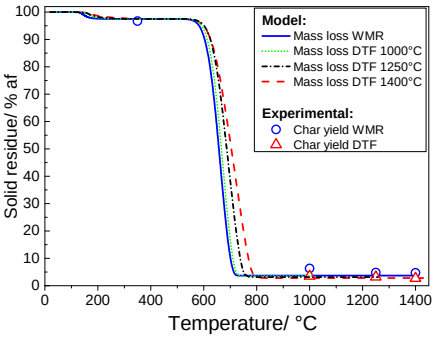

7(f): Leached wheat straw 0.2 mm

Figure 7: Simulated mass loss over the mean particle temperature (% af) of pinewood, beechwood, wheat straw, alfalfa straw and leached wheat straw at 1000, 1250 and 1400°C in the DTF and at 1400°C in the WMR, and comparison with the char yields determined experimentally in the wire mesh reactor at (heat treatment temperature: 350, 800, 1000, 1250 and 1400°C; heating rate: 1000 K s^{-1}; holding time: 1 s) and drop tube reactor at 1000, 1250 and 1400°C as determined by Trubetskaya et al. [33, 34].

The mass loss of smaller particles is shown only at 1400°C in the wire-mesh reactor, since pyrolysis is complete at temperatures below 800°C. The simulation results show that char yields from pyrolysis of wood and leached wheat straw in the drop tube reactor were similar over a temperature range of 1000-1400°C, whereas the char yield of wheat and alfalfa straw decreased slightly from 10.3 % to 7.6 % by weight. The present results show that the model accurately estimates the char yield for smaller (0.2 mm) biomass particles. The char yield from pyrolysis of 1 mm pinewood particles is also estimated well and is about 3 % lower relative to the experimentally determined char yields in the drop tube reactor. The experimental data obtained in the wire mesh reactor agree with the mass loss estimated by the model. The lower WMR heating rate caused the reaction to take place at lower temperatures for an extended period compared to fast pyrolysis conditions in the drop tube reactor.

Figure 8 illustrates the mass fraction of metaplast formed at the surface, middle and center of the particle as a function of time. The simulation results show that both heating rate and particle size influence metaplast formation. In general, high heating rates promote the formation of metaplast. Due to negligible temperature gradients, high heating rates cause small particles first to become fluid and form a molten sphere, then solidify into char [6, 7, 33]. For large particles, significant formation of metaplast at high heating rates is only observed at the surface.

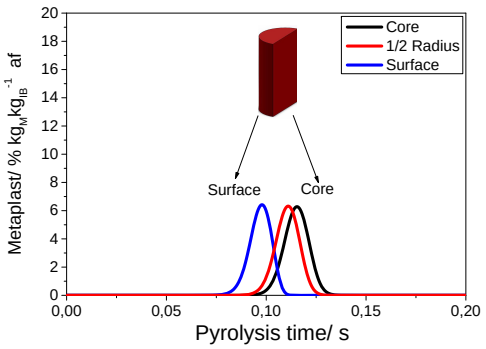

8(a): 0.2 mm, heated by 10^4 K s^{-1} gas flow

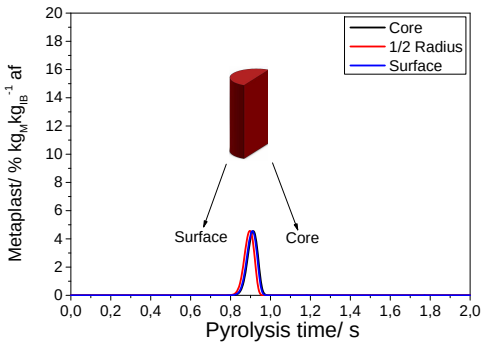

8(b): 0.2 mm, heated by 10^3 K s^{-1} gas flow

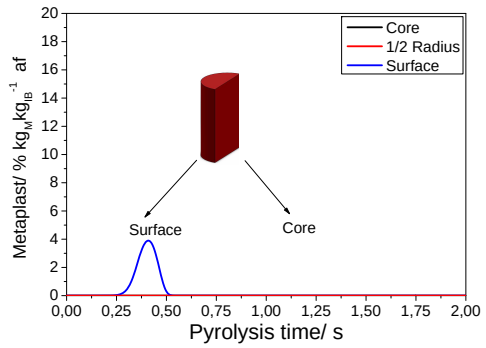

8(c): 3 mm, heated by 10^4 K s^{-1} gas flow

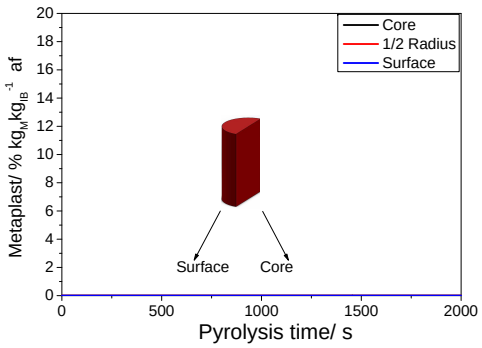

8(d): 3 mm, heated by 10 K min^{-1} gas flow

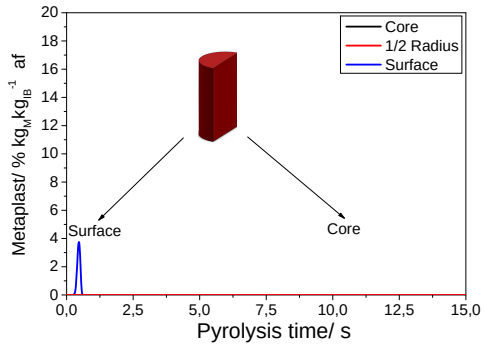

8(e): 10 mm, heated by 10^4 K s^{-1} gas flow

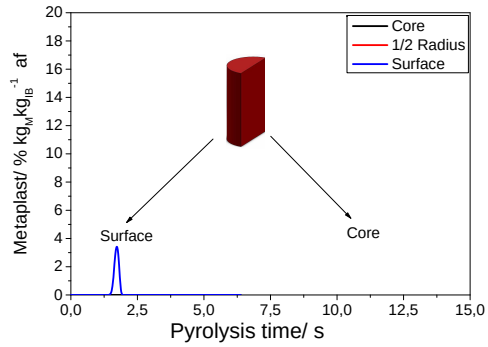

8(f): 10 mm, heated by 10^3 K s^{-1} gas flow

Figure 8: Simulated metaplast formation (% af) from pyrolysis of 0.2, 3 and 10 mm pinewood particles at slow heating rate in the thermogravimetric instrument (10 K min^{-1}), at intermediate heating rate (10^3 K s^{-1}) in the wire mesh reactor and at high heating rates in the drop tube reactor. The metaplast formation (kg$_M$ kg$_{IB}^{-1}$) is showed over the pyrolysis time.

This means that the particle surface melts during pyrolysis, whereas the interior retains the original biomass structure [33]. The rate of metaplast formation was slower than formation of volatiles and char at lower temperatures. Thus, metaplast was formed faster than it was consumed at higher temperatures. At low heating rates, the particle was nearly isothermal, indicating only small differences in metaplast formation as function of position within the particle. Thus, the relatively low heating rate for the particle core increased the time for the three reactions, leading to lower metaplast yields.

3.2. Influence of assumed particle geometry

Figure 9 illustrates the mass loss of 0.2, 1 and 5 mm pinewood particles. Devolatilization time decreased with the higher heating rate in the drop tube reactor compared to the wire mesh reactor. The representation of the 0.2 mm particles using different characteristics lengths does not give large deviations with respect to char yield and devolatilization time among the three particle geometries as shown in Figure 9(a).

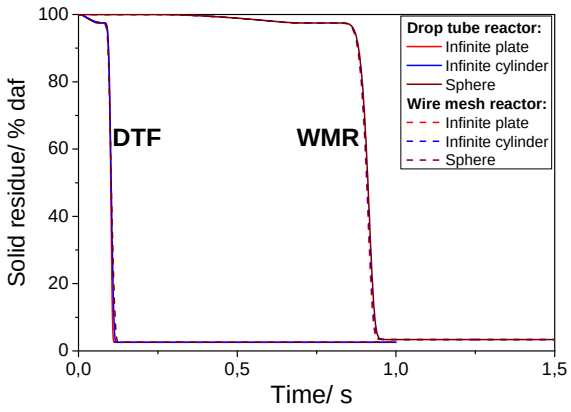

9(a): Pinewood 0.2 mm

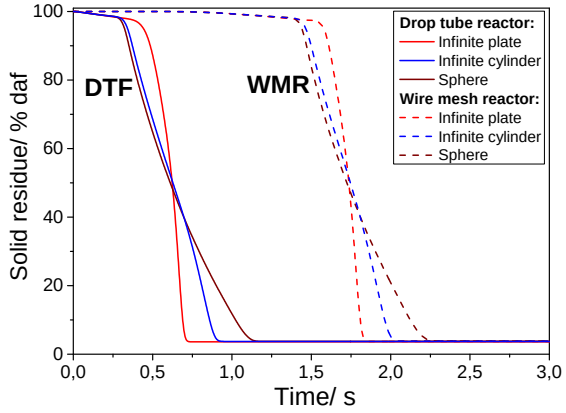

9(b): Pinewood 1 mm

Figure 9: Mass loss histories of pinewood particles (0.2 and 1 mm) with the similar volume to surface ratio and different characteristic lengths which were calculated in plate-like (n=0), cylindrical (n=1) and spherical (n=2) geometries at the final temperature of 1400°C during pyrolysis in the wire mesh and drop tube reactors.

The influence of particle shape becomes more important with the increasing particle size due to the larger internal temperature gradients as

shown in Figure 9(b). The relative influence of heating rate on devolatilization time of 1 mm pinewood was less compared that for smaller particles. This is because of the predominance of internal heat transfer control within the large particles.

3.3. Influence of volumetric shrinkage on devolatilization time

In the model, the shrinkage front moves from the surface towards the center. At high heating rates, the outer layers initially shrink while the inner layers remain unaffected. Later, the fuel particle shrinks due to devolatilization. During slow pyrolysis, internal thermal gradients are small, and therefore, drying followed by devolatilization takes place over throughtout the particle. Particle shrinkage takes place after the original biomass is converted into metaplast. The rate of volatiles formation determines the rate at which the particle shrinks.

Figure 10(a) shows that the particle size of 5 mm particle was reduced by 27 % during pyrolysis at high heating rates. A 26 % reduction in a particle size was measured during devolatilization of 3 mm pinewood particle in a temperature range of 1180-1440°C in the single particle reactor [41].

Figure 10(c) shows that shrinkage has a negligible influence on the devolatilization time of smaller particles, which are practically isothermal. For the large particles, the inclusion of shrinkage increases the devolatilization rate and thereby decreases the devolatilization time. Internal temperature gradients in larger particles becomes smaller as the particle shrinks which enhances the devolatilization rate. The shrinkage of 5 mm pine particle leads to the decrease of devolatilization time by 19 % during pyrolysis in the WMR and DTF.

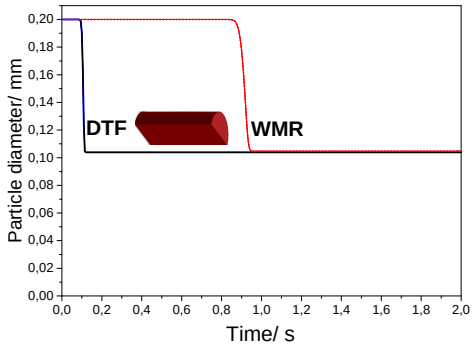

10(a): Pinewood 0.2 mm

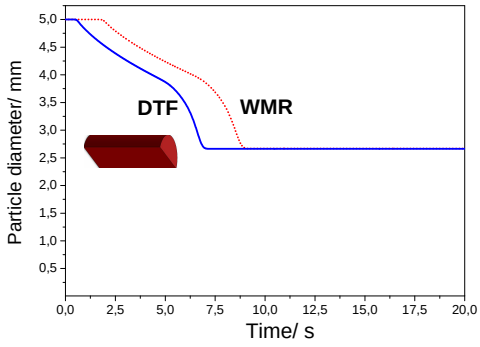

10(b): Pinewood 5 mm

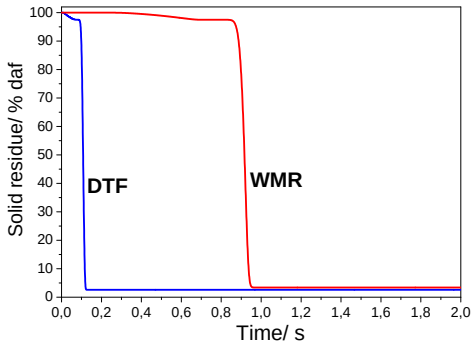

10(c): Pinewood 0.2 mm

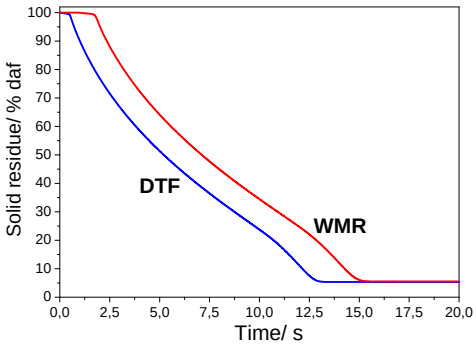

10(d): Pinewood 5 mm

Figure 10: (a)-(b) Simulated pinewood particle shrinking (0.2 and 5 mm) and (c)-(d) Simulated mass loss of shrinking pinewood particles in the wire mesh and drop tube reactors.

3.4. Influence of particle size on devolatilization time

Figure 11 compares the times required for complete devolatilization of 3, 4 and 5 mm pinewood particles in the single particle reactor to those estimated by the model for particles from 0.01 to 10 mm. In the model, the complete devolatilization time is defined as the time when 95 % of the volatile matter in the original pinewood particle has been released [67].

Figure 11 shows that under fast heating particles with mean diameters < 0.25 mm may be considered as thermally thin based on the modeling results with 0.1 s deviation, while the intra-particle heat conduction in larger particles plays a key role in biomass devolatilization. The diameter of 3, 4 and 5 mm pinewood cubes was recalculated for corresponding cylinders under the assumption of a similar volume to surface ratio (3, 4 and 5 mm). A comparison of experimental and estimated devolatilization times showed that the model estimates the devolatilization time of pinewood particles well. In addition, the results showed that the 1 mm pinewood particles require more than 1 s in the WMR and DTF for complete conversion. The estimated devolatilization time by the model showed a similar trend for the experiments in the drop tube reactor.

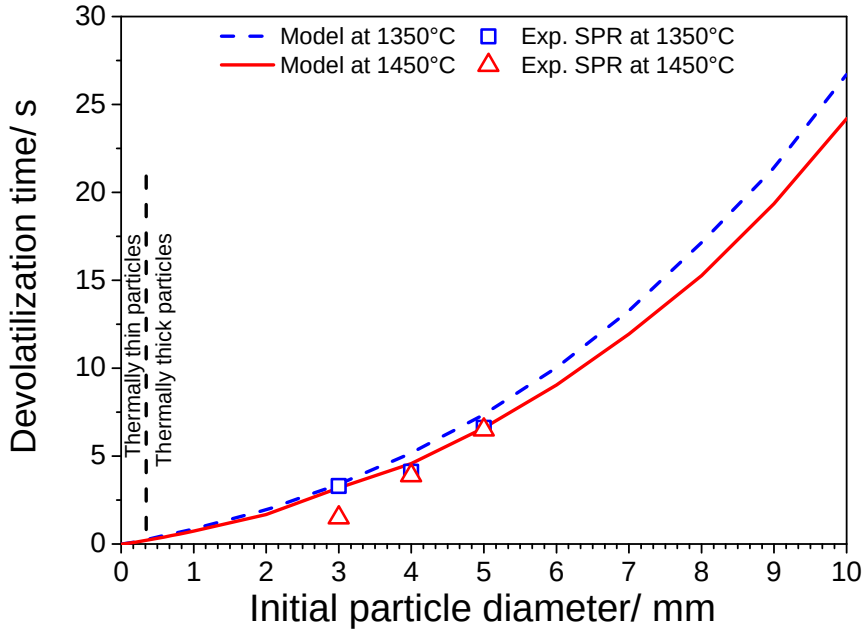

Figure 11: Simulated devolatilization time of shrinking pinewood particles (from 0.01 mm to 10 mm) at 1000, 1250 and 1400°C, and compared with the experimental results obtained in the SPR for 3, 4 and 5 mm particles at 1350 and 1450°C. Experimental data was taken from the investigations of Jepsen [41]. The black dashed line separates the thermally thin regime ($Bi < 0.1$) from the thermally thick ($Bi > 0.1$).

4. Discussion

The present pyrolysis model describes the char yield at high temperatures (up to 1500°C) and high heating rates $> 200\,\mathrm{K\ s^{-1}}$. In the model, an intermediate liquid (so called metaplast) is formed from the decomposition of biomass which reacts further to char and gas. It was assumed that the kinetics for metaplast formation does not depend on the biomass type and that

reaction of metaplast to char and gas is influenced by the biomass potassium content.

The impact of heating rate on the maximum metaplast formation and subsequent reaction to char and gas shown in Figure 12.

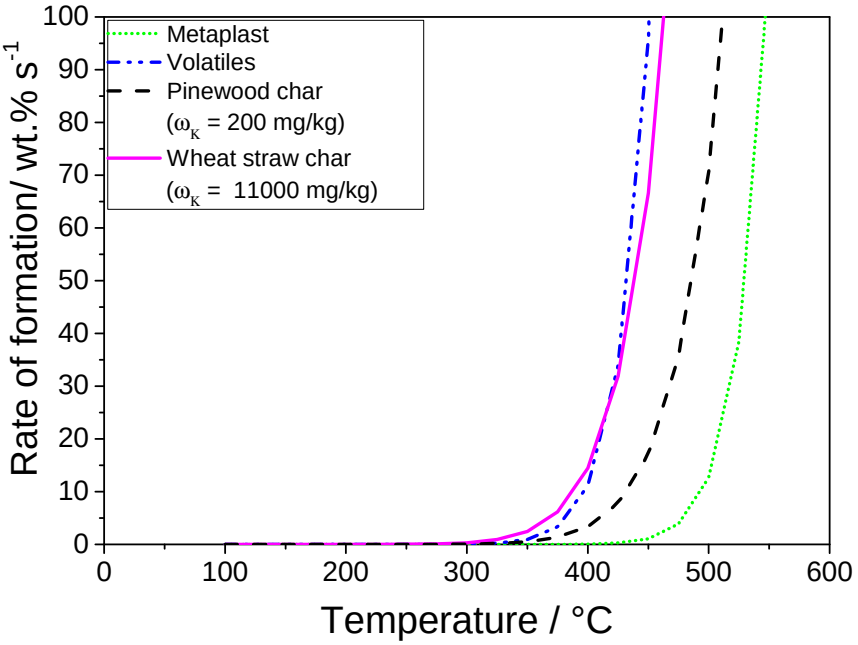

Figure 12: Simulated reaction rates (wt.% s^{-1}) of metaplast, char and volatile formation during fast pyrolysis of 0.2 mm pinewood ($\omega_K = 200\,\mathrm{mg\,kg^{-1}}$, dry basis) and wheat straw ($\omega_K = 11000\,\mathrm{mg\ kg^{-1}}$, dry basis) particles in the wire mesh reactor ($1000\,\mathrm{K\ s^{-1}}$).

Figure 12 demostrates that the rate of metaplast formation is slower than formation of volatiles and char at temperatures below 350°C. Thus, lower concentrations of metaplast are formed at lower heating rates. The particle temperature was nearly uniform over the particle diameter, and therefore,

only small differences in metaplast formation were observed. At higher temperatures, the rate of char formation was lower than the rate of metaplast formation, in agreement with experimental results from Koufopanos [15, 45]. Higher temperatures result in greater metaplast accumulation because its formation rate is faster than its rate of consumption. At high heating rates, such as in the wire mesh and drop tube reactors, lower mass fractions of metaplast were formed in the particle core compared to the particle surface. This could be due to the lower heating rates at the core compared to at the surface. At high heating rates, formation of metaplast is initially fast relative to reaction from metaplast to char and gas, so a high concentration of metaplast is obtained. With a high fraction of metaplast, the particle may become molten (locally or throughtout the whole particle), thereby leading to structural changes of the particle [33].

Particle size demonstrates a greater influence on metaplast, volatile and char formation in the drop tube reactor ($10^{-4}\,\mathrm{K\ s^{-1}}$) than in the wire mesh reactor ($10\,\mathrm{K\ s^{-1}}$). The larger internal temperature gradients led to slower pyrolysis of 3 and 10 mm pinewood particles compared to 0.2 mm particles. For large particles the formation of metaplast mainly takes place at the particle surface at high heating rates, whereas the lower heating rates result in high metaplast concentrations in the interior. At low heating rates, both small and large particles were nearly isothermal, leading to smaller local differences in metaplast formation. Differences in local mass fractions of metaplast became larger with increasing particle size and increasing heating rates because of the predominance of internal heat transfer control within the large particles.

Char yield has been experimentally shown to increase with potassium content in the original biomass [33, 34]. This effect was accounted for in the model by modifying the activation energy for the char formation reaction as a function of the potassium content. The influence of potassium on char formation became stronger with decreasing heating rate, which corresponds to the experimental observations from the wire mesh and drop tube reactors. Calculations suggested that pyrolysis was completed at temperatures below 800°C, and thus, the char yields for woody and herbaceous biomass remain unchanged. The experimental data showed that the biomass char yields decreased with the increasing temperature due to the dehydrogeneration and cross-linking reactions [68], which are not considered in the present simulation. The simulated char yield from wheat straw pyrolysis was slightly lower than the char yield from the wire mesh and drop tube reactor experiments. The ash compositional analysis of char from the pyrolysis in the drop tube reactor showed that close to 70 % potassium in the wheat straw has been released in a temperature range of 1000-1500°C [69]. The remaining potassium in herbaceous biomass samples is still present in a larger amount than in woody chars. The large differences in herbaceous char yields between the model and experimental data might be attributed to the interactions between potassium, other remaining alkali metals and carbonaceous char matrix which were not considered during the model development.

Moreover, the char yield of larger particles is underestimated by the model. It was hypothesized that tar inside larger particles may undergo secondary reactions, leading to higher char yields [36]. At high heat treatment temperatures of 750-1100°C, secondary reactions occurring in larger

particles strongly decrease tar release and increase char formation during pyrolysis. Tar decomposition occurs by secondary reactions (i.e. cracking and polymerization), and tar release to ambient by mass transfer [35]. The evolutionary profiles of the temperatures at the pinewood particle surface and the particle center as a function of time are shown in the supplemental material. Due to the fast heat transfer in 0.2 mm particles, the differences between surface and core temperatures are small and thus, tar release remains unchanged at 1100°C. The differences between surface and core temperatures become more pronouced with the increasing particle size. Tar formation from pyrolysis of larger pinewood particles was stronger, whereas the soot yield was half lower compared to smaller particles [70]. The lower soot yields were related to the less formed PAH precursors. Tar inside larger particles underwent secondary reactions due to the lower heat flux, leading to a slower pyrolysis and thereby higher char yields and less soot, corresponding to investigations of Miller and Bellan [36]. This effect was not included in the model and could be the reason why the model slightly underpredicts the char yield for large particles.

5. Conclusion

The novelty of this work relies on the description of both low and high temperature kinetics for wood and herbaceous biomass using one set of kinetic parameters. The actual particle heating rate of biomass particles was quantitatively defined in wire mesh and drop tube reactors. The results presented in this work emphasize a stronger catalytic effect of potassium on char yield at low and intermediate heating rates compared to high heating rates.

The potassium content and heating rate affected the char yield more than other operational parameters.

An innovative approach was used to implement the influence of potassium on the char yield in the model by reduction in the activation energy of char formation with increasing potassium content, and fitted to the experimental results. The simulation results showed that particle size has a more significant influence on metaplast formation and reaction to char and gas at high heating rates ($10^4\,\mathrm{K\ s^{-1}}$) compared to pyrolysis at low heating rates ($10\,\mathrm{K\ s^{-1}}$).

In addition, the model showed that the impact of shrinkage on devolatilization time increases with increasing particle size, but it has negligible influence on char yields. Results from the 1D model are in agreement with experimental data, and emphasize a key role of intra-particle heat conduction in biomass particle $> 0.25\,\mathrm{mm}$.

Acknowledgements

The authors would like to acknowledge the financial support that they received for this project from Kempestiftelserna. We also acknowledge Professor Anker Degn Jensen (DTU CHEC) for fruitful discussions. Assistant Professor Catherine Brewer is acknowledged for the article proof reading.

References

[1] Sander B, Properties of Danish Biofuels and the Requirements for Power Production, Biomass Bioenergy 12 (3) (1997) 177–83.

[2] Danish Energy Agency: Energy strategy 2050 - from coal, oil and gas to green energy, The Danish Ministry of Climate and Energy (2011) 1–66.

[3] Rosendahl LA, Yin C, Kœr SK, Friborg K, Overgaard P, Physical characterization of biomass fuels prepared for suspension firing in utility boilers for CFD modelling, Biomass Bioenergy 31 (2007) 318–25.

[4] Larsen L, Peteresen MO, Thirup L, Li HW, Iversen FK, The IBUS process - Lignocellulosic bioethanol close to a commercial reality, Chem Eng Technol 31 (2008) 765–77.

[5] Wornat MJ, Hurt RH, Yang NYC, Headley TJ, Structural and compositional transformations of biomass chars during combustion, Combust Flame 100 (1-2) (1995) 131–45.

[6] Cetin E, Moghtaderi B, Gupta R, Wall TF, Influence of pyrolysis conditions on the structure and gasification reactivity of biomass chars, Fuel 83 (2004) 2139–50.

[7] Dall'Ora M, Jensen PA, Jensen AD, Suspension combustion of wood: Influence of pyrolysis conditions on char yield, morphology, and reactivity, Energy Fuels 22 (2008) 2955–62.

[8] Tran DQ, Rai C, Pyrolytic Gasification of Bark, AIChE 75 (184) (1979) 41–9.

[9] Roberts AF, A Review of Kinetic Data for the Pyrolysis of Wood and Related Substances, Combust Flame 14 (2) (1970) 261–72.

[10] Thurner F, Mann U, Kinetic Investigation of Wood Pyrolysis, Ind Eng Chem Process Des Dev 20 (3) (1981) 482–8.

[11] Jegers HF, Klein MT, Primary and Secondary Lignin Pyrolysis Reaction Pathways, Ind Eng Chem Process Des Dev 24 (1) (1985) 173–83.

[12] Shafizadeh F, Introduction to Pyrolysis of Biomass, J Anal Appl Pyrolysis 3 (4) (1982) 283–305.

[13] Sheng C, Azevedo JLT, Modeling biomass devolatilization using the chemical percolation devolatilization model for the main components, Proc Combust Inst 29 (1) (2002) 407–14.

[14] Elfasakhany A, Klason T, Bai XS, Modelling of pulverized wood combustion using a functional group model, Combust Theory Modelling 12 (5) (2008) 883–904.

[15] Koufopanos CA, Maschio G, Lucchesi A, Kinetic Modelling of the Pyrolysis of Biomass and Biomass Components, Can J Chem Ing 67 (1) (1989) 75–84.

[16] Grønli MG, A Theoretical and Experimental Study of the Thermal Degradation of Biomass. PhD thesis, Norwegian University of Science and Technology (1996).

[17] Bellais M, Modelling of the pyrolysis of large wood particles. PhD thesis, KTH Royal Institute of Technology (2007).

[18] Di Blasi C, Modeling chemical and physical processes of wood and biomass pyrolysis, Prog Energy Combust Sci 34 (1) (2008) 47–90.

[19] Di Blasi C, Comparison of semi-global mechanisms for primary pyrolysis of lignocellulosic fuels, J Anal Appl Pyrolysis 47 (1) (1998) 43–64.

[20] Di Blasi C, Modeling and Simulation of Combustion Processes of Charring and Non-Charring Solid Fuels, Prog Energy Combust Sci 19 (1) (1993) 71–104.

[21] Chan WR, Kelbon M, Krieger BB, Modelling and experimental verification of physical and chemical processes during pyrolysis of a large biomass particle, Fuel 64 (11) (1985) 1505–13.

[22] Liden AG, Berruti F, Scott DS, A kinetic model for the production of liquids from the flash pyrolysis of biomass, Chem Eng Comm 65 (1) (1988) 207–21.

[23] Bradbury AGW, Sakai Y, Shafizadeh F, A kinetic model for pyrolysis of cellulose, J Appl Pol Sci 23 (11) (1979) 3271–80.

[24] Shafizadeh F, Bradbury AGW, Thermal Degradation of Cellulose in Air and Nitrogen at Low Temperatures, J Appl Pol Sci 23 (5) (1979) 1431–42.

[25] Ranzi E, Cuoci A, Faravelli T, Frassoldati A, Migliavacca G, Pierucci S et al., Chemical kinetics of biomass pyrolysis, Energy & Fuels 22 (6) (2008) 4292–300.

[26] Debiagi PE, Pecchi C, Gentile G, Frassoldati A, Cuici A, Ranzi E et al., Extractives extend the applicability of multistep kinetic scheme of biomass pyrolysis, Energy & Fuels 29 (10) (2015) 6544–55.

[27] Nik-Azar M, Hajaligol MR, Sohrabi M, Dabir B, Mineral matter effects in rapid pyrolysis of beechwood, Fuel Process Technol 51 (1-2) (1997) 7–17.

[28] Jensen AD, Dam-Johansen K, Wojtowicz MA, Serio MA, TG-FTIR Study of the Influence of Potassium Chloride on Wheat Pyrolysis, Energy Fuels 12 (5) (1998) 929–38.

[29] Umeki K, Kirtania K, Chen L, Bhattacharya S, Fuel Particle Conversion of Pulverized Biomass during Pyrolysis in an Entrained Flow Reactor, Ind Eng Chem Res 51 (2012) 13973–9.

[30] Lede J, Authier O, Characterization of biomass fast pyrolysis: Advantages and drawbacks of different possible criteria, Biomass Conv Bioref 1 (2011) 133–47.

[31] Narayan R, Antal MJ, Thermal lag, fusion and the compensation effect during biomass pyrolysis, Ind Eng Chem 35 (1996) 1711–21.

[32] Umeki K, Biswas AK, Simplification of devolatilization models for thermally-thick particles: Differences between wood logs and pellets, Chem Eng J 274 (2015) 181–91.

[33] Trubetskaya A, PA Jensen, Jensen AD, Steibel M, Spliethoff H, Glarborg P, Influence of fast pyrolysis conditions on yield and structural transformation of biomass char, Fuel Process Technol 140 (2015) 205–14.

[34] Trubetskaya A, Jensen PA, Garcia Llamas AD, Umeki K, Jensen AD,

Glarborg P, Effect of fast pyrolysis conditions on biomass solid residues at high temperatures, Fuel Process Tech 143 (2016) 118–29.

[35] Hajaligol MR, Howard JB, Longwell JP, Peters WA, An Experimental and Modeling Study of Pressure Effects on Tar Release by Rapid Pyrolysis of Cellulose Sheets in a Screen Heater, Combust Flame 95 (1993) 47–60.

[36] Miller RS, Bellan J, Tar Yield and Collection from the Pyrolysis of Large Biomass Particles, Combust Sci Tech 127 (1-6) (1997) 97–118.

[37] Boutin O, Ferrer M, Lede J, Flash pyrolysis of cellulose pellets submitted to a concentrated radiation: experiments and modeling, Chem Eng Sci 57 (2002) 15–25.

[38] Liu Q, Wang S, Wang K, Guo X, Luo Z, Cen K, Mechanism of Formation and Consequent Evolution of Active Cellulose during Cellulose Pyrolysis, Acta Phys Chim Sin 24 (11) (2008) 1957–63.

[39] Dauenhauer PJ, Colby JL, Balonek CM, Suszynski WJ, Schmidt LD, Reactive boiling of cellulose for integrated catalysis through an intermediate liquid, Green Chem 11 (2009) 1555–61.

[40] Teixeira AR, Mooney KG, Kruger JS, Williams CL, Suszynski WJ, Schmidt LD and etc., Aerosol generation by reactive boiling ejection of molten cellulose, Energy Environ Sci 4 (2011) 4306–21.

[41] Jepsen MS, Pyrolysis of Large Biomass Particles in a Single Particle Combustion Reactor. MSc thesis, DTU Chemical Engineering, Technical University of Denmark (2014).

[42] Anca-Couce A, Zobel N, Numerical analysis of a biomass pyrolysis particle model: Solution method optimized for the coupling to reactor models, Fuel 97 (2012) 80–8.

[43] Arseneau DF, Competitive Reactions in the Thermal Decomposition of Cellulose, Can J Chem 49 (4) (1971) 632–8.

[44] Mok WSL, Antal MJ, Effects of pressure on biomass pyrolysis. I. Cellulose pyrolysis products, Thermochimica Acta 68 (1983) 155–64.

[45] Koufopanos CA, Papayannakos N, Maschio G, Lucchesi A, Modelling of the Pyrolysis of Biomass Particles. Studies on Kinetics, Thermal and Heat Transfer Effects, Can J Chem Ing 69 (4) (1991) 907–15.

[46] Haseli Y, van Oijen JA, de Goey LPH, Modeling biomass particle pyrolysis with temperature-dependent heat of reactions, J Anal Appl Pyrolysis 90 (2) (2011) 140–54.

[47] Haseli Y, van Oijen JA, de Goey LPH, Numerical study of the conversion time of single pyrolyzing biomass particles at high heating conditions, Chem Eng J 169 (2011) 299–312.

[48] Mack CH, Donaldson DJ, Effects of Bases on the Pyrolysis of Cotton Cellulose, Textile Research J 37 (12) (1967) 1063–71.

[49] Rath J, Wolfinger MG, Steiner G, Krammer G, Barontini F, Cozzani V, Heat of wood pyrolysis, Fuel 82 (2003) 81–91.

[50] Gubba SR, Ma L, Pourkashanian M, Williams A, Influence of particle shape and internal thermal gradients of biomass particles on pulverized

coal/biomass co-fired flames, Fuel Process Technol 92 (11) (2011) 2185–95.

[51] Qin K, Lin W, Jensen PA, Jensen AD, High-temperature entrained flow gasification of biomass, Fuel 93 (2012) 589–600.

[52] Ragland KW, Boerger JC, Baker AJ, A model of chunkwood combustion, Forest Prod J 38 (1988) 27–32.

[53] Borman GL, Ragland KW, Combustion engineering, McGraw Hill Book Company, 1998.

[54] Tosun I, Modeling in Transport Phenomena. A conceptual approach, Elsevier, 2007.

[55] Clement KH, Fangel P, Jensen AD, Thomsen K, Kemiske enhedsoperationer, Polyteknisk Forlag, 2004.

[56] Alves SS, Figueiredo JL, A model for pyrolysis of wet wood, Chem Eng Sci 44 (12) (1989) 2861–9.

[57] Janse AMC, Westerhout RWJ, Prins W, Modelling of flash pyrolysis of a single wood particle, Chem Eng Proc 39 (3) (2000) 239–52.

[58] Bryden KM, Hagge MJ, Modeling the combined impact of moisture and char shrinkage on the pyrolysis of a biomass particle, Fuel 82 (13) (2003) 1633–44.

[59] Fan LS, Miyanami K, Chen TY, Walawender WP, A mathematical model for pyrolysis of a solid particle: Effects of the Lewis number, Can J Chem Eng 55 (1) (1977) 47–53.

[60] Celaya EA, Aguirrezabala JJA, Chatzipantelidis P, Implementation of an Adaptive BDF2 Formula and Comparison with the MATLAB ode15s, Proc Comp Sci 29 (2014) 1014–26.

[61] Lu H, Robert W, Peirce G, Ripa B, Baxter LL, Comprehensive Study of Biomass Particle Combustion, Energy Fuels 22 (4) (2008) 2826–39.

[62] Jensen PA, Sander B, Dam-Johansen K, Pretreatment of Straw for Power Production, Biomass Bioenergy 20 (6) (2001) 431–46.

[63] Miller RS, Bellan J, Numerical Simulation of Vortex Pyrolysis Reactors for Condensable Tar Production from Biomass, Energy Fuels 12 (1) (1998) 25–40.

[64] Perry R, Perry's chemical engineers' handbook, McGraw Hill Book Company, 2007.

[65] Di Blasi C, Russo G, Modeling of Transport Phenomena and Kinetics of Biomass Pyrolysis, Adv Thermochem Biomass Conv (1994) 906–21.

[66] Di Blasi C, Modelling the Fast Pyrolysis of Cellulosic Particles in Fluid-Bed Reactors, Chem Eng Sci 55 (24) (2000) 5999–6013.

[67] Johansen JM, Jensen PA, Glarborg P, Mancini M, Weber R, Mitchell RE, Extension of apparent devolatilization kinetics from thermally think to thermally thick particles in zero dimensions for wood biomass, Energy 95 (2016) 279–90.

[68] Solomon PR, Hamblen DG, Carangelo RM, Serio MA, Deshpande GV, General Model of Coal Devolatilization, Energy Fuels 2 (1988) 405–22.

[69] Trubetskaya A, Jensen PA, Glarborg P, Steibel M, Spliethoff H, Hofmann Larsen F, Comparison of high temperature chars of wheat straw and rice husk with respect to chemistry, morphology and reactivity, Biomass Bioenergy 86 (2016) 76–87.

[70] Trubetskaya A, Fast pyrolysis of biomass at high temperatures. PhD thesis, Technical University of Denmark (2016).

Supplemental material

Click here to download Supplementary Interactive Plot Data (CSV): supplemental_material_revised.pdf

LaTeX Source Files bibtex

Click here to download LaTeX Source Files: myref6.bib

LaTeX Source Files supplemental material

Click here to download LaTeX Source Files: supplemental_material_revised.tex

LaTeX Source Files manuscript with marked changes

Click here to download LaTeX Source Files: article6_20160918_revised_marked_corrections.tex

LaTeX Source Files manuscript without marked changes

Click here to download LaTeX Source Files: article6_20160918_revised.tex

image12.pdf

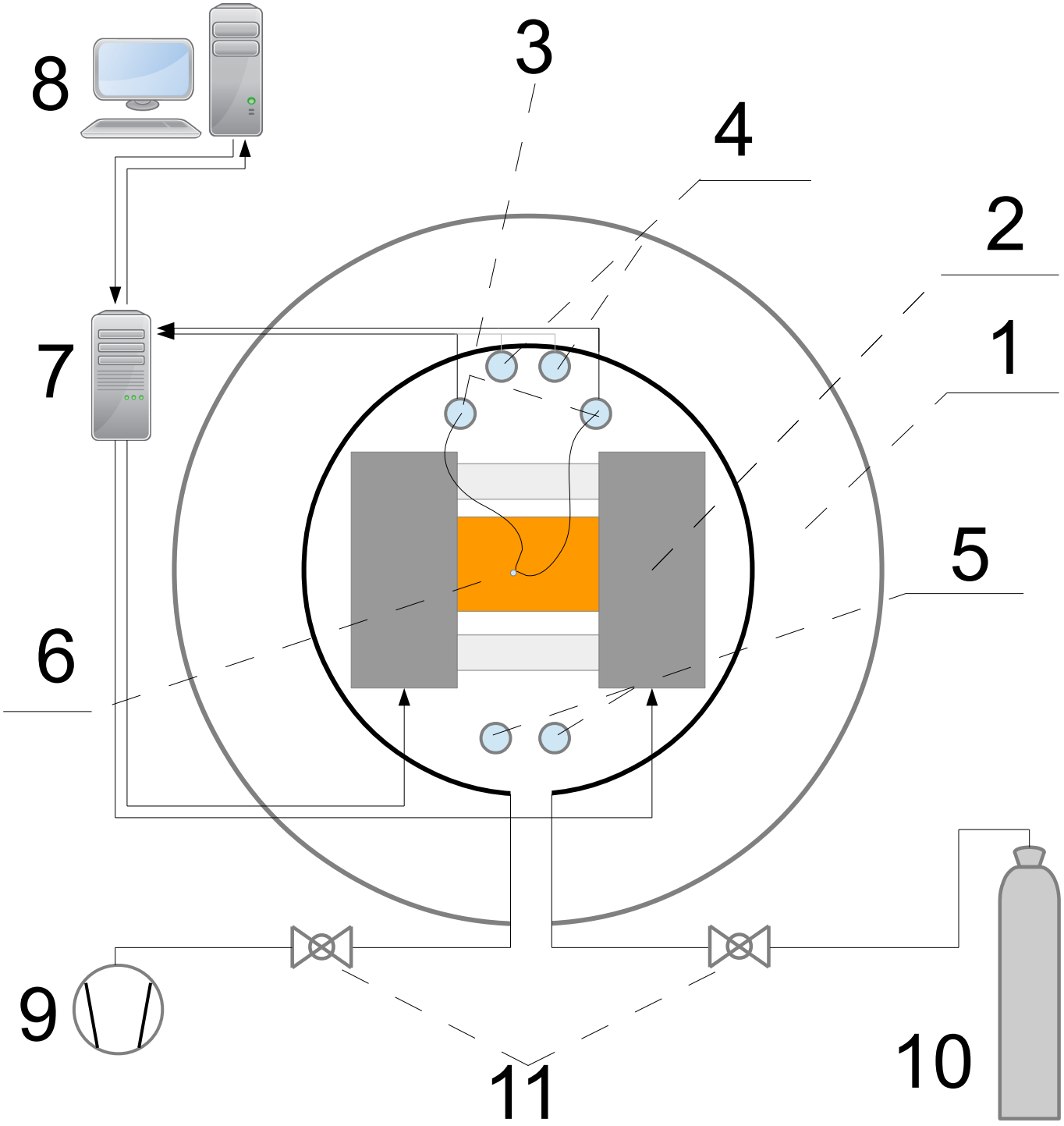

image13.jpg
Click here to download high resolution image

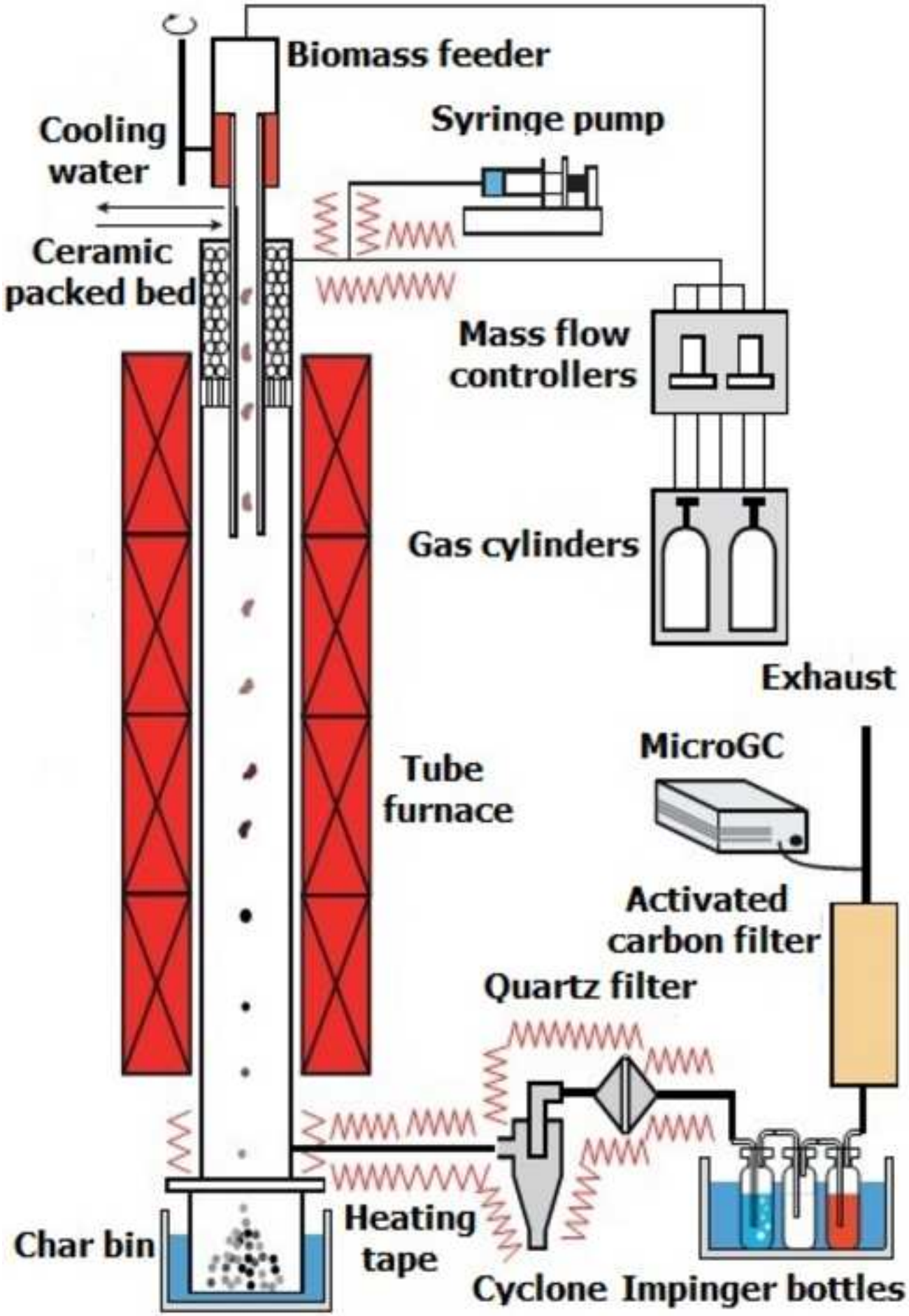

image14.pdf

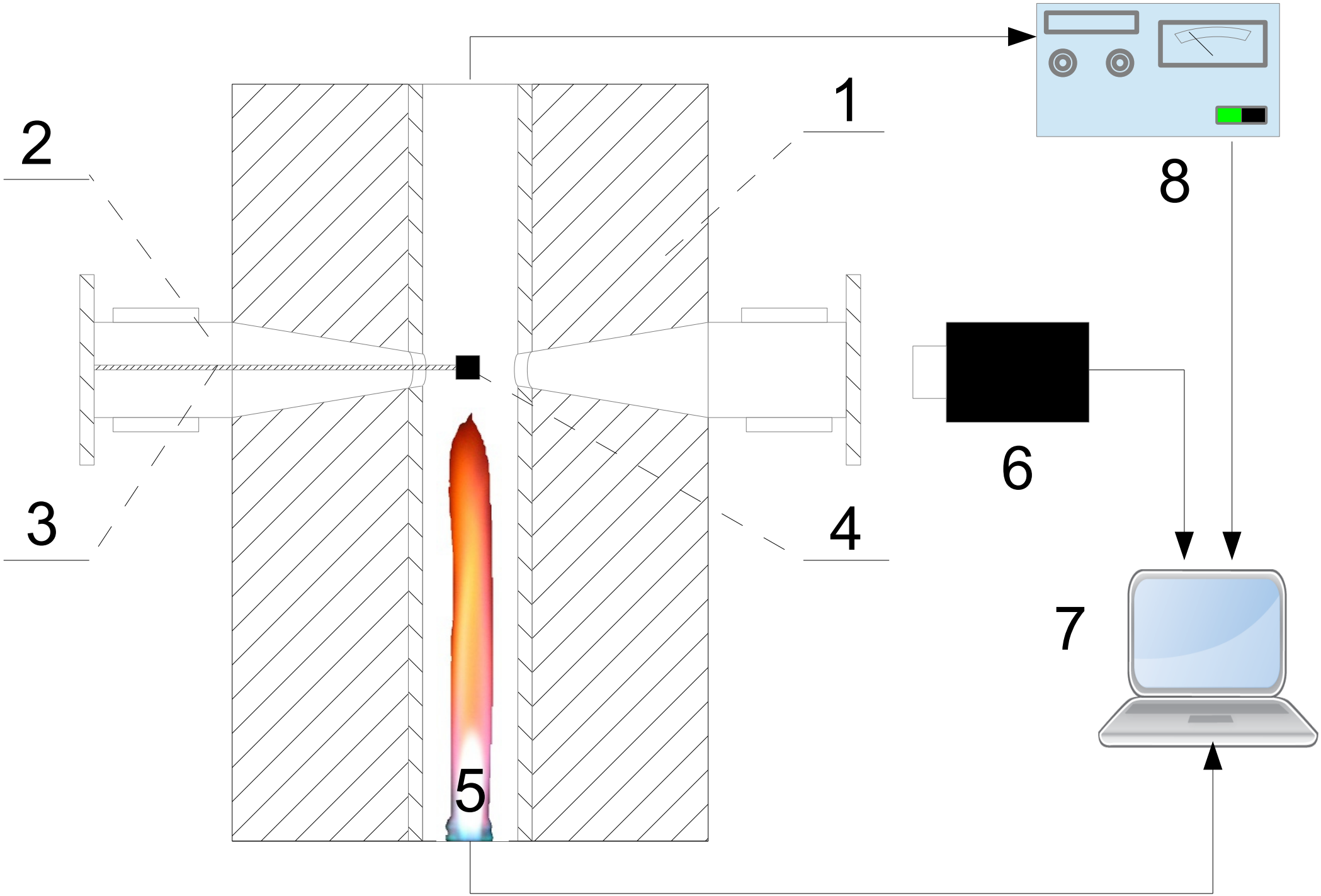

image15.pdf

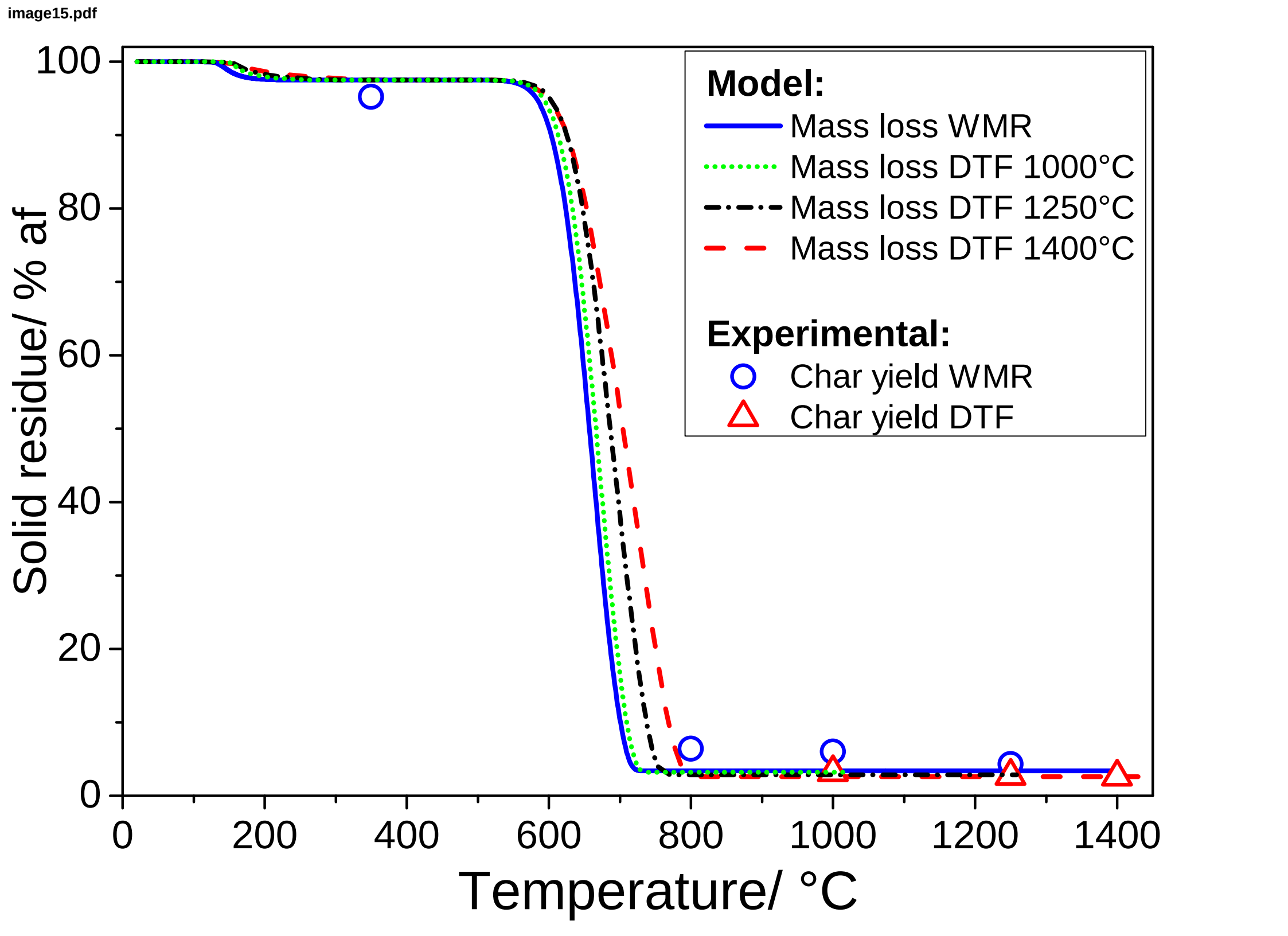
Model:
Mass loss WMR
Mass loss DTF 1000°C
Mass loss DTF 1250°C
Mass loss DTF 1400°C
Experimental:
Char yield WMR
Char yield DTF
Solid residue/ % af
Temperature/ °C
0
20
40
60
80
100
0
200
400
600
800
1000
1200
1400

image16.pdf

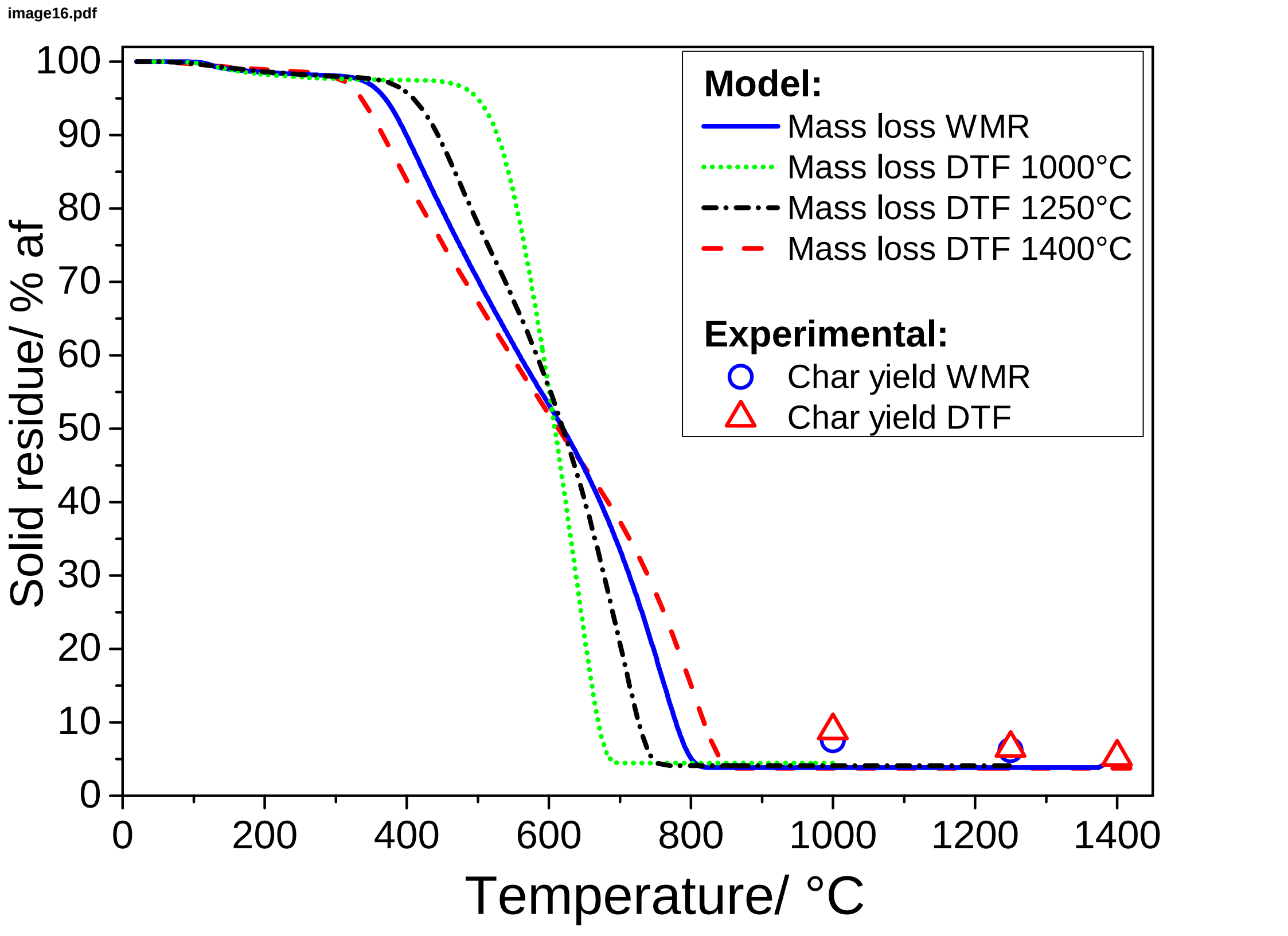
Model:
Mass loss WMR
Mass loss DTF 1000°C
Mass loss DTF 1250°C
Mass loss DTF 1400°C
Experimental:
Char yield WMR
Char yield DTF
Solid residue/ % af
Temperature/ °C
0
10
20
30
40
50
60
70
80
90
100
0
200
400
600
800
1000
1200
1400

image17.pdf

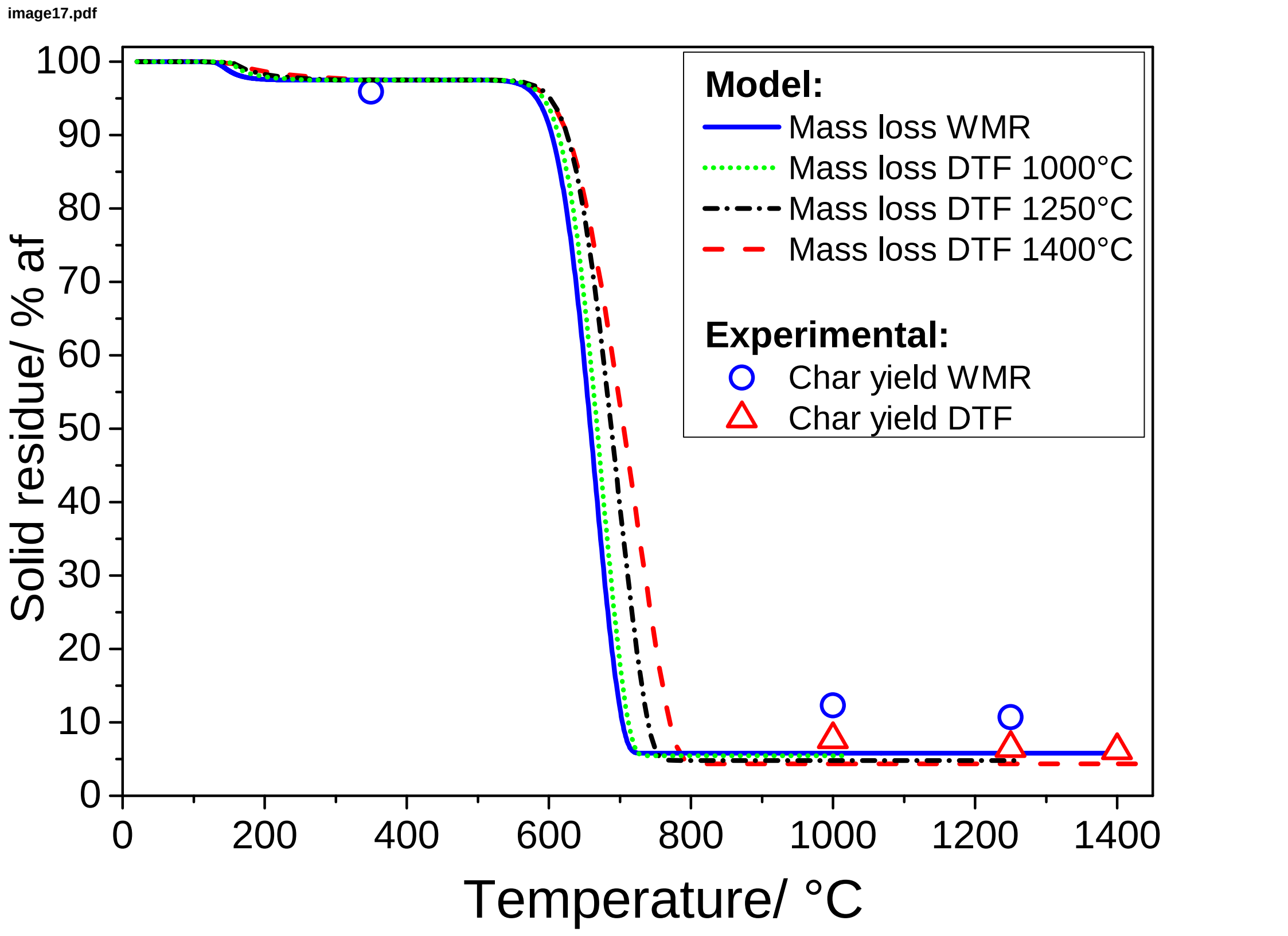
Model:
Mass loss WMR
Mass loss DTF 1000°C
Mass loss DTF 1250°C
Mass loss DTF 1400°C
Experimental:
Char yield WMR
Char yield DTF
Solid residue/ % af
Temperature/ °C
0
10
20
30
40
50
60
70
80
90
100
0
200
400
600
800
1000
1200
1400

image18.pdf

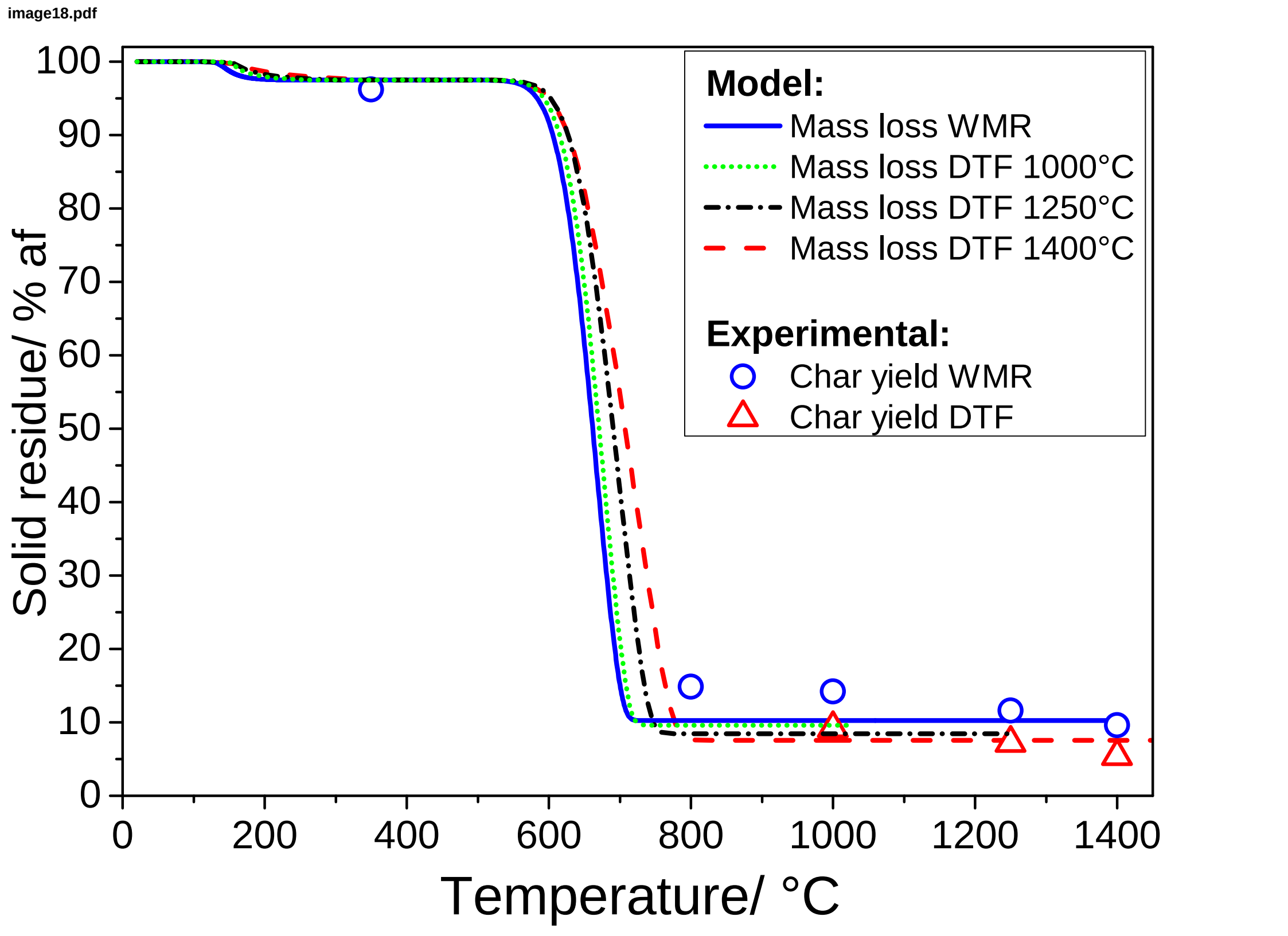
Model:
Mass loss WMR
Mass loss DTF 1000°C
Mass loss DTF 1250°C
Mass loss DTF 1400°C
Experimental:
Char yield WMR
Char yield DTF
Solid residue/ % af
Temperature/ °C
0
10
20
30
40
50
60
70
80
90
100
0
200
400
600
800
1000
1200
1400

image19.pdf

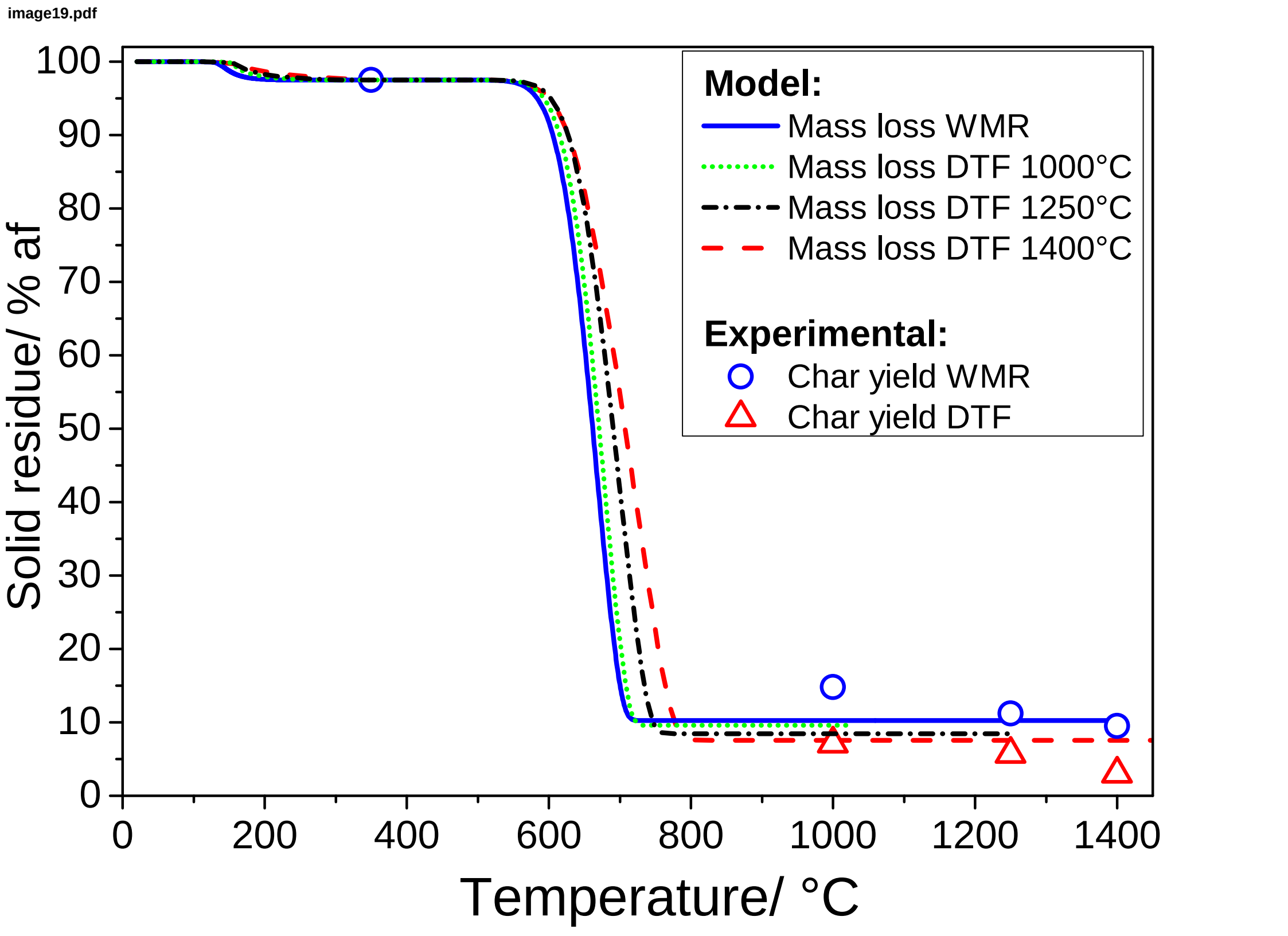
Model:
Mass loss WMR
Mass loss DTF 1000°C
Mass loss DTF 1250°C
Mass loss DTF 1400°C
Experimental:
Char yield WMR
Char yield DTF
Solid residue/ % af
Temperature/ °C
0
10
20
30
40
50
60
70
80
90
100
0
200
400
600
800
1000
1200
1400

image20.pdf

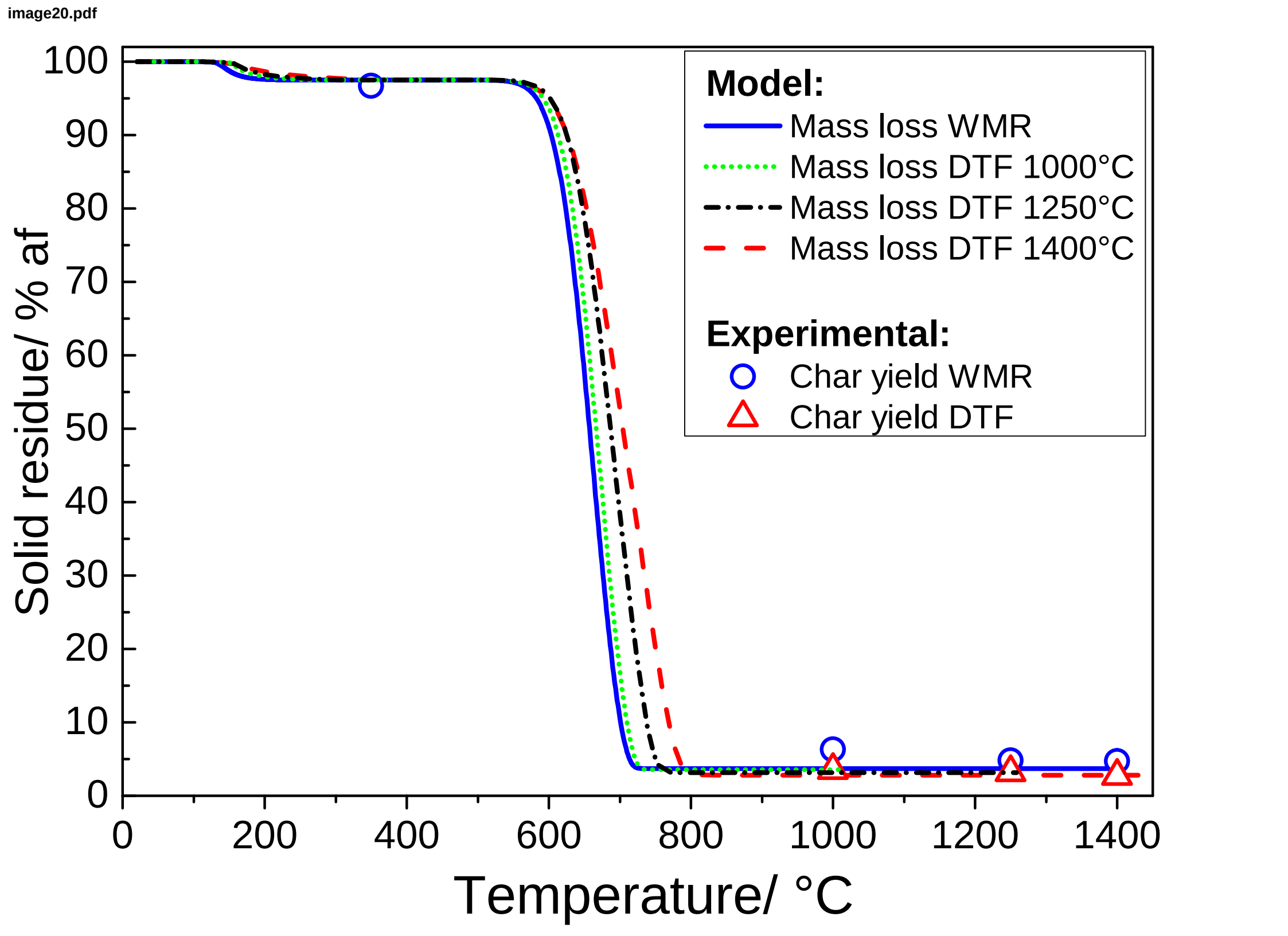
Model:
Mass loss WMR
Mass loss DTF 1000°C
Mass loss DTF 1250°C
Mass loss DTF 1400°C
Experimental:
Char yield WMR
Char yield DTF
Solid residue/ % af
Temperature/ °C
0
10
20
30
40
50
60
70
80
90
100
0
200
400
600
800
1000
1200
1400

image24.pdf

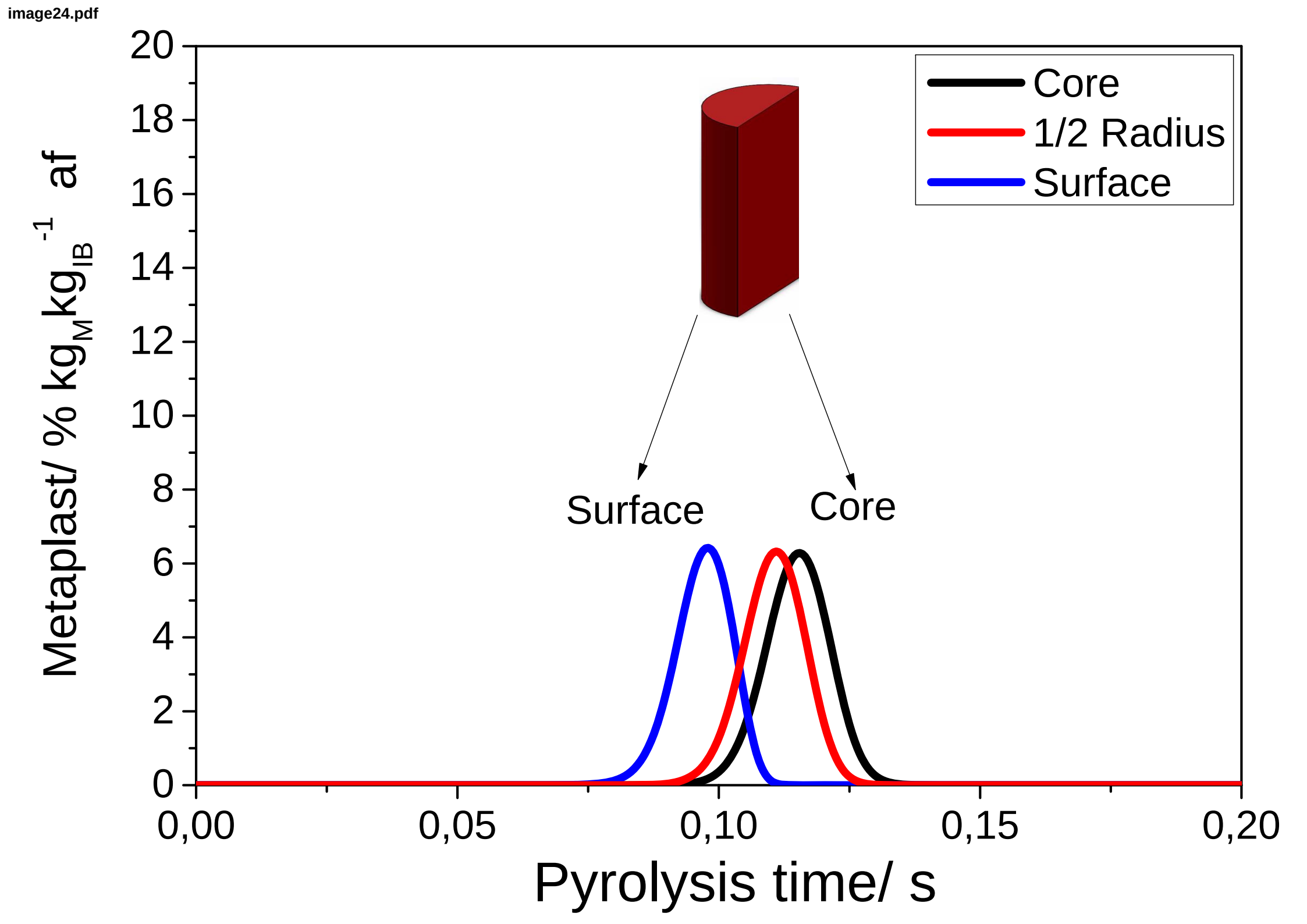
Core
1/2 Radius
Surface
Surface
Core
Metaplast/ % kg$_M$kg$_{IB}$$^{-1}$ af
Pyrolysis time/ s
0
2
4
6
8
10
12
14
16
18
20
0,00
0,05
0,10
0,15
0,20

image25.pdf

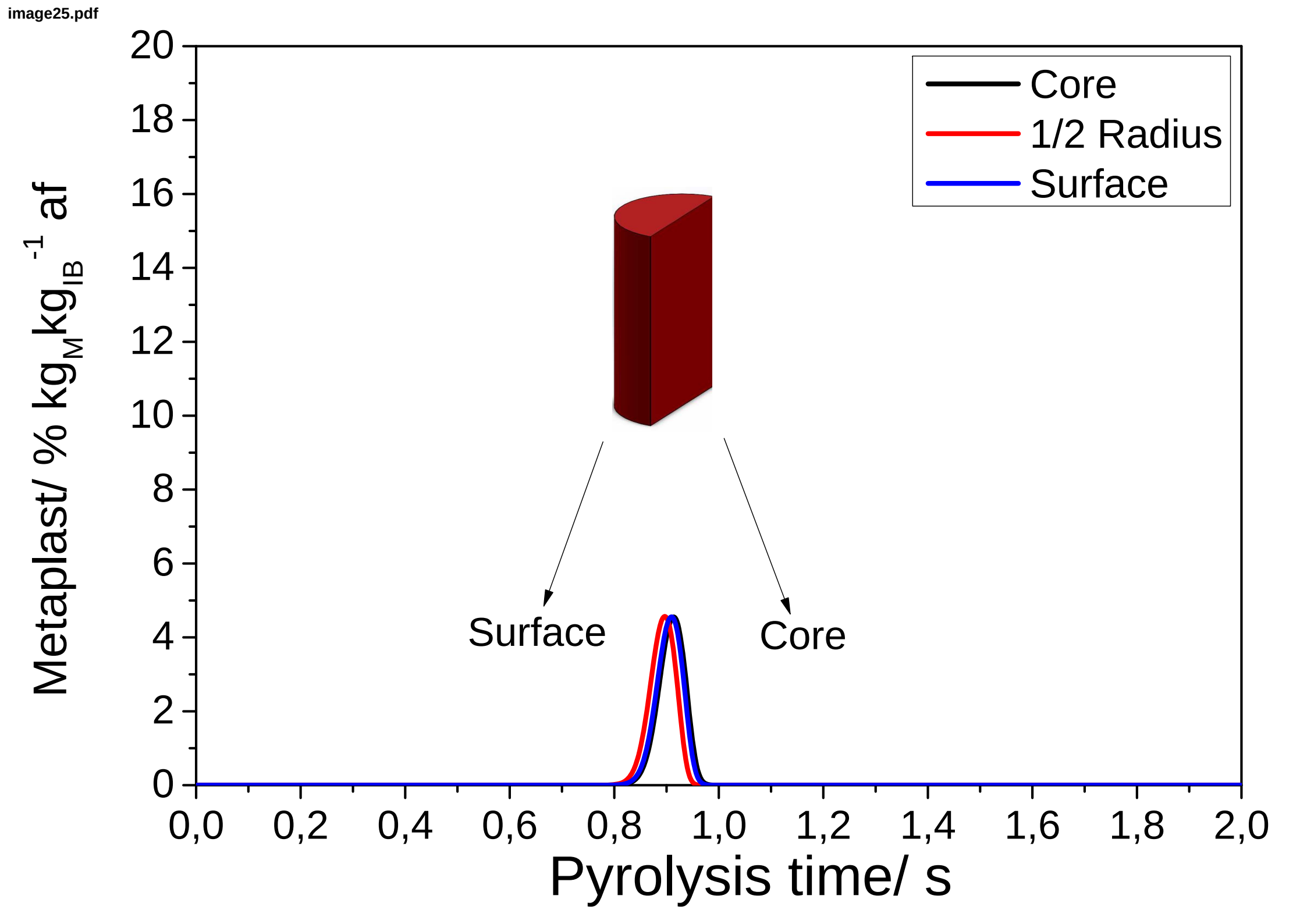
Core
1/2 Radius
Surface
Surface
Core
Metaplast/ % kg$_M$kg$_{IB}^{-1}$ af
Pyrolysis time/ s
0
2
4
6
8
10
12
14
16
18
20
0,0
0,2
0,4
0,6
0,8
1,0
1,2
1,4
1,6
1,8
2,0

image26.pdf

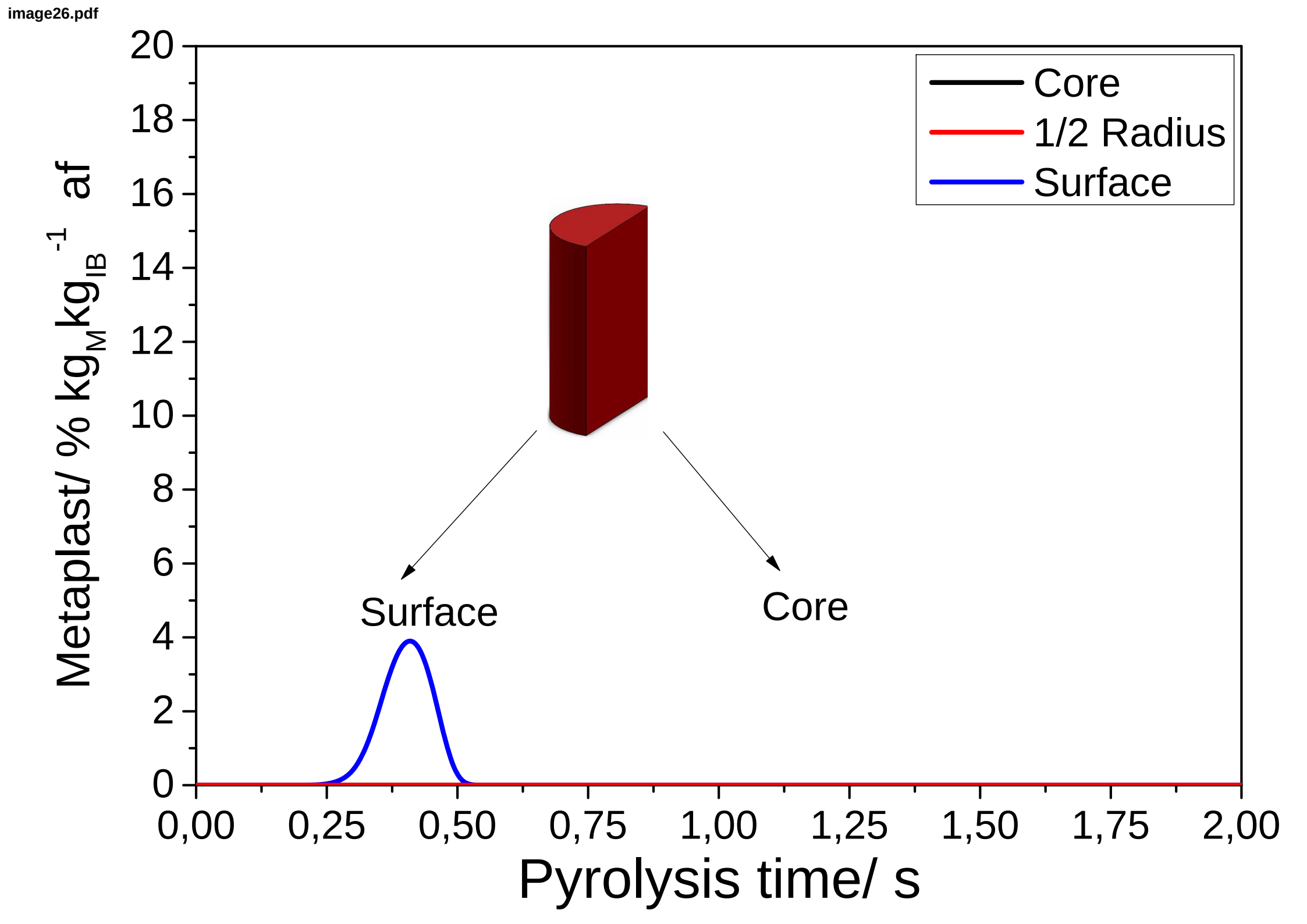
Core
1/2 Radius
Surface
Surface
Core
Metaplast/ % kg$_M$kg$_{IB}^{-1}$ af
Pyrolysis time/ s
0
2
4
6
8
10
12
14
16
18
20
0,00
0,25
0,50
0,75
1,00
1,25
1,50
1,75
2,00

image28.pdf

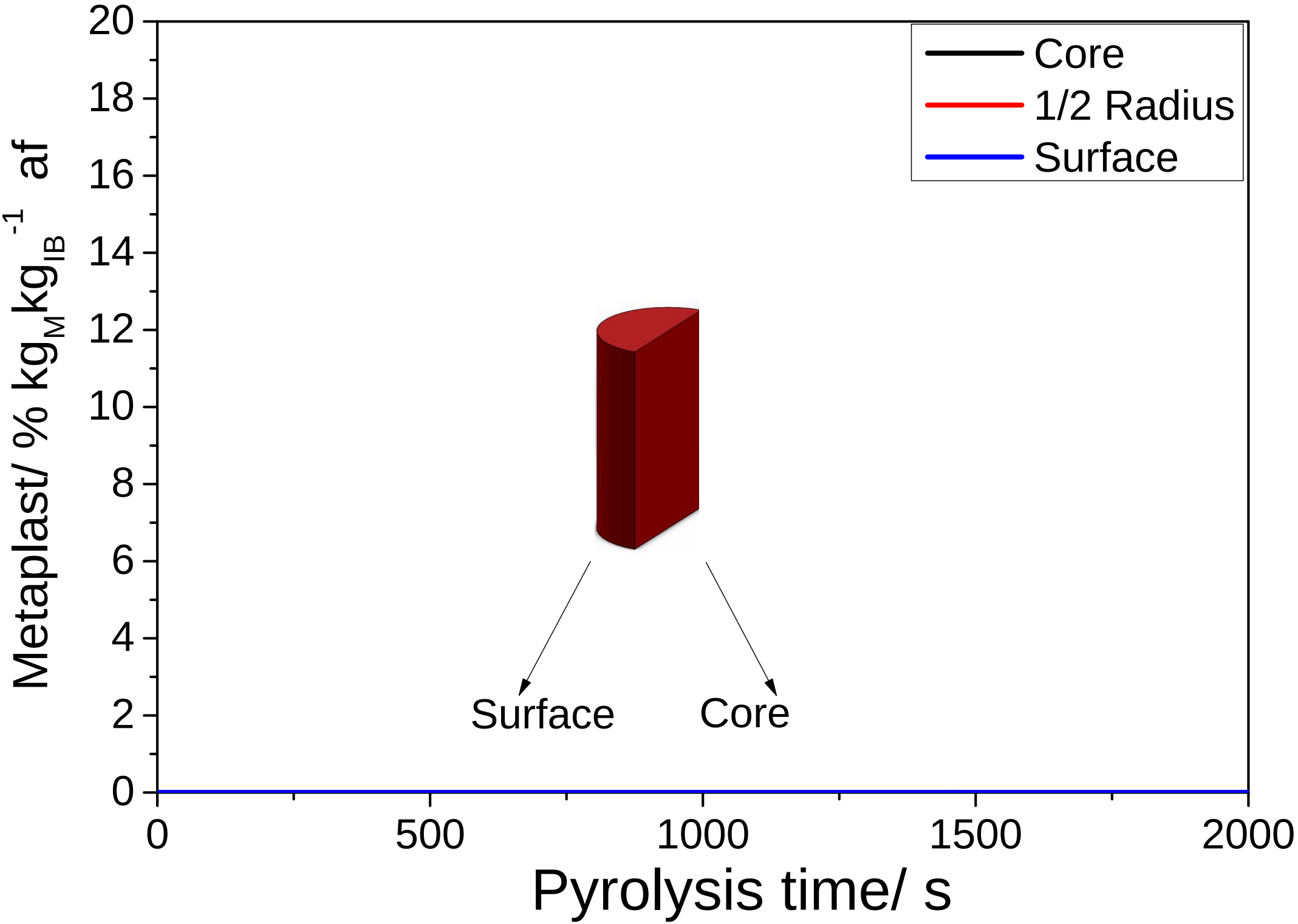
Core
1/2 Radius
Surface
Metaplast/ % kg$_M$kg$_{IB}$$^{-1}$ af
Pyrolysis time/ s
0
2
4
6
8
10
12
14
16
18
20
0
500
1000
1500
2000
Surface
Core

image29.pdf

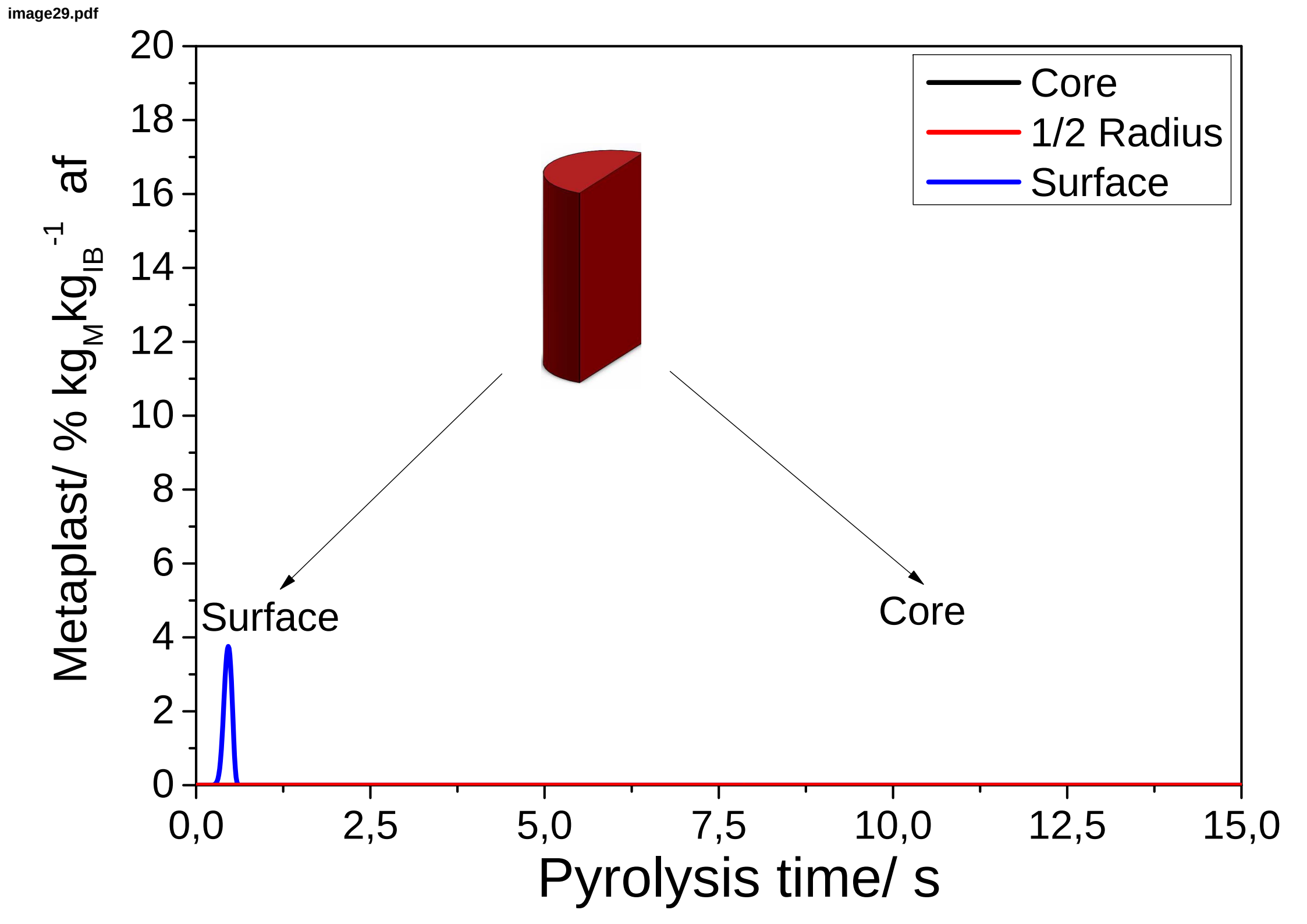
Core
1/2 Radius
Surface
Surface
Core
Metaplast/ % $kg_M kg_{IB}^{-1}$ af
Pyrolysis time/ s
0
2
4
6
8
10
12
14
16
18
20
0,0
2,5
5,0
7,5
10,0
12,5
15,0

image30.pdf

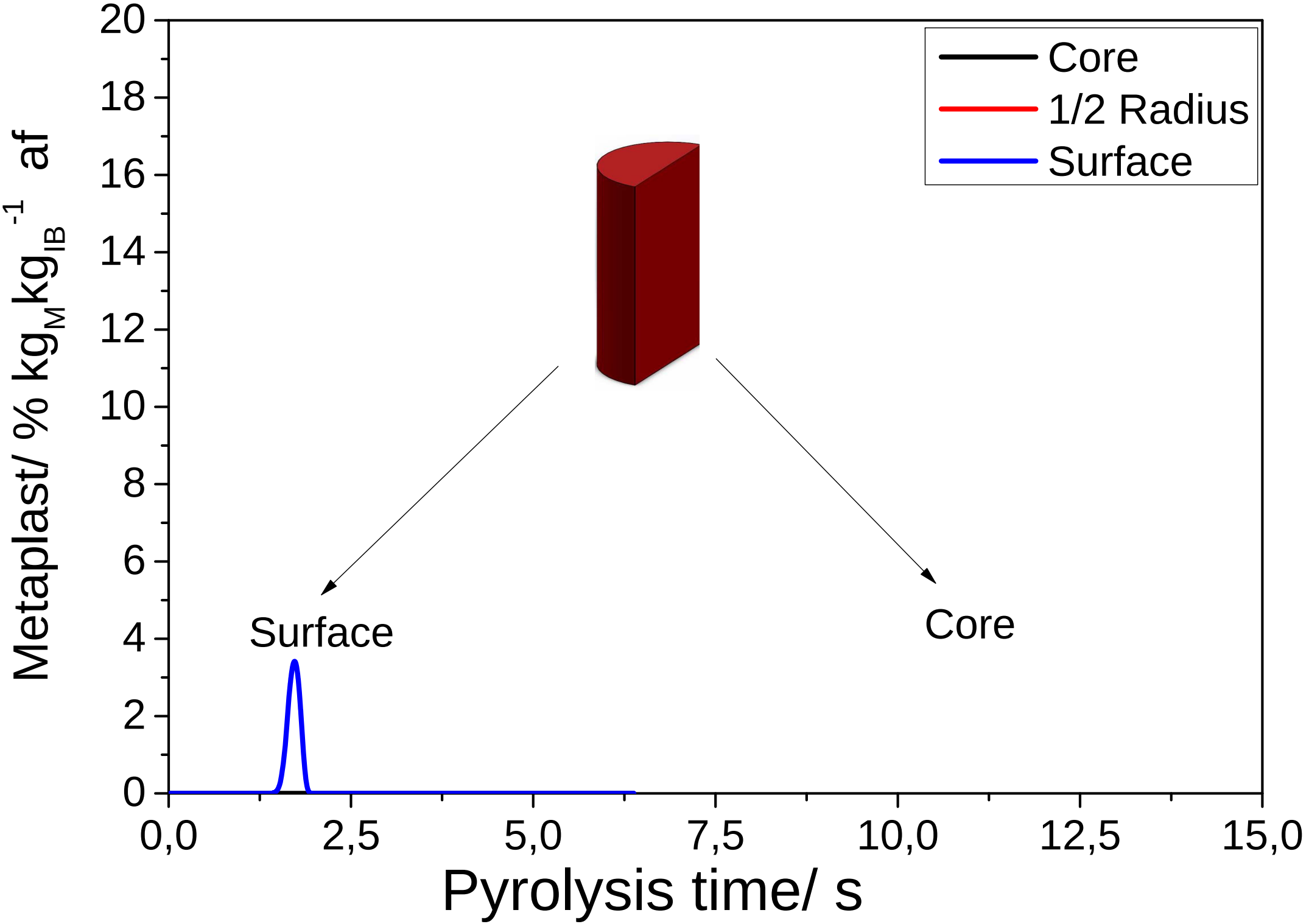
Core
1/2 Radius
Surface
Surface
Core
Metaplast/ % kg$_M$kg$_{IB}^{-1}$ af
Pyrolysis time/ s
0
2
4
6
8
10
12
14
16
18
20
0,0
2,5
5,0
7,5
10,0
12,5
15,0

image32.pdf

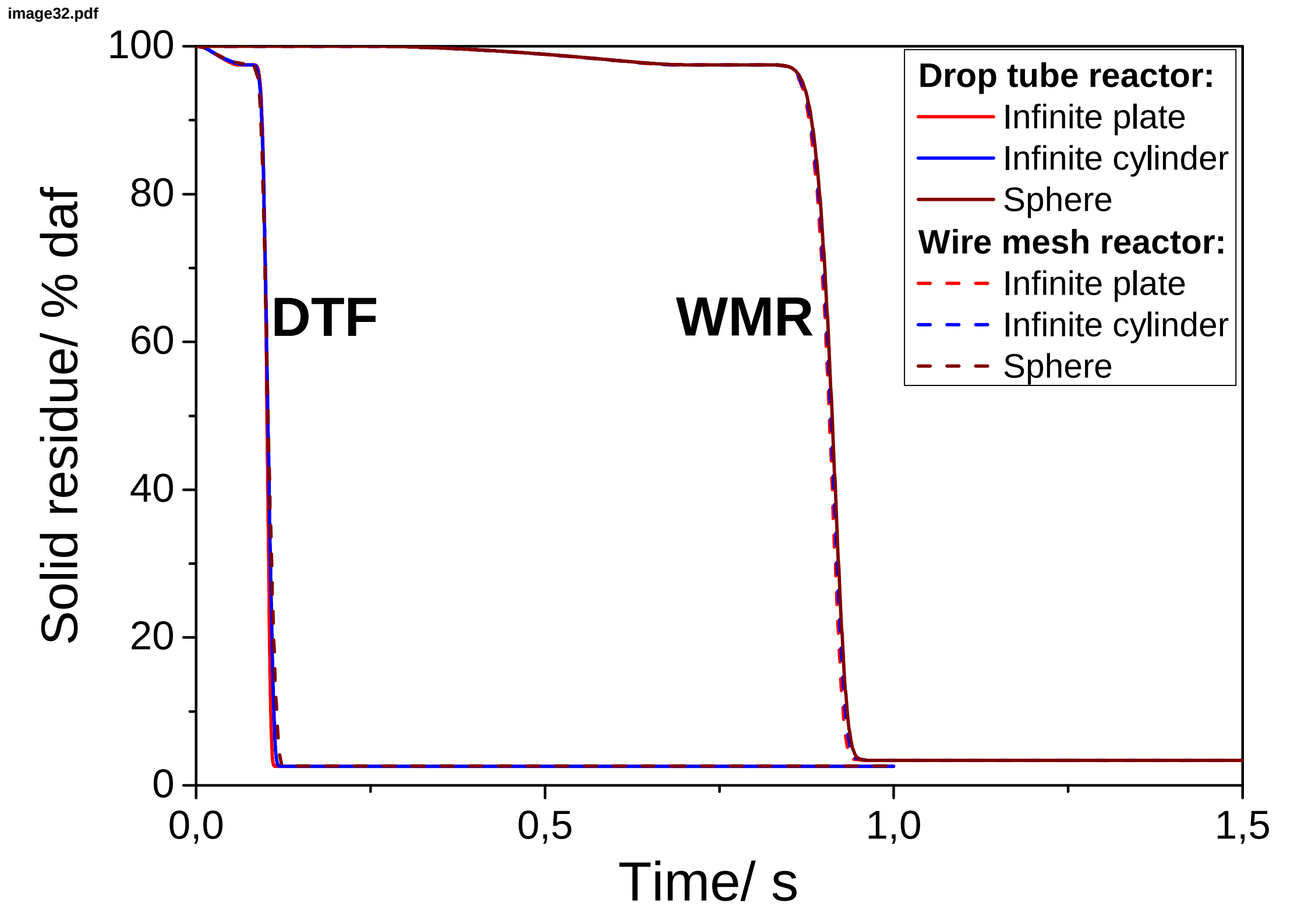
Drop tube reactor:
Infinite plate
Infinite cylinder
Sphere
Wire mesh reactor:
Infinite plate
Infinite cylinder
Sphere
DTF
WMR
Solid residue/ % daf
Time/ s
100
80
60
40
20
0
0,0
0,5
1,0
1,5

image33.pdf

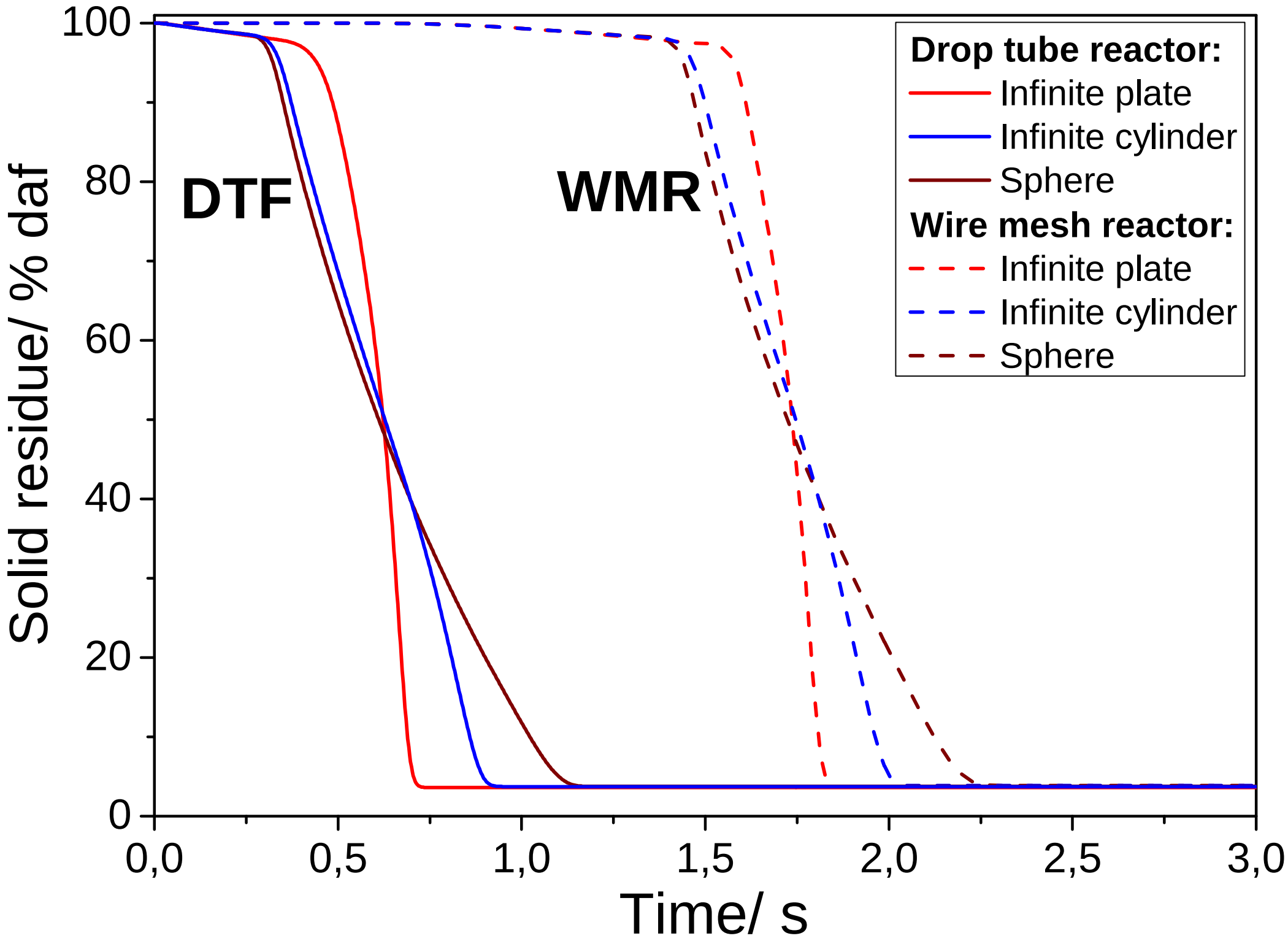
Drop tube reactor:
Infinite plate
Infinite cylinder
Sphere
Wire mesh reactor:
Infinite plate
Infinite cylinder
Sphere
DTF
WMR
Solid residue/ % daf
Time/ s
100
80
60
40
20
0
0,0
0,5
1,0
1,5
2,0
2,5
3,0

image36.pdf

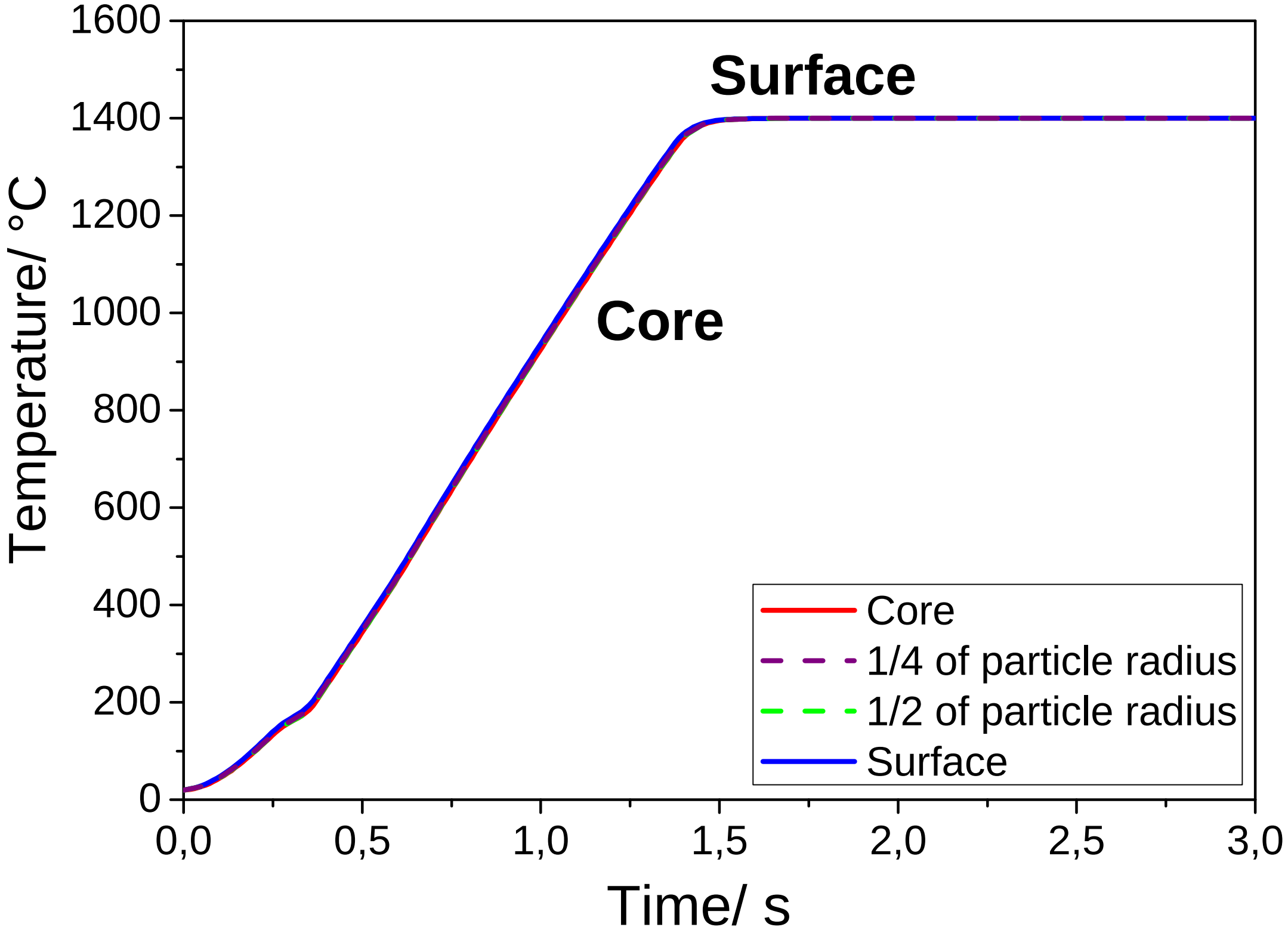
Surface
Core
Temperature/ °C
Time/ s
1600
1400
1200
1000
800
600
400
200
0
0,0
0,5
1,0
1,5
2,0
2,5
3,0
Core
1/4 of particle radius
1/2 of particle radius
Surface

image37.pdf

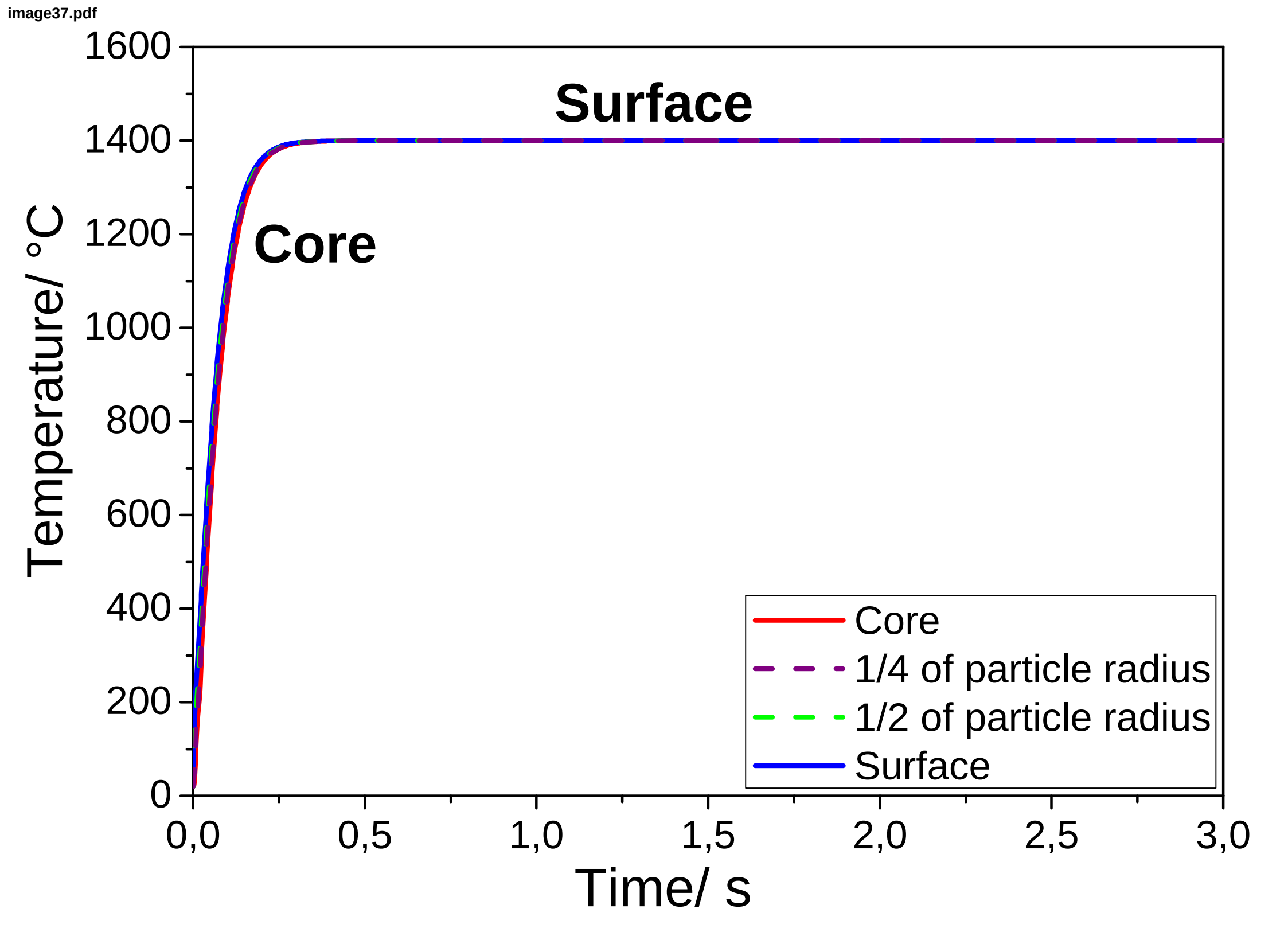
Surface
Core
Temperature/ °C
Time/ s
1600
1400
1200
1000
800
600
400
200
0
0,0
0,5
1,0
1,5
2,0
2,5
3,0
Core
1/4 of particle radius
1/2 of particle radius
Surface

image38.pdf

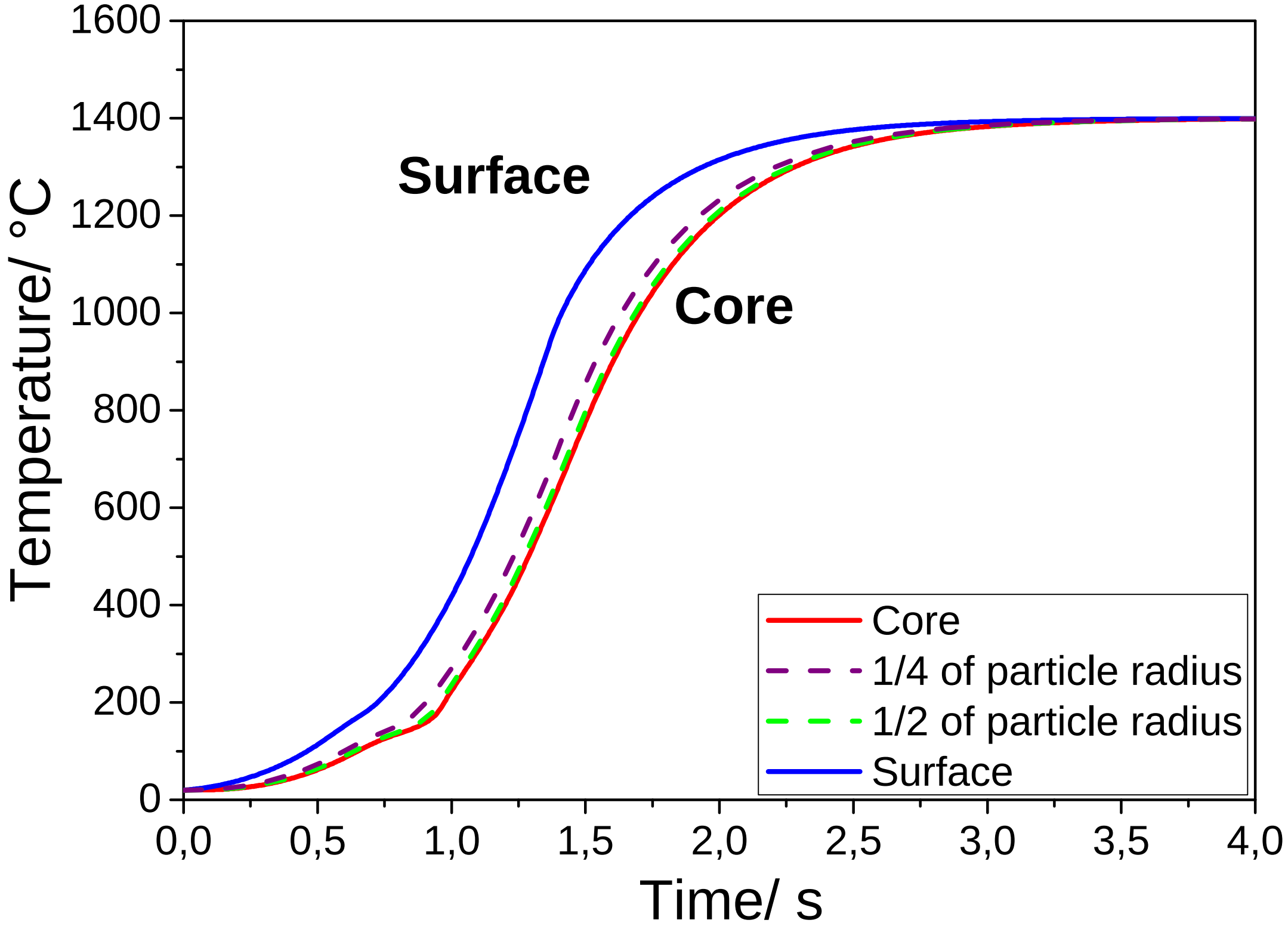
Surface
Core
Temperature/ °C
Time/ s
1600
1400
1200
1000
800
600
400
200
0
0,0
0,5
1,0
1,5
2,0
2,5
3,0
3,5
4,0
Core
1/4 of particle radius
1/2 of particle radius
Surface

image39.pdf

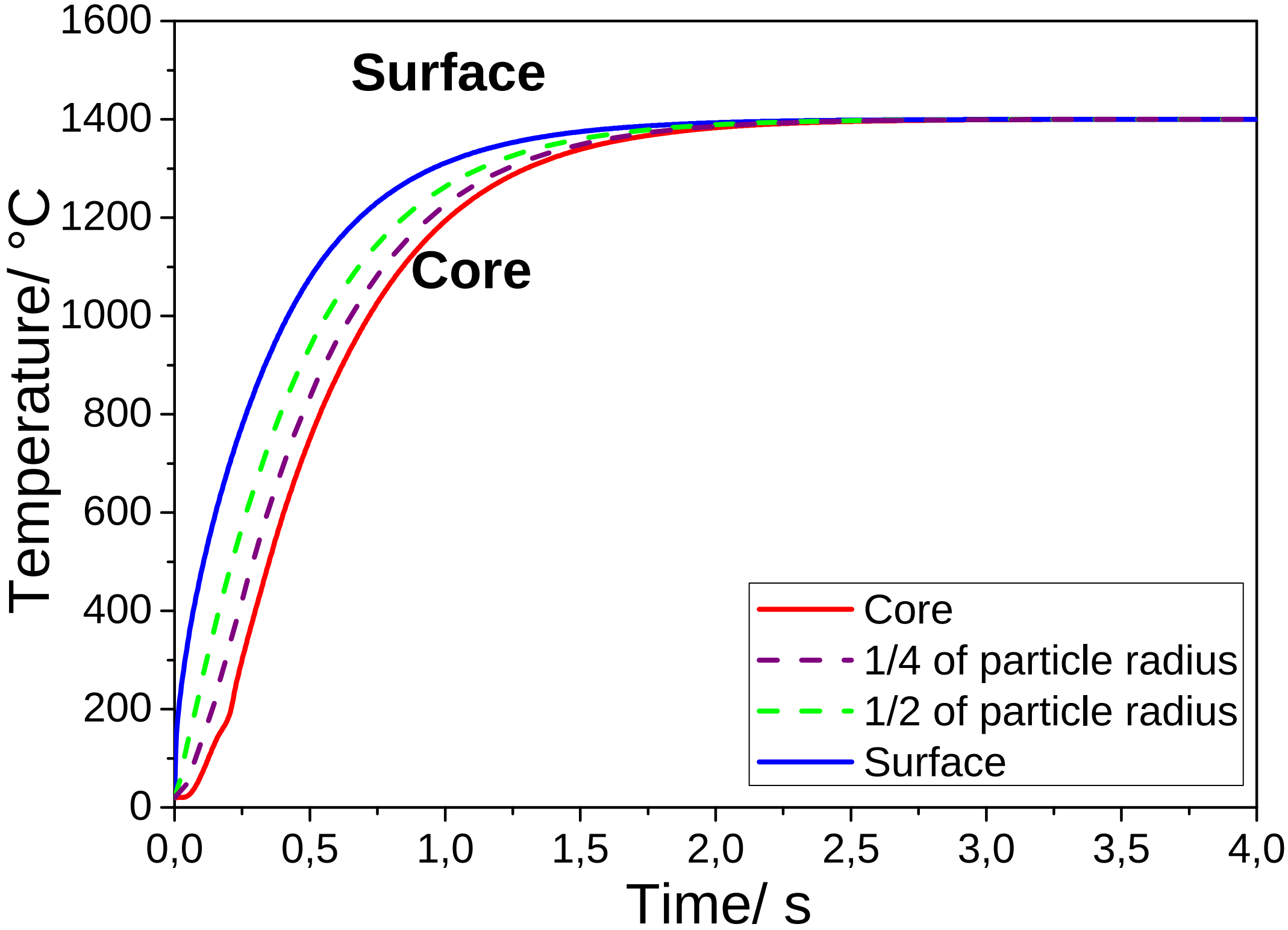
Surface
Core
Temperature/ °C
Time/ s
1600
1400
1200
1000
800
600
400
200
0
0,0
0,5
1,0
1,5
2,0
2,5
3,0
3,5
4,0
Core
1/4 of particle radius
1/2 of particle radius
Surface

image40.pdf

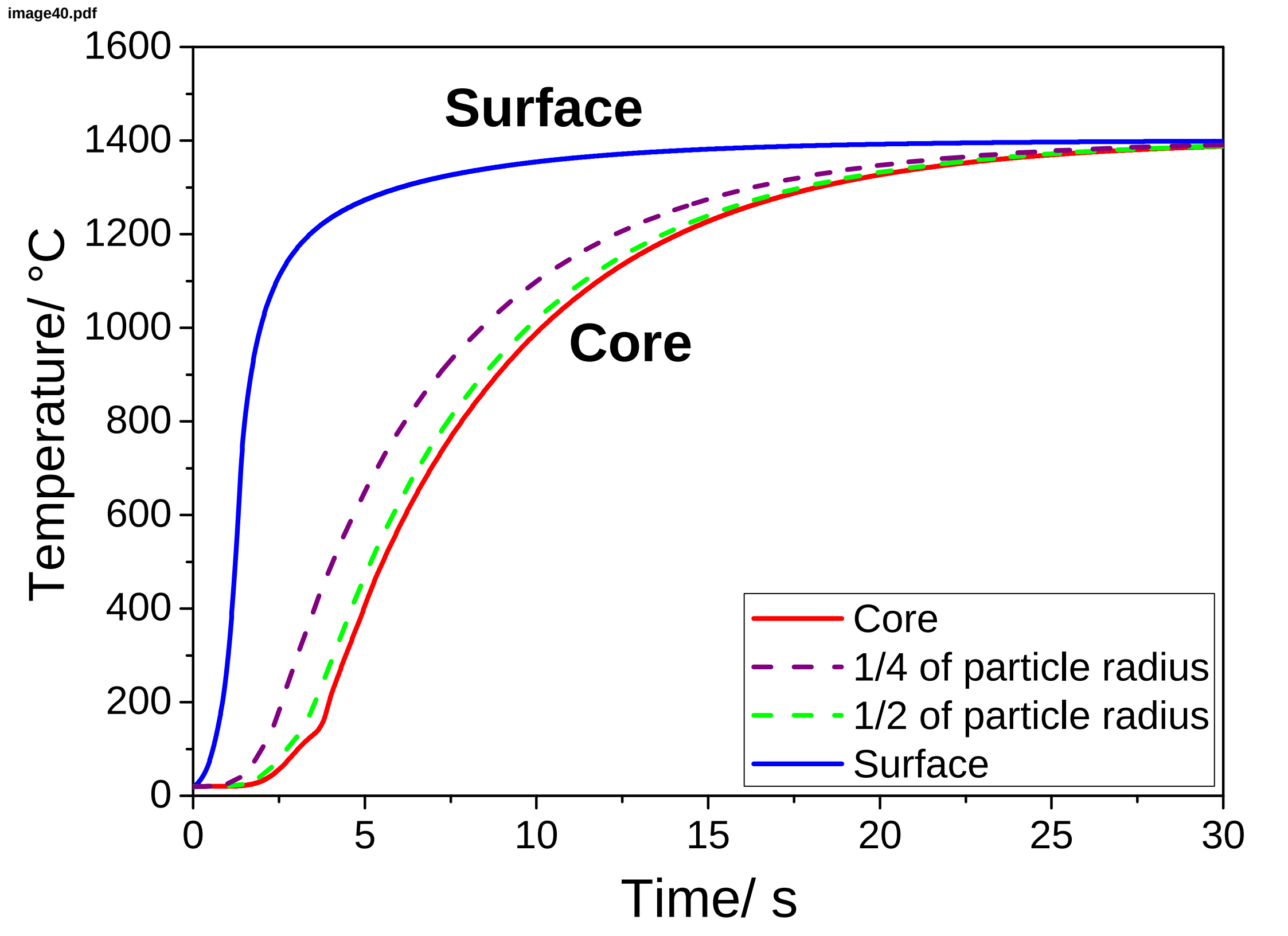
Surface
Core
Temperature/ °C
Time/ s
0
200
400
600
800
1000
1200
1400
1600
0
5
10
15
20
25
30
Core
1/4 of particle radius
1/2 of particle radius
Surface

image41.pdf

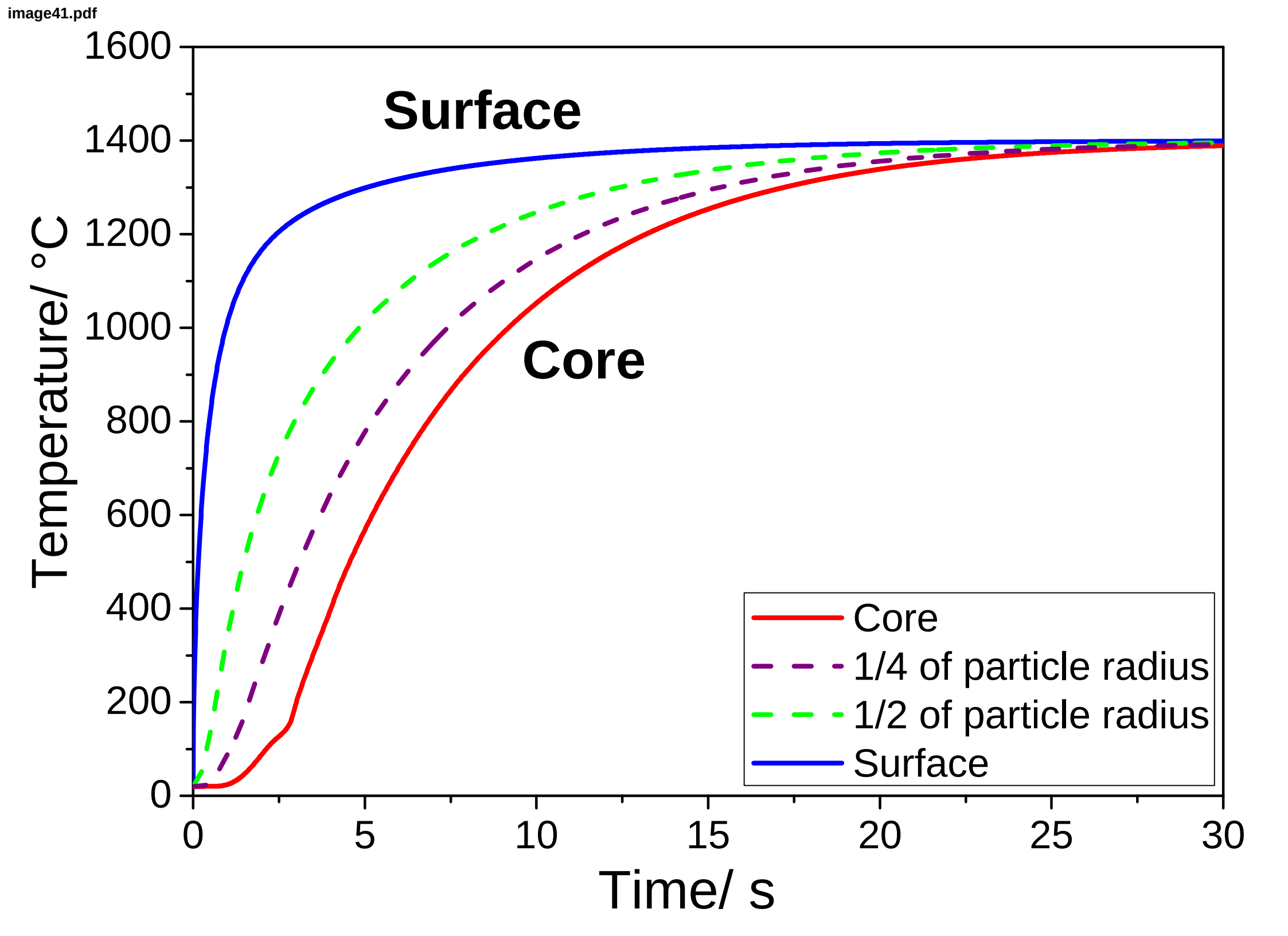
Surface
Core
Temperature/ °C
Time/ s
0
200
400
600
800
1000
1200
1400
1600
0
5
10
15
20
25
30
Core
1/4 of particle radius
1/2 of particle radius
Surface

image43.pdf

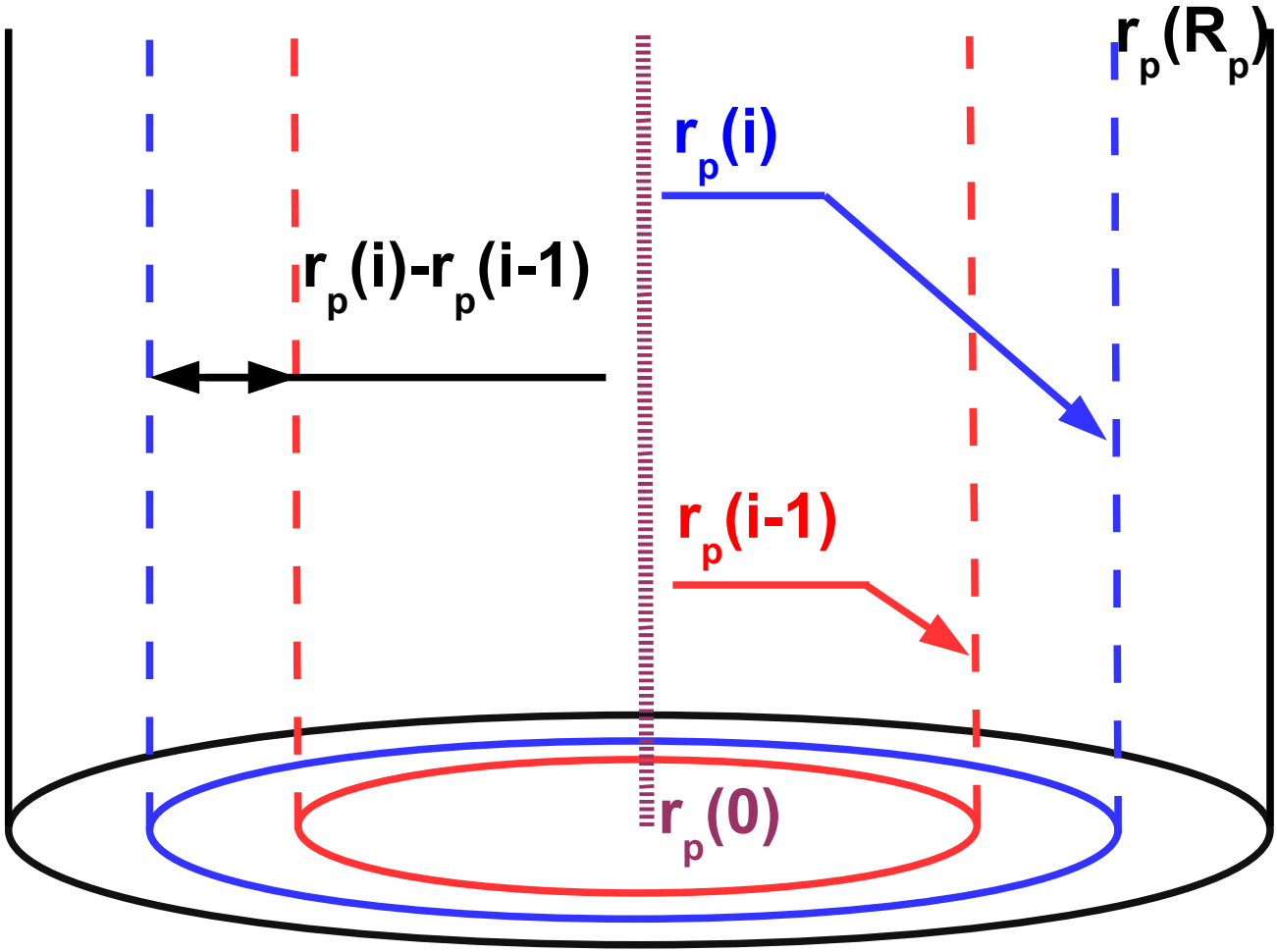

image44.pdf

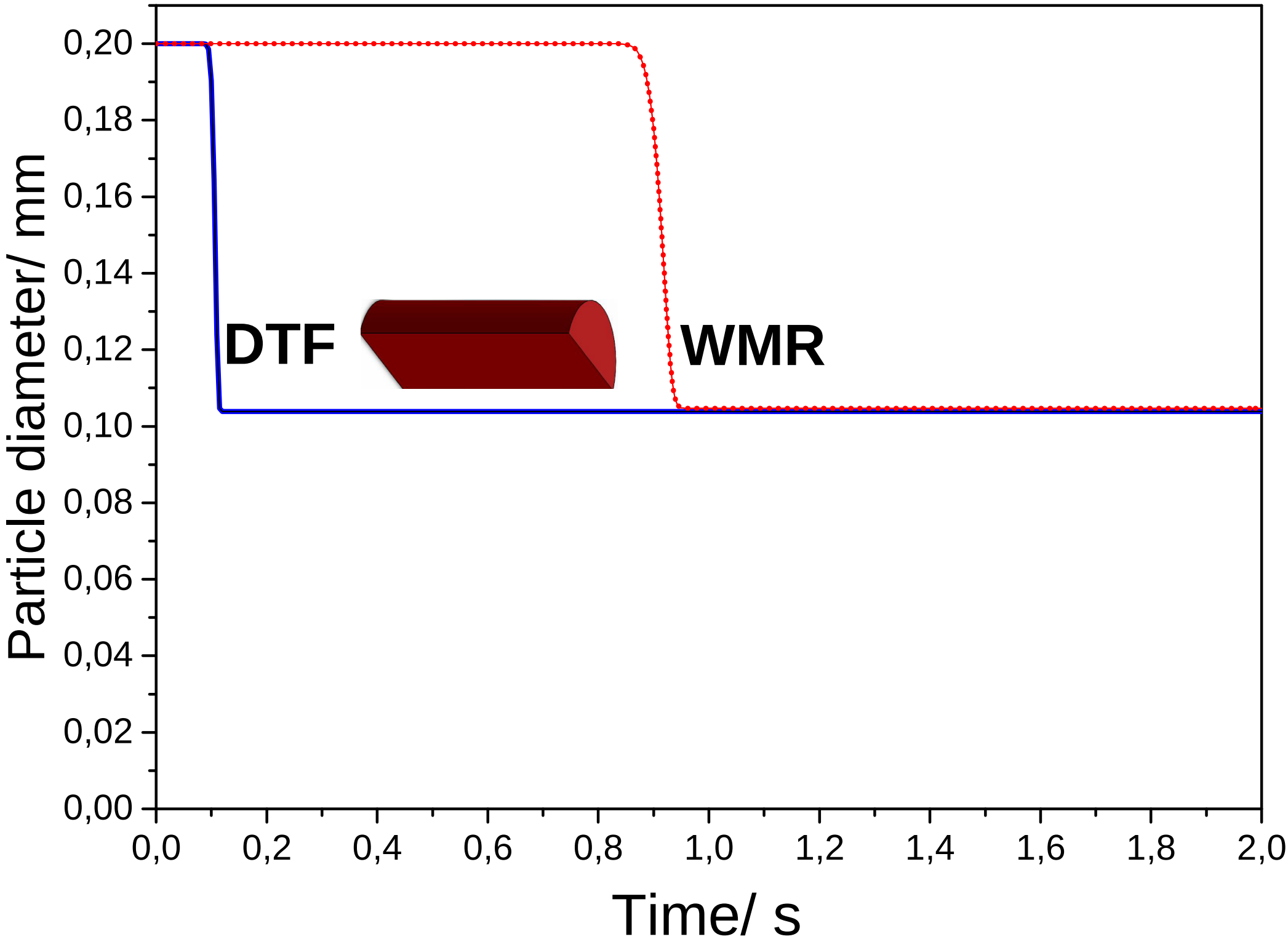
0,20
0,18
0,16
0,14
0,12
0,10
0,08
0,06
0,04
0,02
0,00
Particle diameter/ mm
DTF
WMR
0,0
0,2
0,4
0,6
0,8
1,0
1,2
1,4
1,6
1,8
2,0
Time/ s

image45.pdf

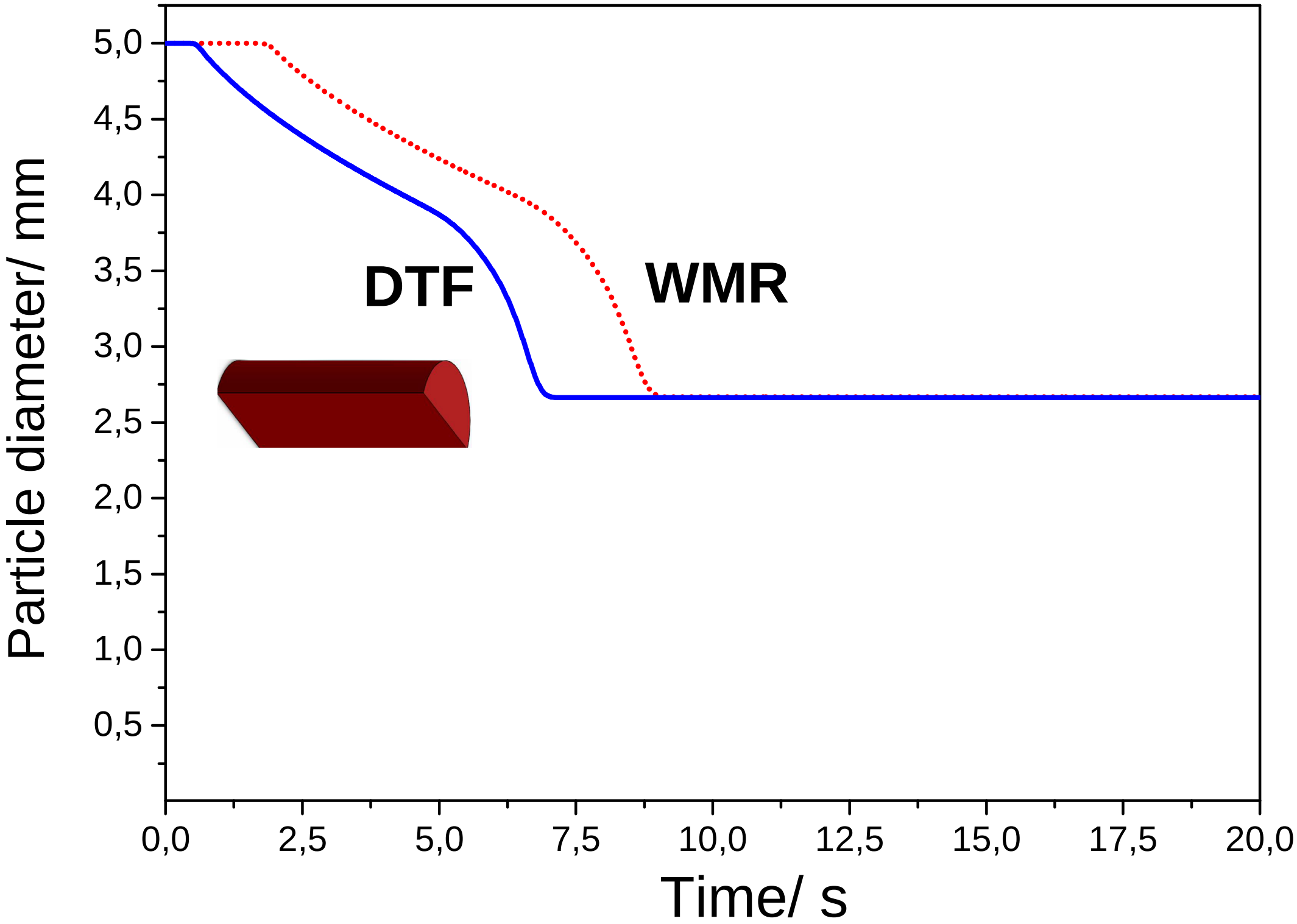
Particle diameter/ mm
5,0
4,5
4,0
3,5
3,0
2,5
2,0
1,5
1,0
0,5
DTF
WMR
0,0
2,5
5,0
7,5
10,0
12,5
15,0
17,5
20,0
Time/ s

image46.pdf

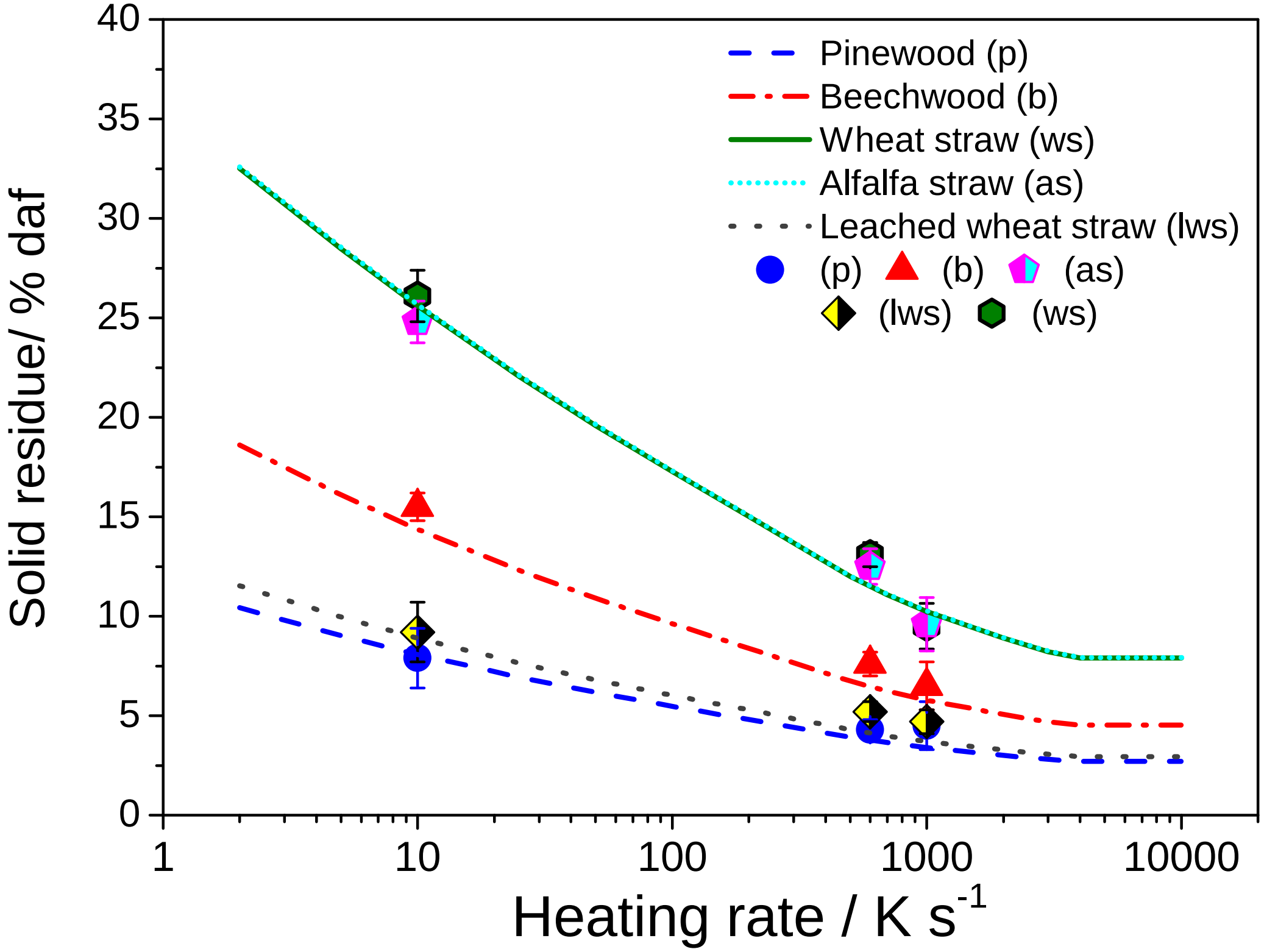
Pinewood (p)
Beechwood (b)
Wheat straw (ws)
Alfalfa straw (as)
Leached wheat straw (lws)
(p)
(b)
(as)
(lws)
(ws)
Solid residue/ % daf
Heating rate / K s-1
0
5
10
15
20
25
30
35
40
1
10
100
1000
10000

image47.pdf

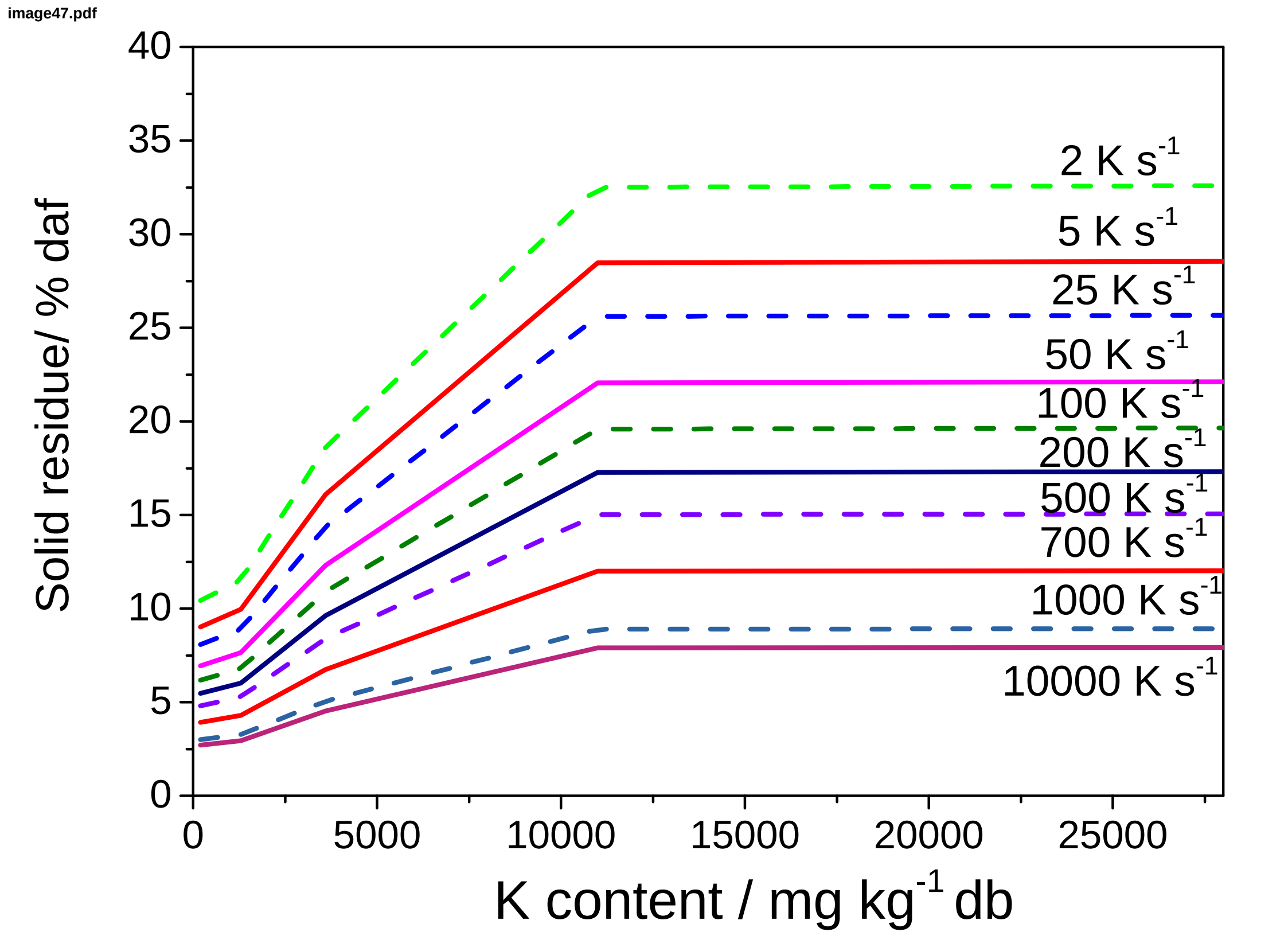
Solid residue/ % daf
K content / mg kg-1 db
0
5
10
15
20
25
30
35
40
0
5000
10000
15000
20000
25000
2 K s-1
5 K s-1
25 K s-1
50 K s-1
100 K s-1
200 K s-1
500 K s-1
700 K s-1
1000 K s-1
10000 K s-1

image48.pdf

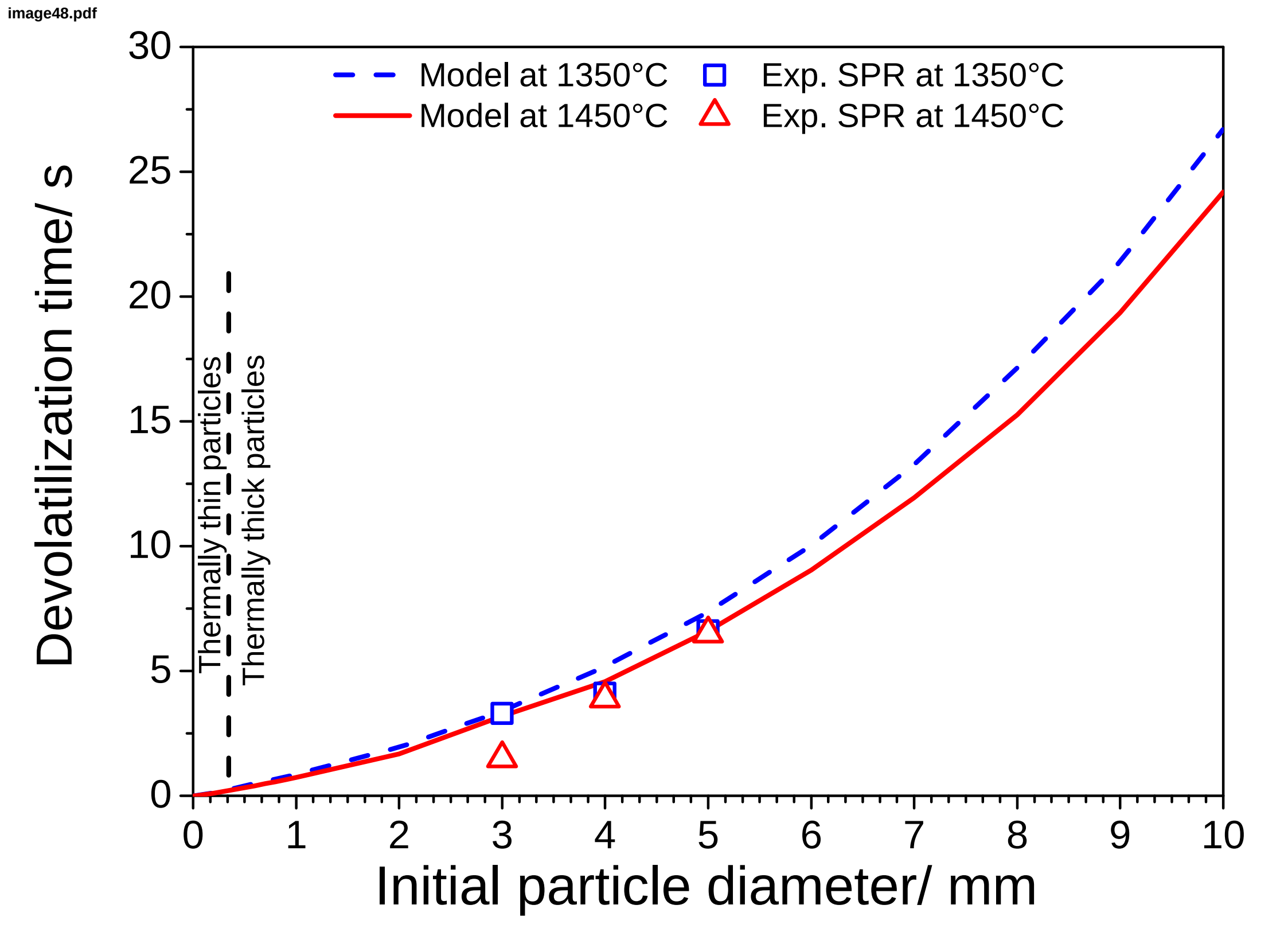
Model at 1350°C
Model at 1450°C
Exp. SPR at 1350°C
Exp. SPR at 1450°C
Thermally thin particles
Thermally thick particles
Devolatilization time/ s
Initial particle diameter/ mm
0
5
10
15
20
25
30
0
1
2
3
4
5
6
7
8
9
10

image49.pdf

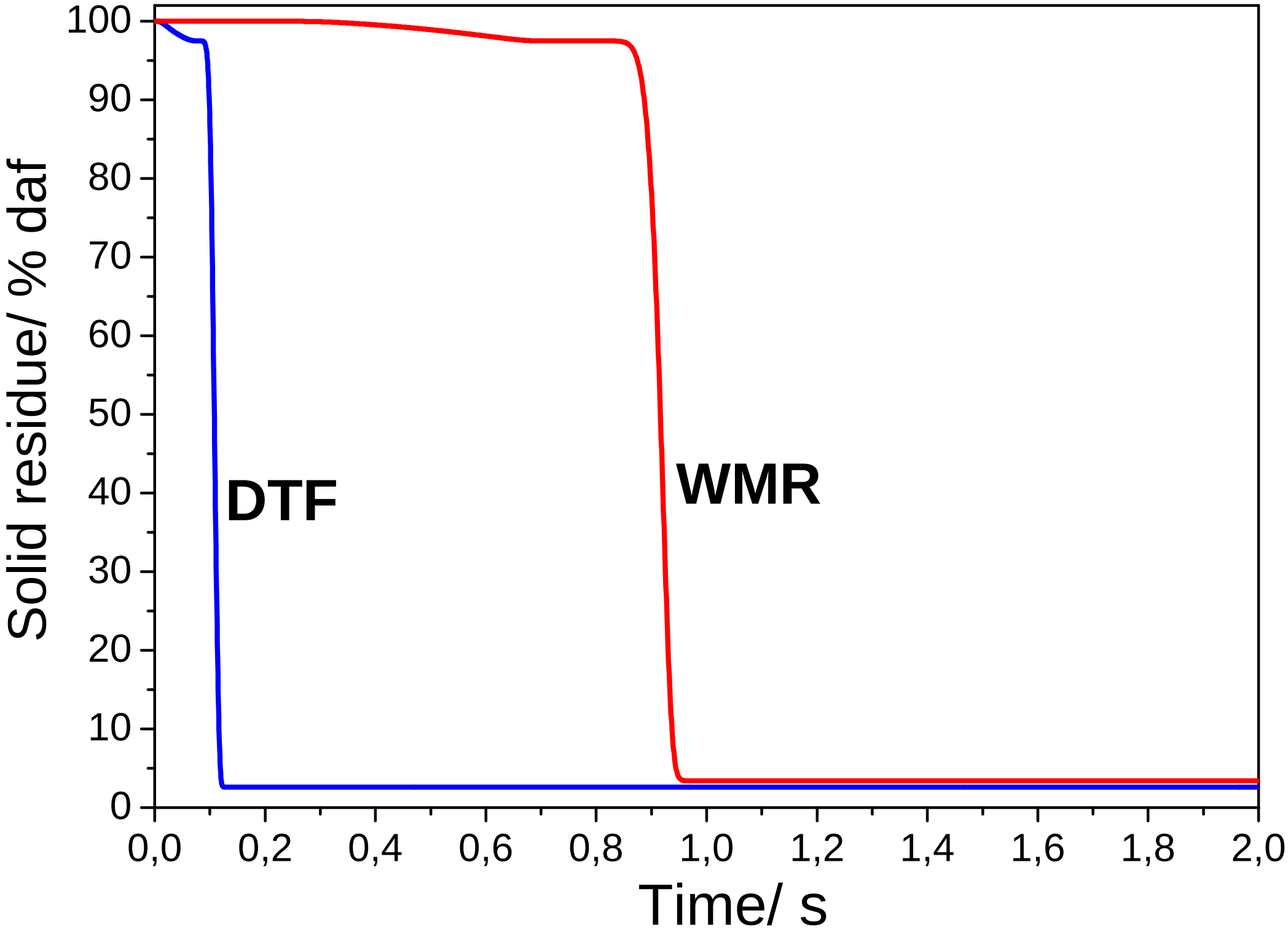
Solid residue/ % daf
100
90
80
70
60
50
40
30
20
10
0
0,0
0,2
0,4
0,6
0,8
1,0
1,2
1,4
1,6
1,8
2,0
Time/ s
DTF
WMR

image50.pdf

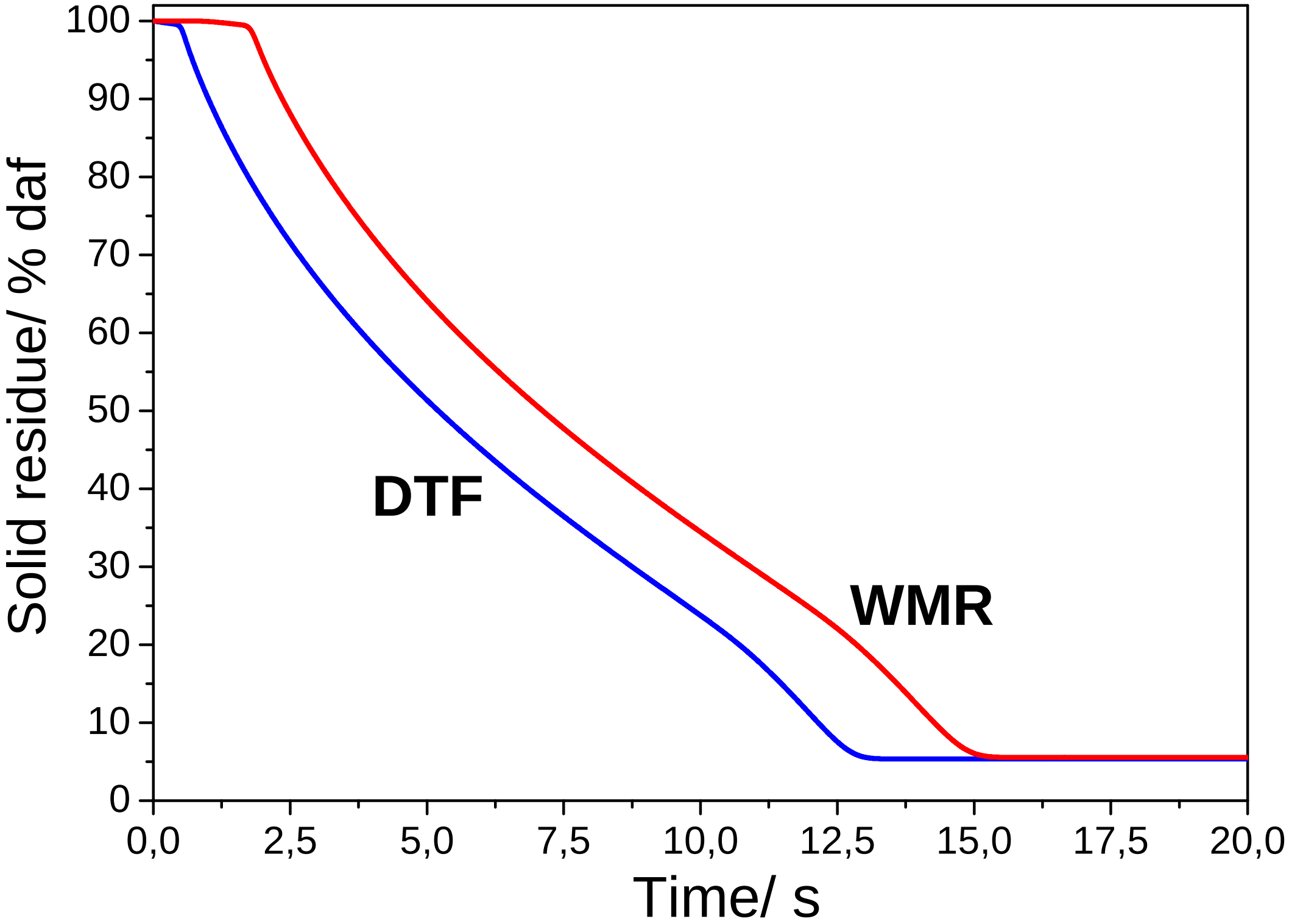
Solid residue/ % daf
100
90
80
70
60
50
40
30
20
10
0
0,0
2,5
5,0
7,5
10,0
12,5
15,0
17,5
20,0
Time/ s
DTF
WMR

image51.pdf

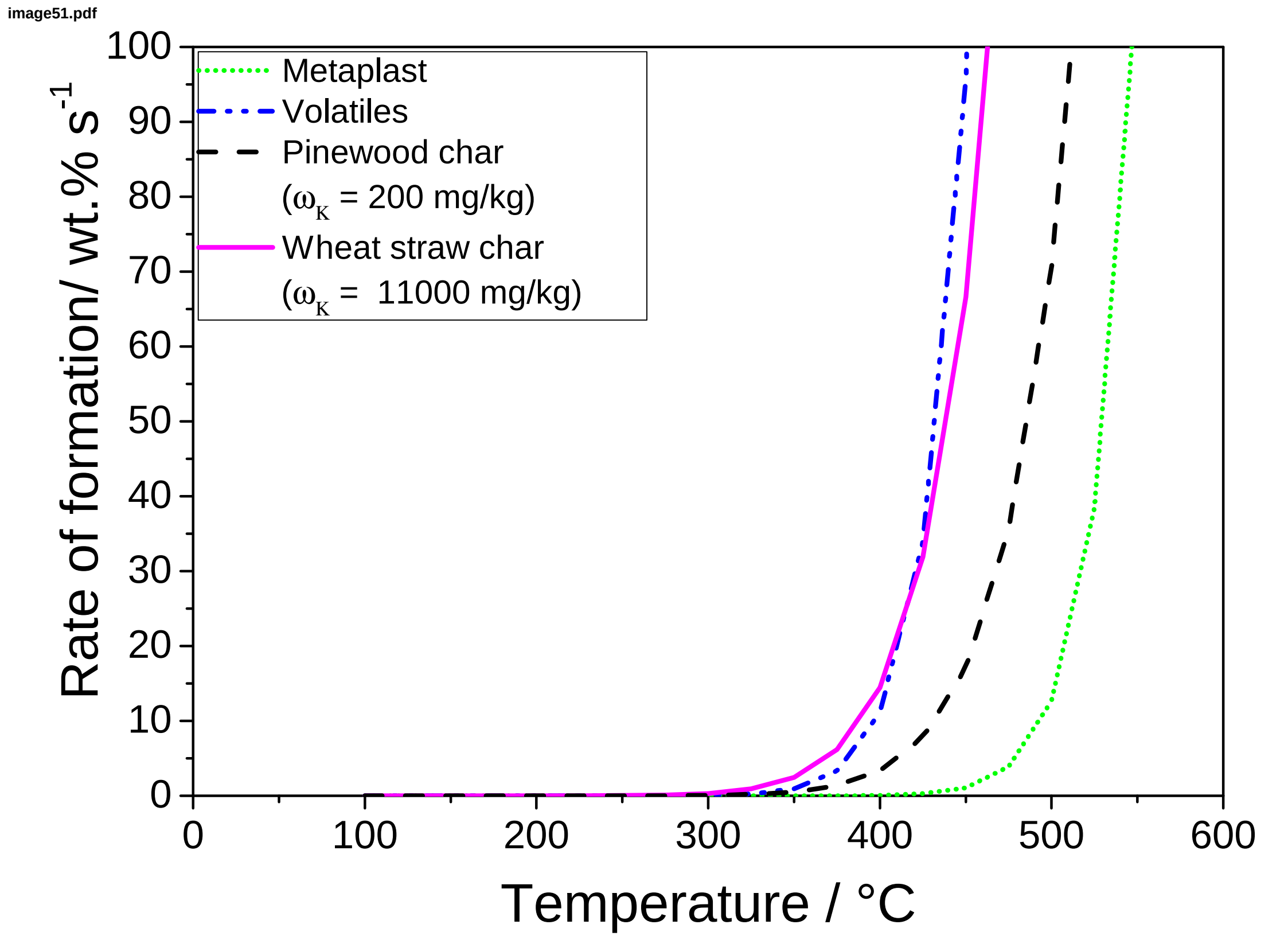
Metaplast
Volatiles
Pinewood char
(ω_K = 200 mg/kg)
Wheat straw char
(ω_K = 11000 mg/kg)
Rate of formation/ wt.% s^-1
Temperature / °C
0
10
20
30
40
50
60
70
80
90
100
0
100
200
300
400
500
600